NPS 68-90-003

NAVAL POSTGRADUATE SCHOOL

Monterey, California

SUBMESOSCALE STRUCTURE OF THE CALIFORNIA CURRENT NEAR SAN CLEMENTE ISLAND

C.M. Tsai, Paul F. Jessen, P.C. chu
and Curtis A. Collins

April 1990

Data Report for Period

17 July 1989 - 6 September 1989

Approved for public release: distribution is unlimited.

Prepared for;

Naval Facilities Engineering Command
Chesapeake Division (FPO-1)
Naval Yard
D.C. 20374

FedDocs
D 208.14/2
NPS-68-90-003

NAVAL POSTGRADUATE SCHOOL
Monterey, California

Rear Admiral R. W. West, Jr.
Superintendent

Harrson Shull
Provost

This report was prepared for Naval Facilities Engineering Command and funded by the Naval Postgraduate School.

Reproduction of all or part of this report is authorized.

This report was prepared by:

DUDLEY KNOX LIBRARY
NAVAL POSTGRADUATE SCHOOL
MONTEREY CA 93943-5101

SECURITY CLASSIFICATION OF THIS PAGE

REPORT DOCUMENTATION PAGE

Form Approved
OMB No 0704-0188

1a REPORT SECURITY CLASSIFICATION Unclassified	1b RESTRICTIVE MARKINGS
2a SECURITY CLASSIFICATION AUTHORITY	3 DISTRIBUTION / AVAILABILITY OF REPORT Approved for public release distribution unlimited.
2b DECLASSIFICATION / DOWNGRADING SCHEDULE	
4 PERFORMING ORGANIZATION REPORT NUMBER(S) NPS - 68-90-003	5 MONITORING ORGANIZATION REPORT NUMBER(S)
6a NAME OF PERFORMING ORGANIZATION Naval postgraduate School 6b OFFICE SYMBOL (If applicable) 68	7a NAME OF MONITORING ORGANIZATION
6c. ADDRESS (City, State, and ZIP Code) Monterey, CA 93943-5000	7b ADDRESS (City, State, and ZIP Code)
8a NAME OF FUNDING / SPONSORING ORGANIZATION Naval Postgraduate School 8b OFFICE SYMBOL (If applicable)	9 PROCUREMENT INSTRUMENT IDENTIFICATION NUMBER O&MN, Direct funding
8c. ADDRESS (City, State, and ZIP Code) Monterey, CA 93943-5000	10 SOURCE OF FUNDING NUMBERS PROGRAM ELEMENT NO / PROJECT NO / TASK NO / WORK UNIT ACCESSION NO

11 TITLE (Include Security Classification)
SUBMESOSCALE STRUCTURE OF THE CALIFORNIA CURRENT NEAR SAN CLEMENTE ISLAND

12 PERSONAL AUTHOR(S)
C.M. TSAI, PAUL F. JESSEN, P.C. CHU, AND CURTIS A. COLLINS

13a TYPE OF REPORT	13b TIME COVERED	14 DATE OF REPORT (Year, Month, Day)	15 PAGE COUNT
Data	FROM 7/17/89 TO 9/6/89	April 1990	96

16 SUPPLEMENTARY NOTATION

17 COSATI CODES			18 SUBJECT TERMS (Continue on reverse if necessary and identify by block number)
FIELD	GROUP	SUB-GROUP	Coastal circulation, Upper ocean currents, San Clemente Basin , Nearshore eddies.

19 ABSTRACT (Continue on reverse if necessary and identify by block number)

The purpose of the San Clemente Basin Experiment (SCBE) was to survey the upper ocean currents and temperature in a region southwest of San Clemente Island(SCI).

To accomplish this, two cruises were made in this area during which currents were measured by using a shipboard mounted Acoustic Doppler Current Profile (ADCP), and temperature was measured during the second cruise by deploying Expendable Bathythermographs(XBT). The first cruise took place during 17-21th July 1989 and the second one during 2nd-6th September 1989.

Data indicate a variety of features. Two different flow patterns were observed:

Strong poleward alongshore flow(about 40 cm/s) occured 40-60 km west of SCI and small scale eddies were seen further offshore, (conti. on next page)

20 DISTRIBUTION / AVAILABILITY OF ABSTRACT	21 ABSTRACT SECURITY CLASSIFICATION
☐ UNCLASSIFIED/UNLIMITED ☐ SAME AS RPT ☐ DTIC USERS	UNCLASSIFIED
22a NAME OF RESPONSIBLE INDIVIDUAL Ching-Mao Tsai	22b TELEPHONE (Include Area Code) (408) 6463266 22c OFFICE SYMBOL

DD Form 1473, JUN 86 *Previous editions are obsolete* SECURITY CLASSIFICATION OF THIS PAGE

S/N 0102-LF-014-6603

ACKNOWLEDGEMENTS

This research was supported by the Naval Postgraduate School Research Council and the Naval Facilities Engineering Command.

TABLE OF CONTENTS

1. INTRODUCTION 1

2. FIELD PROGRAM 2

3. DATA PROCESSING 4

4. CURRENT STRUCTURE 7

5. THERMAL STRUCTURE 11

6. CONCULSION 13

LIST OF FIGURES

Figure 1.
Cruise track off San Clemente Island during 17-21 July, 1989 (SCBE-I). 14

Figure 2.
Vertically averaged currents measured during SCBE-I (1920 UT 18 July - 1411 UT, 20 July). a. 12 - 28m, b. 42 - 58m, c.92 - 108m, d. 142 - 158m, e. 192 - 208m, f. 242 - 258m, g. 292 - 308m, h. 342 - 358m, i. 392 - 408m. 14

Figure 3.
Cruise track followed during the first pass through the study area off San Clemente Island during 2-6 September, 1989 (SCBE-II)..... 19

Figure 4.
Vertically averaged currents measured during SCBE-II (2240 UT 3 September - 2330 UT, 4 September). a. 12 - 28m, b. 42 - 58m, c.92 - 108m, d. 142 - 158m, e. 192 - 208m, f. 242 - 258m, g. 292 - 308m, h. 342 - 358m, i. 392 - 408m. 19

Figure 5.
Cruise track followed during the second pass through the study area off San Clemente Island during 2-6 September, 1989 (SCBE-II). 24

Figure 6.
Vertically averaged currents measured during SCBE-II (2240 UT 4 September - 0640 UT 6 September). a. 12 - 28m, b. 42 - 58m, c. 92 - 108m, d. 142 - 158m, e. 192-208m, f. 242-258m, g. 292-308m, h. 342 - 358m, i. 392 - 408m. 24

Figure 7.
Location of vertical profiles of currents measured by the ADCP. 29

Figure 8.
Vertical profiles of currents (u,v) at locations given in Fig. 7.
a. M1, b. M2, c. M3, d. M4, e. M5, f. M6, g. M7, h. M8, i. M9. 29

Figure 8.
Vertical profiles of currents (u,v) at locations given in Fig. 7.
j. E1, k. E2, l. E3, m. E4, n. E5, o. E6. 34

Figure 8.
Vertical profiles of currents (u,v) at locations given in Fig. 7.
p. D1, q. D2, r. D3, s. D4, t. D5. 37

Figure 8.u
Mean vertical profiles of currents (u,v) at study area given in
Fig. 5. 39

Figure 9.
Coordinate system and primary cruise lines along which most
shipboard current measurements were made. 40

Figure 10.
Across-shore sections of onshore and alongshore current components
using coordinate geometry of Fig. 9. a. 54km, b. 46km, c. 39km, d.
31km, e. 23km, f. 15km, g. 8km, h. 0km line. 41

Figure 11.
Across-shore sections of the standard deviation of onshore and
alongshore current components using coordinate geometry of Fig. 9.
a. 54km, b. 46km, c. 39km, d. 31km, e. 23km, f. 15km, g. 8km, h.
0km line. 45

Figure 12.
Across-shelf sections of temperature using the coordinate geometry of Fig. 9 a. 54km, b. 46km, c. 39km, d. 31km, e. 23km, f. 15km, g. 8km, h. 0km line. 49

Figure 13.
Isotherm depth in the study area a. 8° C b. 9° C c. 10° C. 53

Figure 14.
Vertical profiles of temperature measured by XBT at stations shown in Fig. 3, No. 15 - No. 42. 55

Figure 15.
Vertical profiles of temperature measured by XBT at stations shown in Fig. 5, No. 43 - No. 74. 69

Figure 16.
Comparison of vertical profiles of temperature between first and second pass over the study area for stations (18-70), (25-62), (32-72), (37-57), (39-65), (41-48). 85

Figure 17.
Mean temperature profile at study area given in Fig. 3 and Fig. 5. 86

I. INTRODUCTION

Two surveys were conducted in San Clememte Basin by the R/V Point Sur to measure the structure of ocean currents and temperature. The first cruise took place during 17-21 July 1989 and the second during 2-6 September 1989. The ocean currents were measured by a shipboard Acoustic Doppler Current Profiler (ADCP) and the temperature was measured by eXpendable BathyThermograph (XBT). Presented in this report are velocity and temperature data collected from ADCP and XBT during these two cruises. The XBT was used only doing the second cruise. In this report, we focus on the second cruise in which the ADCP/XBT data can be combined in some detail.

This report consists of six sections. Section two discusses the data processing and calibration. Section three contains ship tracks for the study area off San Clemente Island, the locations where XBTs were launched, vertically averaged currents for different layers, and twenty current profiles. Section four includes sections of onshore and alongshore currents, as well as sections of standard deviation of onshore and alongshore current components. Section five consists of 74 profiles of temperature and the temperature gradient microstructure on the 8°C, 9°C and 10°C isotherm. The final section discusses the flow pattern in San Clemente Basin and possible causes of these flow patterns. This project was sponsored by the Naval Engineering Systems Command.

II. FIELD PROGRAM

1). Observations during the first cruise (SCBE I)

The R/V Point Sur departed Moss Landing on the morning (1600 UT) of 17 July 1989. The course followed during the steam to the study area is shown in Figure 1 [**a** (32° 52.8′ N 119° 09.2′ W), **b** (33° 06.3′ N 118° 54.2′ W), **c** (32° 35.2′ N 118° 46.7′ W), **d** (32° 48.8′ N 118° 31.8′ W).] The track was designed to minimize course changes while allowing the ship to remain in water shallower than 400 m (the depth range of the ADCP). This allowed for current observations through the entire water column during the transit down the coast. Ship speed to the study area was approximately 10 knots.

The ship arrived at the northwest corner of the study area on 18 July at 1920 UT. Ship speed was reduced to approximately 5 knots to increase spatial resolution for the ADCP. The course followed in the study area consisted of 8 transects and a reciprocal course (Figure 1).

Following completion of the grid, the ship increased speed to 10 knots and steamed back to Moss Landing. The ship arrived in Moss Landing at 2230 UT on 21 July, 1989.

2). Observations during the second cruise (SCBE II)

During the second cruise, ship's speed was increased to approximately 9 knots while in the study area thus allowing the grid to be completed twice.

The ship departed Moss Landing on the morning of 2 September, 1989 at 1700 UT. The track followed to the study area was the same as the first cruise on 17 July 1989. XBTs were dropped every two hours starting at 2000 UT on the way to the study area.

The ship arrived at the northwest corner of the study area on 3 September at 2240 UT. The course followed during the first pass over the study area consisted of eight transects

(Figure 3). The transects were made in a northwest to southeast directions back and forth. The eight transects were finished at 2330 UT on September 4.

The frequency of XBT drops was increased to one per hour in the study area. The station numbers and positions of XBTs dropped during the first pass of the grid are shown in Figure 3.

The second pass over the study area consisted of eight transects oriented perpendicular to those of the first pass. During this pass the ship speed was reduced to 7.5 knots allowing slightly better spatial resolution of ADCP data as compared to the first pass. The time needed to complete each transect was increased to about 4 hours.

Position and station number of XBT deployment during the second pass of the grid are shown in Figure 5. Transect eight of the second grid was completed at 0640 UT on 6 September .

Following the completion of two passes, the ship increased speed to 10 knots and steamed for Santa Barbara, arriving at about 2000 UT on September 6.

III. DATA PROCESSING

1). Raw data processing

The ADCP data were processed by Paul Jessen of the NPS Oceanography Department. The first step is the correction of navigation data. "Bad" navigation data are replaced with values linearly interpolated from the preceding and following "good" data. From the corrected navigation data, the ship velocity is calculated. The second step in processing the data is the initial determination of the depth (bin number) to which the data of each ensemble remains reliable. If the percent of good returns drops below 50%, all deeper data are dropped.

After the first and second steps a reference layer five bins wide (62-78 m) was chosen. The choice of a reference layer depth is some what arbitrary, but appears to have little affect on the final calculated water velocities. Subtracting the ships velocity from the average velocity within the chosen reference layer yields an absolute reference layer velocity for each ensemble. The series of absolute reference velocity was filtered with a low pass Hanning window filter. The cutoff frequency of this filter is in the range of 0.03-0.05 cycles per minute.

2). Rotation (pitch, roll and heading)

The ADCP measured currents are relative to the ADCP, which can be oriented arbitrarily and moved relative to the earth. It is necessary to correct the data for ADCP attitude and motion. There are two kinds of motion that require correction: rotation (pitch, roll and heading) and translation (ship velocity). There are many ways to measure rotation and translation. The use of one of the following specific methods depend on a variety of factors:

Rotation (heading)

1. Gyrocompass
2. Flux-gate compass

Rotation (pitch and roll)

1. vertical gyro
2. pendulums

Translation

1. Navigation device (LORAN-C system)
2. Bottom tracking
3. Assume a 'layer of no motion' (reference layer)

A scheme for ADCP calibration which may take advantage of bottom tracking by the ADCP if water depths are not too large, is illustrated as follows (Joyce,1989). Let(u',v') represent the east and north velocity components as measured in the (x',y') coordinate frames and (u,v) the east and north components in the true (x,y) coordinates. Velocity in the two coordinate systems is related by

$$\begin{pmatrix} u' \\ v' \end{pmatrix} = \begin{pmatrix} \cos\alpha & \sin\alpha \\ -\sin\alpha & \cos\alpha \end{pmatrix} \begin{pmatrix} u \\ v \end{pmatrix} \tag{1}$$

Thus the water velocities in the true (x,y) coordinate frame are:

$$u_w = u_s + (1+\beta)(u_d cos\alpha - v_d sin\alpha) \tag{2}$$

$$v_w = v_s + (1+\beta)(u_d sin\alpha + v_d cos\alpha)$$

Where (u_w,v_w) is the water velocity, (u_s,v_s) is the ship velocity, and (u_d,v_d) is the Doppler velocity, β is the scale factor, and α is the heading angle between true north and meas-

ured north direction. The water velocity (u_w,v_w) is further decomposed into offshore (U) and alongshore (V) components by using a similar rotation formula:

$$\begin{pmatrix} U \\ V \end{pmatrix} = \begin{pmatrix} u_w \\ v_w \end{pmatrix} \begin{pmatrix} \cos\gamma & \sin\gamma \\ -\sin\gamma & \cos\gamma \end{pmatrix} \tag{3}$$

where γ is 313°. This coordinate system is shown in figure 8.

3). Other Data Collection

In addition to ADCP and XBT data, meteorological and surface oceanographic data were collected by a Serial ASCII Interface Loop (SAIL) system. This system monitors, averages, and stores: ship position, speed and heading, relative wind speed and direction, air temperature, dew point temperature, sea surface salinity, sea surface temperature, visible and infrared solar insolation, and sea surface skin temperature. These data were averaged over 30 second intervals and recorded on an HP9826 computer.

AVHRR imagery is being processed by the Oceanography Department of the Naval Postgraduate School.

IV. CURRENT STRUCTURE

Two flow patterns can be discerned from these surveys, a strong alongshore poleward current (centered at 5-15 km from San Clemente Island) and two small-scale eddies (further than 30 km from San Clemente Island). In figure 3, ADCP data were missing from station 35 to station 37. In figure 4.i, a lot of data were dropped due to bad return signals around 400 m depth.

1) Horizontal Current Patterns

Figure 4 shows the vertically averaged current in following layers : 12-28 m, 42-58 m, 92-108 m, 142-158 m, 192-208 m, 242-258 m, 292-308 m, 342-358 m and 392-408 m. These were made during the first pass over San Clemente Basin on cruise SCBE II. Results are:

(1) The poleward flow center is located 11 km offshore. Strongest currents are in the 12-58 m layers with flow speeds of over 50 cm/s and are located offshore 16 km near 32° 50′ N 118° 46′ W from the surface to a depth of 400m.

(2) The first eddy center is located at 32° 50′ N 118° 59′ W and the second eddy center is located at 32° 45′ N 118° 50′ W. The length-scale of these two eddies is approximately 10 km.

Figure 6 shows the vertically averaged current in the following layers: 12-28 m, 42-58 m, 92-108 m, 142-158 m, 192-208 m, 242-258 m, 292-308 m, 342-358 m and 392-408 m. These were obtained during the second pass over San Clemente Basin on cruise SCBE II.

Figure 5 shows the cruise track during the 2nd pass. Station 42 and 48 were in the same location but 6 hours apart, and stations 57 and 64 are seven hours apart. Associated with this time difference is a change in the direction of the mean flow at these stations.

The circulation measured during the second pass, figure 6.a to 6.i, was much different from the circulation measured during the first pass, figure 4.a to figure 4.i, especially in the poleward flow area. Nevertheless, the current flows poleward strongly at both times.

2) Current Profiles

Twenty current (u,v) profiles were plotted (figure 8.a - 8.t). Each profile consists of U and V components from the sea surface to a depth of 400 m over the San Clemente Basin, where U and V are onshore and alongshore velocity respectively.

The location of these data was shown in figure 7 where stations M1, M2 ....M9 were in the poleward flow area, stations E1, E2.....E6 represent the region of the first eddy area, and stations D1, D2.....D5 represent the second eddy area.

(1) Figure 8.b shows strong alongshore flow at station M2 of over 50 cm/s at the surface with the velocity decreasing rapidly at about 30 m depth. Stations M3, M4, M5, M6, M8 (figure 8.c, 8.d, 8.e, 8.f, 7.h) show a strong alongshore flow pattern.

(2) Figure 8.k and 8.l at the center of the first eddy showed a weak flow from the surface to a depth of 400 m.

(3) The mean flow pattern in the study area was shown at Fig. 8.u. The strong poleward flow velocity (15 cm/s) from the surface to a depth of 30 m decreased gradually with increase of depth to a velocity of approximately 5 cm/s at a depth of 400 m. The mean offshore flow velocity of 5 cm/s in the upper layer decreased to 1 cm/s at a depth of 250 m.

3). Sections of Onshore and Alongshore Currents

Figure 9 shows the coordinate system and the primary cruise track along which most shipboard current measurements were made during the second pass over the study area from 4-6 September, 1989 during SCBE-II. The coordinate origin is at 32° 47′ N, 118° 26′ W, and the Y-axis has been rotated to 313°, i.e. from a north to a northwest direction. The study area is located in the minus X direction. Primary lines were separated approximately 7-8 km from 0 km to 54 km from southeast to northwest.

Figure 10 shows the section of onshore and alongshore currents from the 54 km to the zero km line.

(1) The figure indicates strong poleward current on the surface at an offshore distance approximately 5-10 km with weak flow offshore 20-30 km. Equatorward current increased farther offshore beginning at a distance of 35 km. Each primary line from north to south displays strong mean current flow of approximately 20 cm/s, located offshore 10 km, from the surface to 400 m depth.

(2) Onshore currents are variable. The 15 km line in Fig. 10.f shows a strong onshore current of 15-30 cm/s. The 31 km and 23 km line also show a somewhat strong onshore current, but the 54 km and 39 km line show offshore flow.

(3) A jet appeared in Fig. 10.e to 10.h with a speed of around 35-45 cm/s. The core of the jet appears to accelerate and move onshore from South to North.

(4) Cyclonic eddy structure can be found from a transition zone on the 31 km primary line (figure 10.d). The 39 km line (figure 10.c) contains opposing alongshore flows and the 31 km line onshore current. The 39 km line has offshore flow.

4). Sections of Standard Deviation of Onshore and Alongshore Currents

The standard deviation of fluctuations are a measure of the variability of the current velocity. Fluctuations in U and V about their mean values (Fig. 11.a - Fig. 11.h) are at least as large as the mean velocity. Far from shore, the fluctuations in U and V are weaker. As the coast is approched the fluctuation in V are stronger.

V. THERMAL STRUCTURE

Temperature data were collected using XBT probes during the SCBE II (4-6 September 1989). 74 XBTs were launched; about 60 XBTs were dropped in the study area.

Data reveals the thermal structure: 1) The thickness of the upper mixed layer was very shallow (< 10m) and varied slightly during the SCBE II second pass, and 2) the temperature was between 6° C and 10° C in the upper 400 m.

1). Section of temperature at the primary onshore and offshore line

Vertical temperature cross-sections from the 54 km primary line to the 0 km line are shown on Fig. 12.a-12.h. From these plots, the temperature stratification over the study area is distinct from surface to 30 m depth. The 8° C contour varied from 200m-300m depth on each primary line.

2). Isotherm depth in the study area

Figure 13.a-13.c are the depths of the 8°, 9°, 10° C isotherms. In figure 13.a, the depth of the 8° C isotherm showed a strong offshore temperature gradient, 10-30 km to the west of SCI. The 9° and 10° isotherms also showed an offshore temperature gradient; the gradient became larger when closer to SCI.

3). Temperature profiles

Figures 14.1-14.28 show temperature profiles from station 15-42 on SCBE II during the first pass over the study area.

In Fig 15.1-15.74, temperature profiles are shown from station 43-74 on SCBI II during the second pass over the study area. By comparing XBT drops between the first and second passes, 6 pairs of XBT stations were found at almost the same place (stations 18-70, 25-62, 32-72, 37-57, 39-65, 41-48.)

Fig. 16 shows the comparison of temperature profiles at three stations (37-57, 39-65, 41-48) located in the mean flow area. The vertical profiles of temperature varied only ($< 1°$ C) for passes 10-24 hours apart. In the eddy area (stations 18-70 and 25-62), mixed layer temperatures dropped 0.5° C in the 24-48 hours between passes. There was little temperature change below the mixed layer in the eddy regime.

Mean temperature profile in figure 17 shows a very shallow mixed layer (less then 10 m). The thermocline extends from 15 m to 50 m depth and the temperature across the thermocline is about 9° C. Below the thermocline temperature decreases slowly with depth. The lapse rate in the layer below the thermocline is around 0.8° C/100 m.

VI. CONCLUSIONS

Data from this report show 1) the topographic effects on the coastal currents near San Clemente Island. 2) The the transition zone of the Southern California Current system.

(1) Two different flow patterns were observed. Strong alongshore poleward (northwest) currents were (centered at 40-60 km west SCI) and small-scale eddies (farther than 60 km west of SCI).

(2) The alongshore poleward currents intensify in the poleward direction. This intensification can reach 300 m depth.

(3) Two small-scale cyclonic eddies were observed during the second cruise. They were located at (119° 5′ W,32° 55′ N) and (118° 53′ W, 32° 47′ N). The length-scale of these two eddies is approximately 10 km .

(4) The appearance of the eddies beween the northwestward coastal current and the California Current offshore is believed to be due to the horizontal shear.

(5) The XBT data show that the mixed layer depth was very shallow (< 10 m) during the second cruise.

(6) The 8° C isotherm thickness indicates a strong baroclinic zone (i.e. a strong across-coastal temperature gradient), which is nearly parallel to and 10-30 km west of SCI.

(7) The coincidence of the strong alongshore poleward currents with the baroclinic zone and the disappearance of these two systems 35 km farther from the SCI suggests a large impact of the topography in the San Clemente Island regime on the oceanic currents and thermal structure.

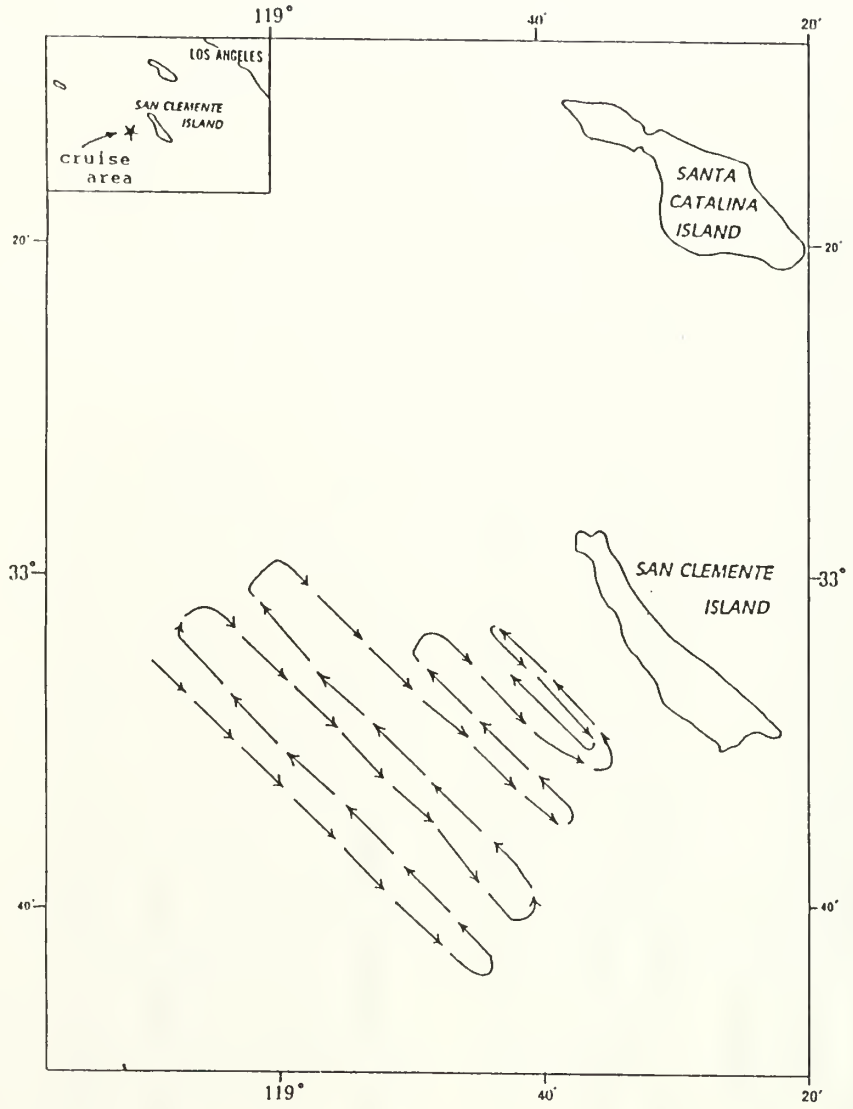

Figure 1. Cruise track followed during occupation of the study area off San Clemente Island during the first curise SCBE-1, 17-21 July, 1989.

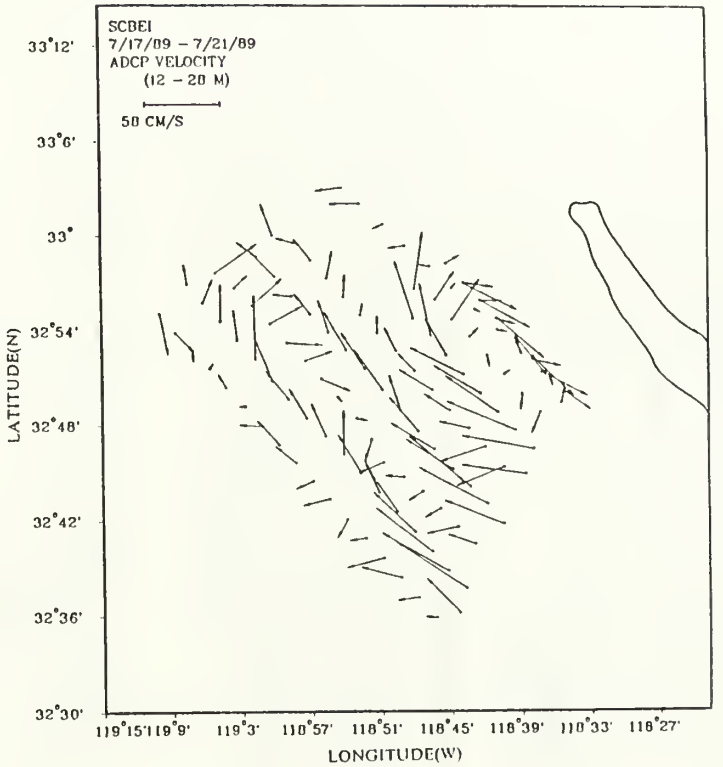

Figure 2a. Vertically averaged currents (12-28m) measured during the cruise SCBE-1 (1920 UT, 18 July - 1411 UT, 20 July).

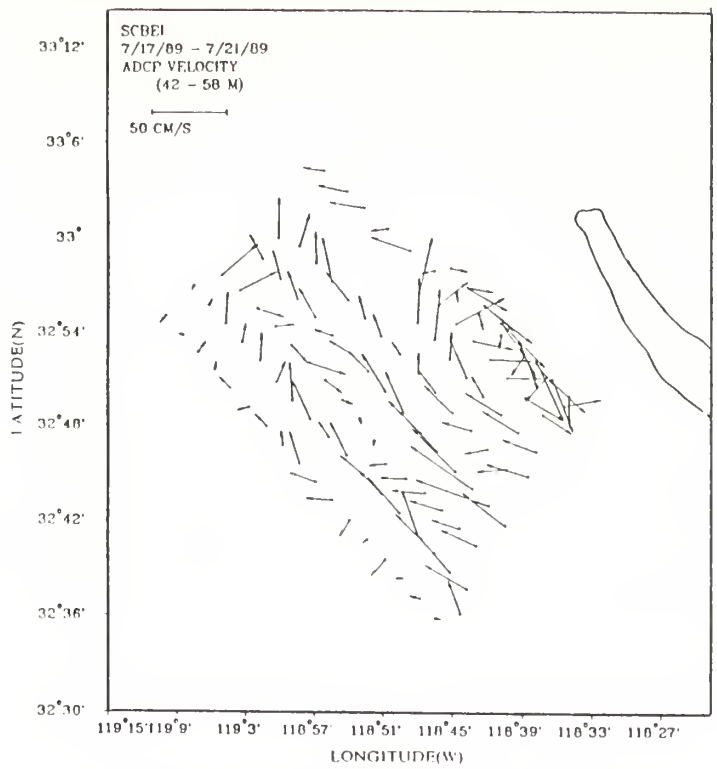

Figure 2b. Vertically averaged currents (42-58m) measured during the cruise SCBE-I (1920 UT, 18 July - 1411 UT, 20 July)

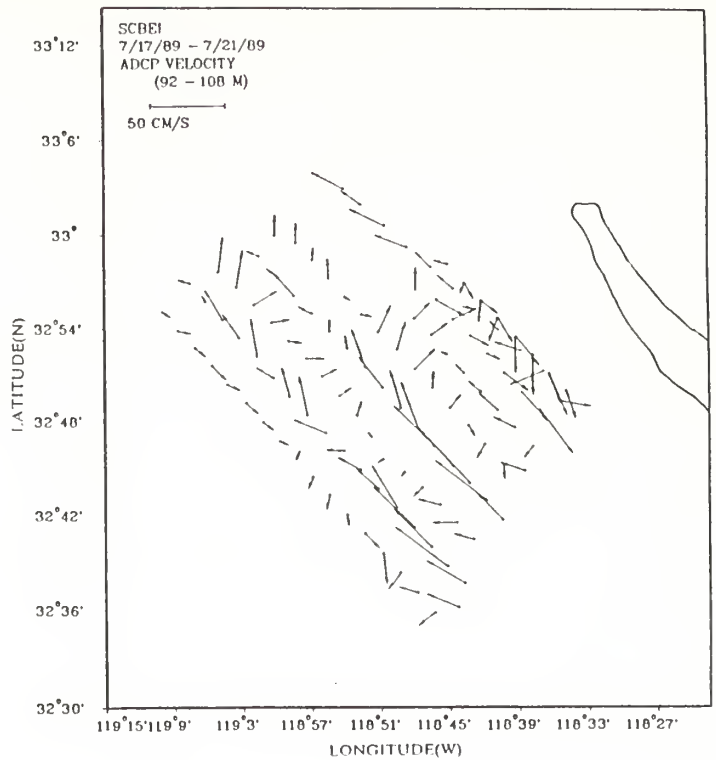

Figure 2c. Vertically averaged currents (92-108m) measured during the cruise SCBE-I (1920 UT, 18 July - 1411 UT, 20 July).

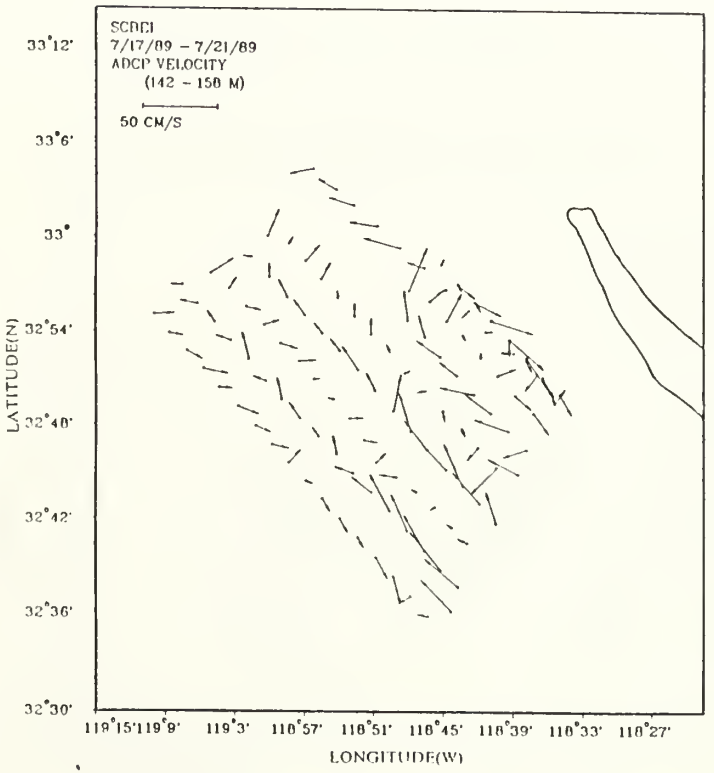

Figure 2d. Vertically averaged currents (142-158m) measured during the cruise SCBE-I (1920 UT, 18 July - 1411 UT, 20 July).

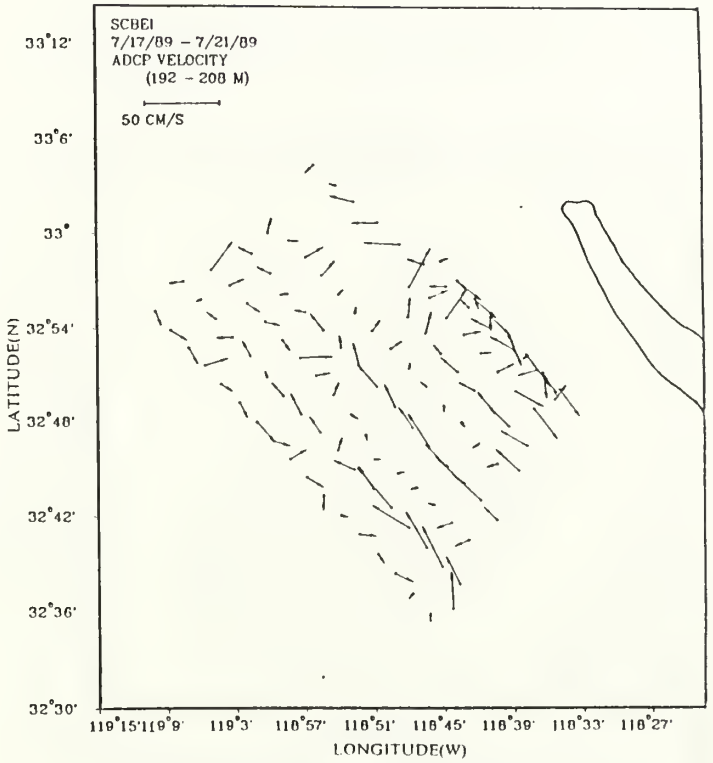

Figure 2e. Vertically averaged currents (192-208m) measured during the cruise SCBE-I (1920 UT, 18 July - 1411 UT, 20 July).

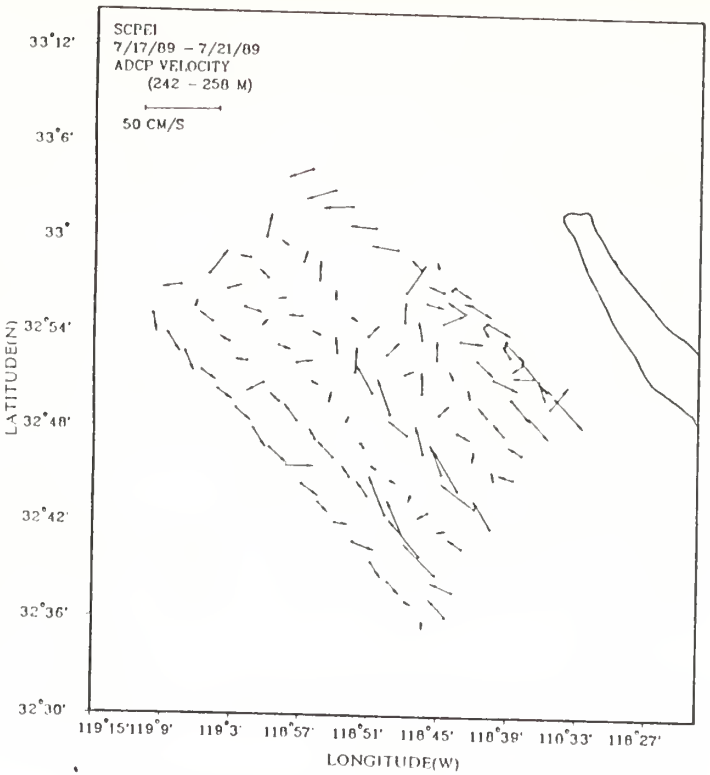

Figure 2f. Vertically averaged currents (242-258m) measured during the cruise SCBE-I (1920 UT, 18 July - 1411 UT, 20 July)

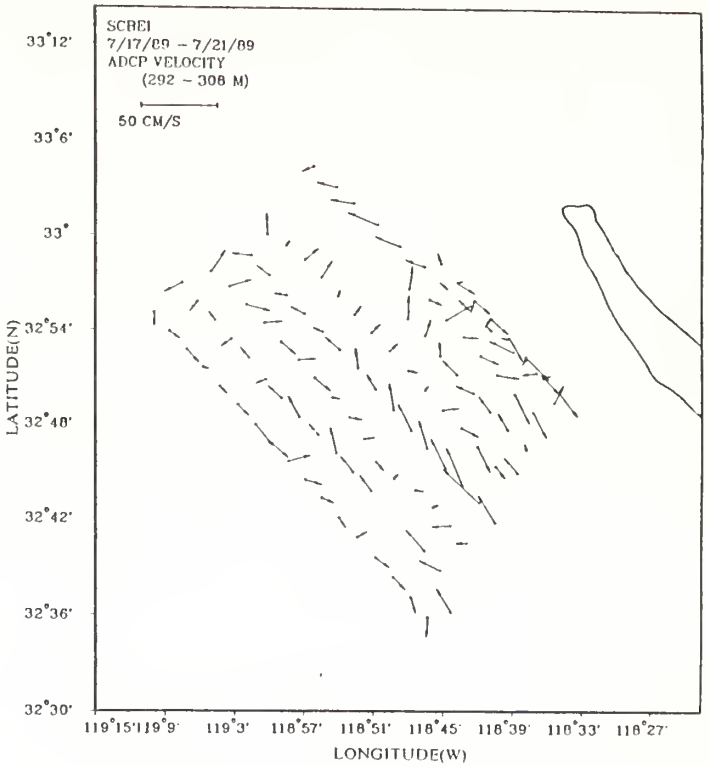

Figure 2g. Vertically averaged currents (292-308m) measured during the cruise SCBE-I (1920 UT, 18 July - 1411 UT, 20 July).

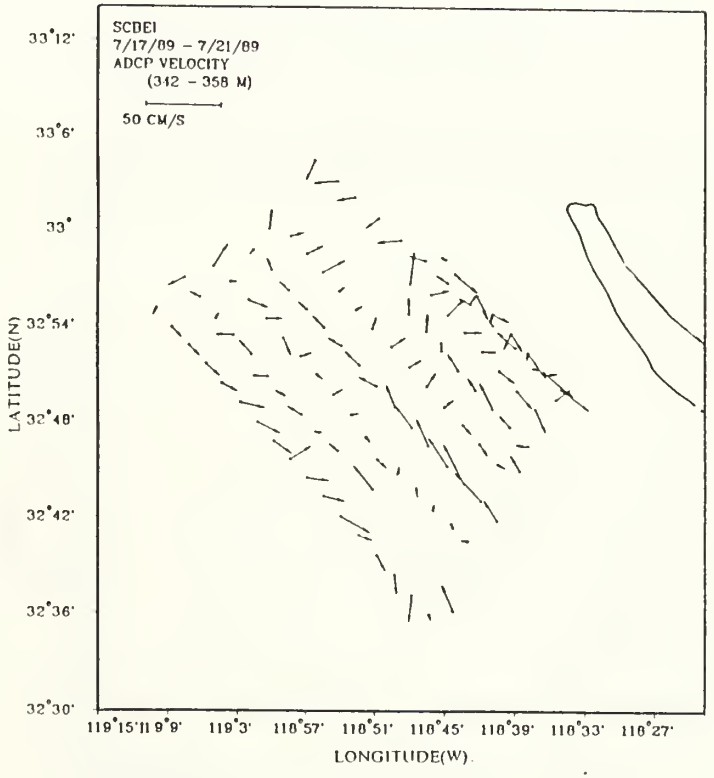

Figure 2h. Vertically averaged currents (342-358m) measured during the cruise SCBE-I (1920 UT, 18 July - 1411 UT, 20 July).

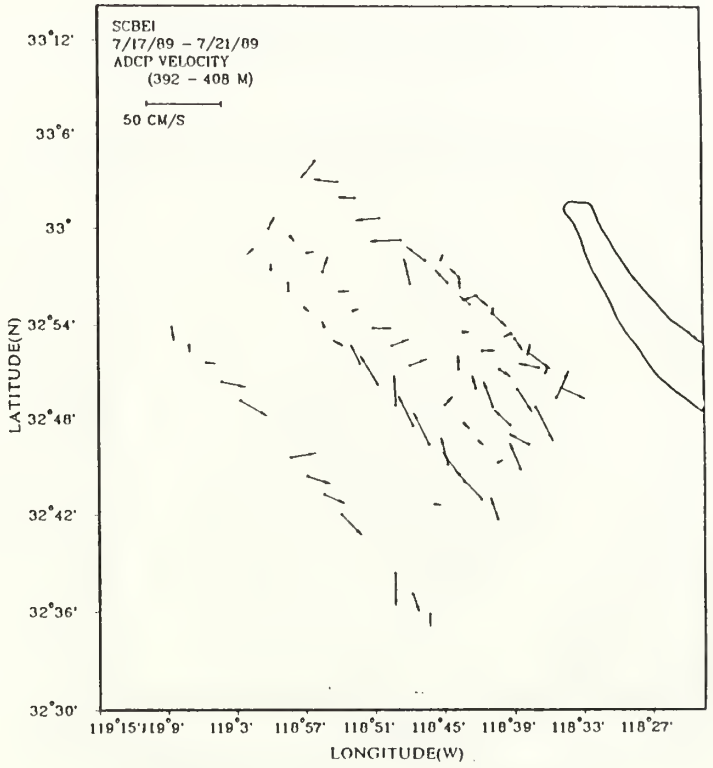

Figure 2i. Vertically averaged currents (392-408m) measured during the cruise SCBE-I (1920 UT, 18 July - 1411 UT, 20 July).

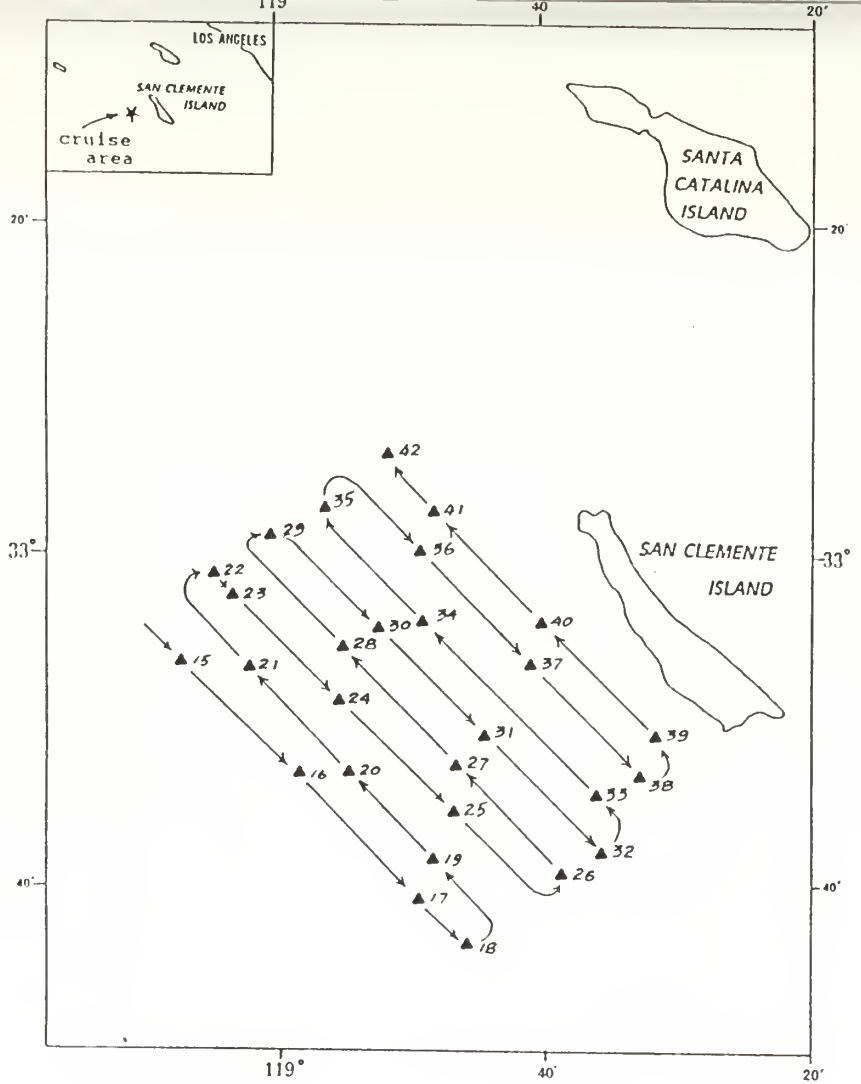

Figure 3. Cruise track followed during the first pass over the study off San Clemente Island during the second cruise SCBE-II 2-6 September, 1989. The solid triangle ▲ denotes location of XBT soundings.

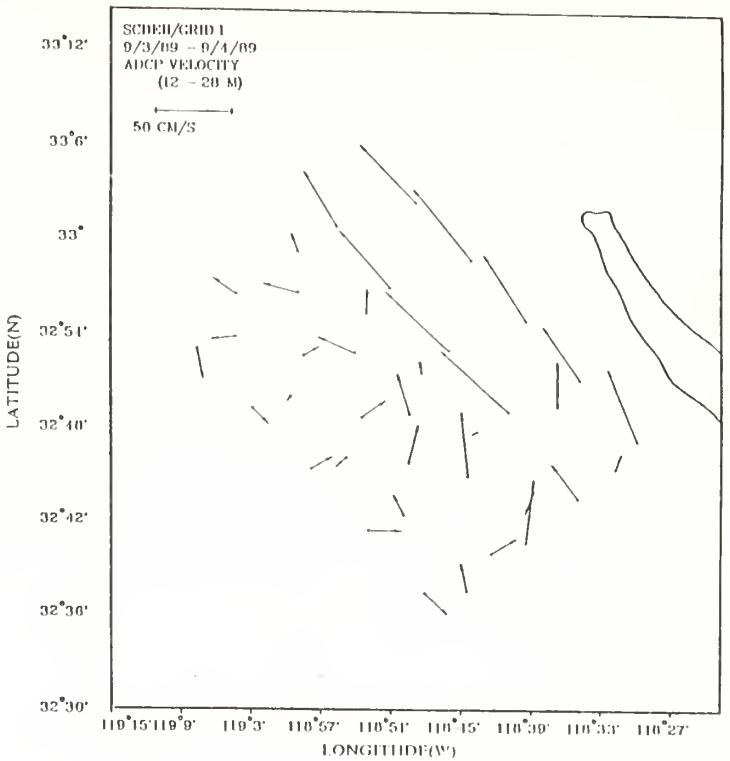

Figure 4a. Vertically averaged currents (12-28m) measured during the cruise SCBE-II (2240 UT, 3 September - 2330 UT, 4 September)

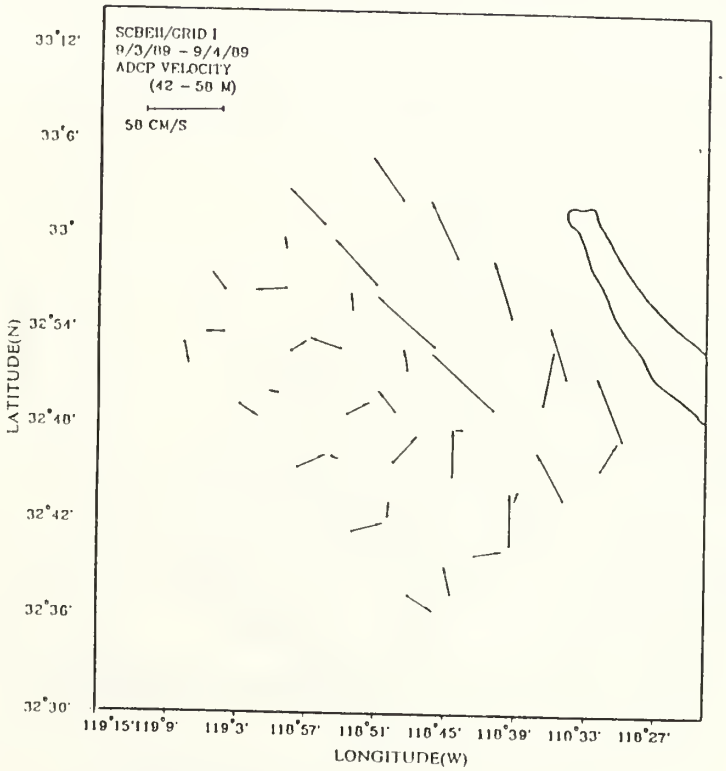

Figure 4b. Vertically averaged currents (42-58m) measured during the cruise SCBE-II (2240 UT, 3 September - 2330 UT, 4 September)

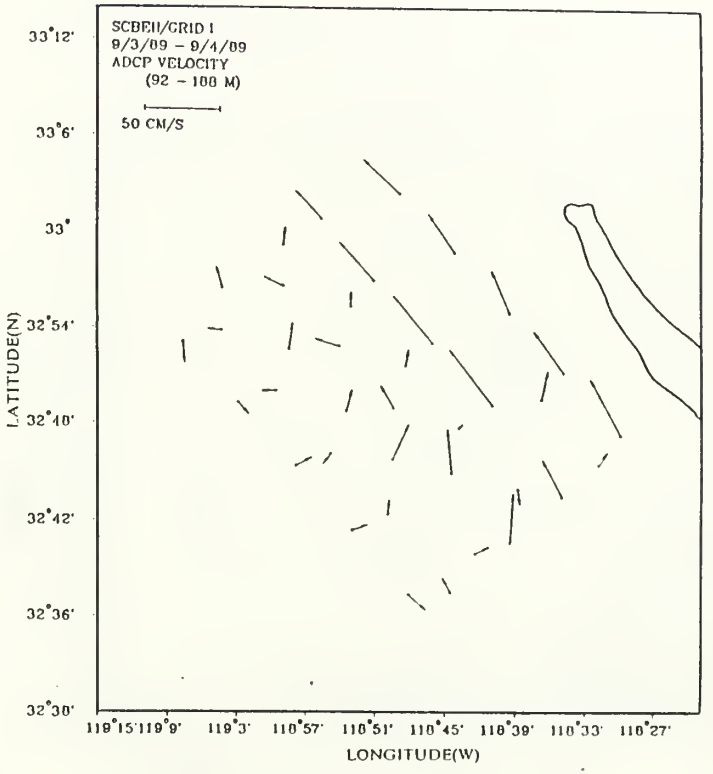

Figure 4c. Vertically averaged currents (92-108m) measured during the cruise SCBE-II (2240 UT, 3 September - 2330 UT, 4 September)

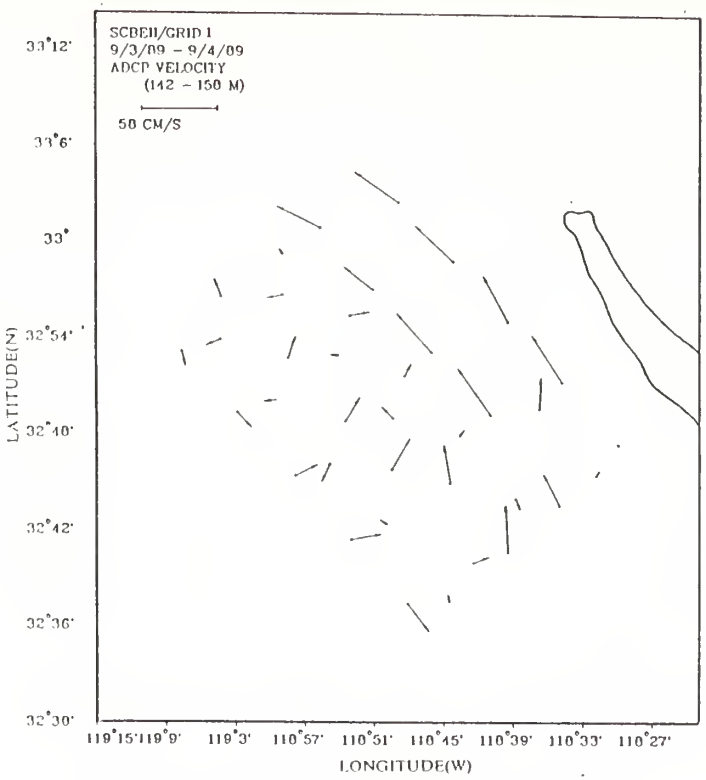

Figure 4d. Vertically averaged currents (142-158m) measured during the cruise SCBE-II (2240 UT, 3 September - 2330 UT, 4 September).

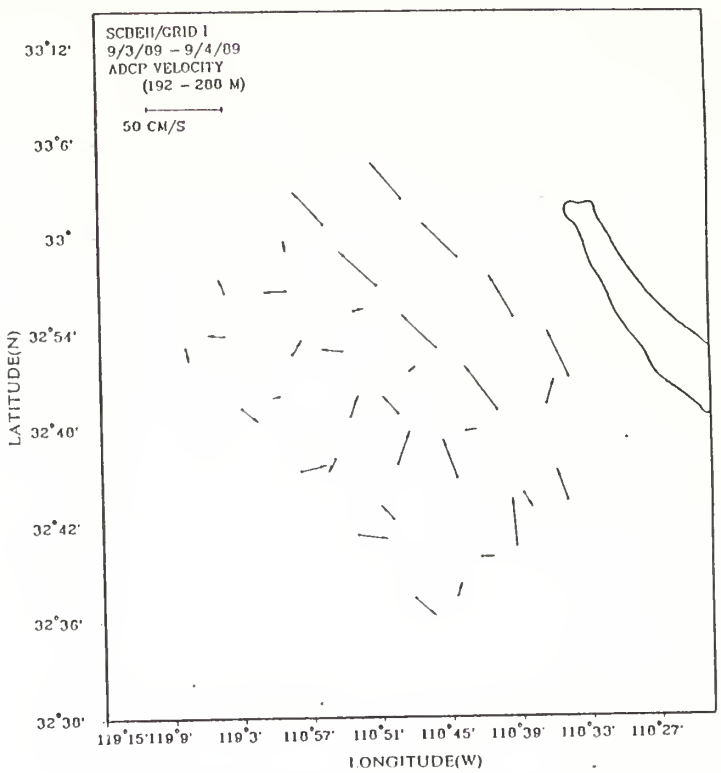

Figure 4e. Vertically averaged currents (192-208m) measured during the cruise SCBE-II (2240 UT, 3 September - 2330 UT, 4 September)

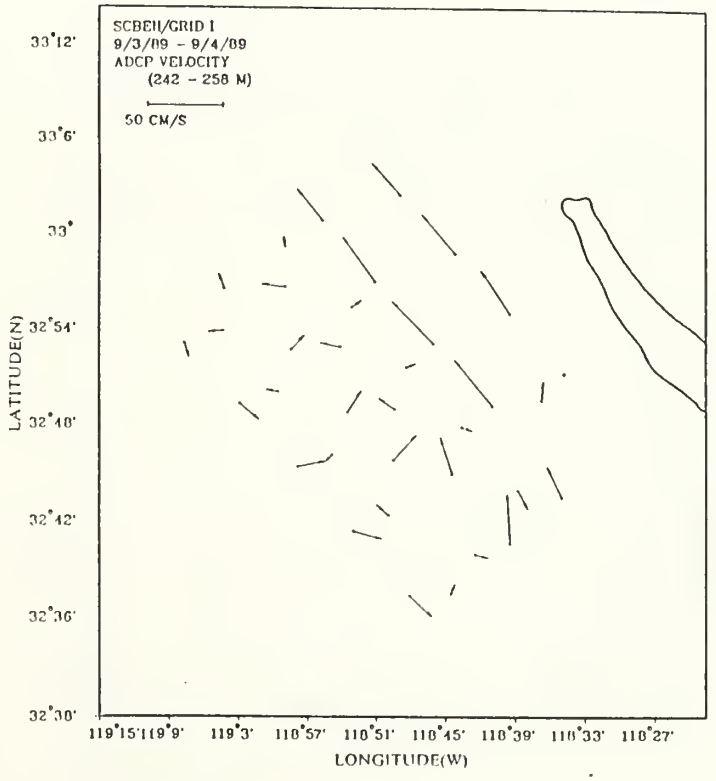

Figure 4f. Vertically averaged currents (242-258m) measured during the cruise SCBE-II (2240 UT, 3 September - 2330 UT, 4 September)

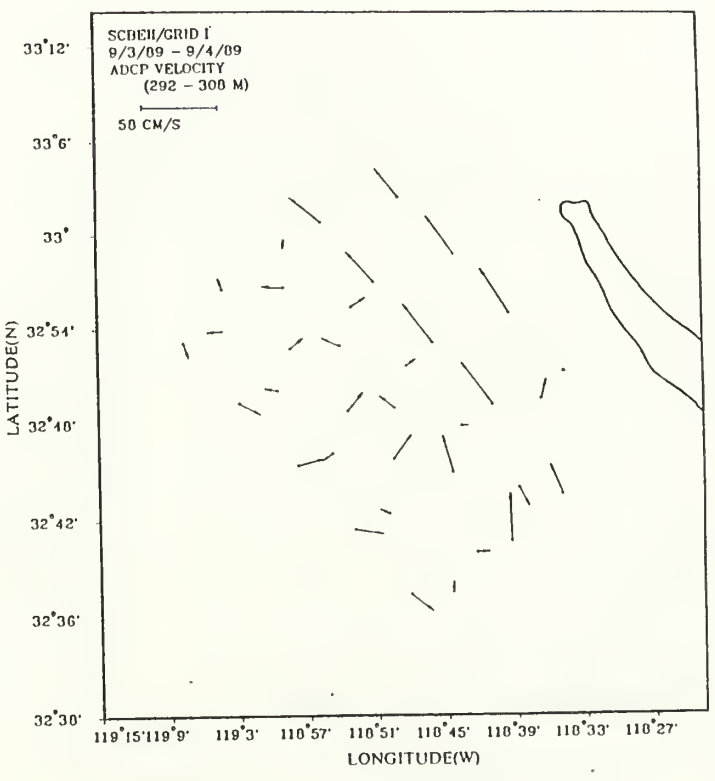

Figure 4g. Vertically averaged currents (292-308m) measured during the cruise SCBE-II (2240 UT, 3 September - 2330 UT, 4 September).

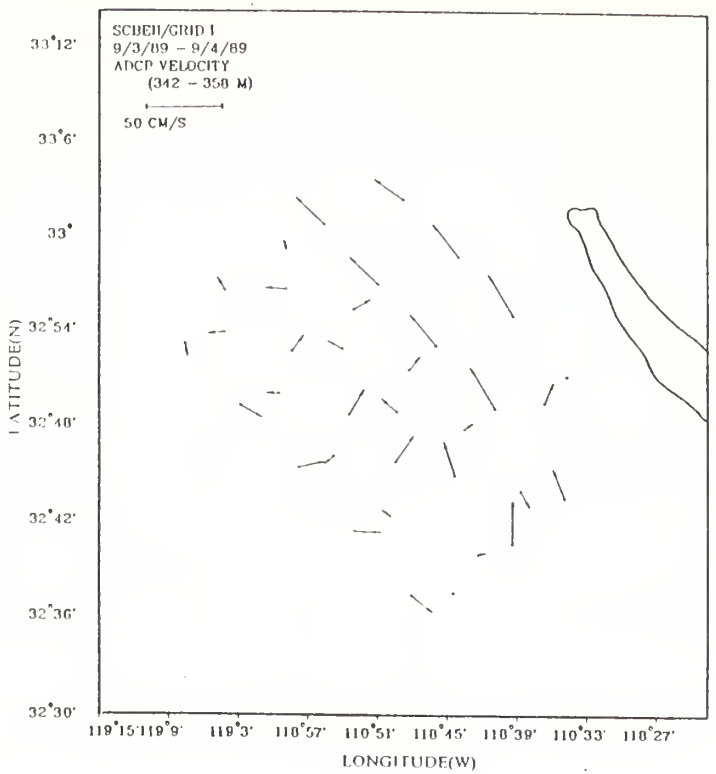

Figure 4h. Vertically averaged currents (342-358m) measured during the cruise SCBE-II (2240 UT, 3 September - 2330 UT, 4 September)

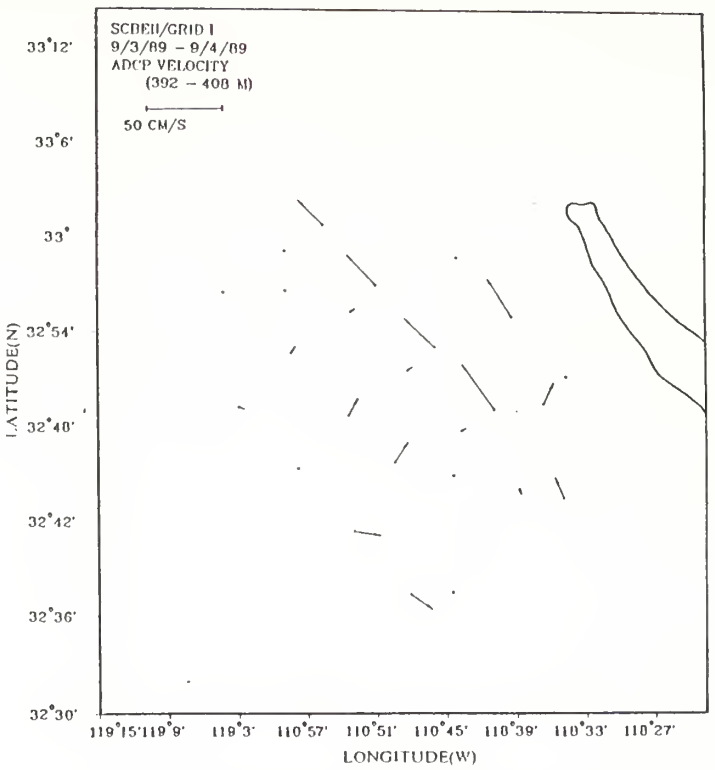

Figure 4i. Vertically averaged currents (392-408m) measured during the cruise SCBE-II (2240 UT, 3 September - 2330 UT, 4 September).

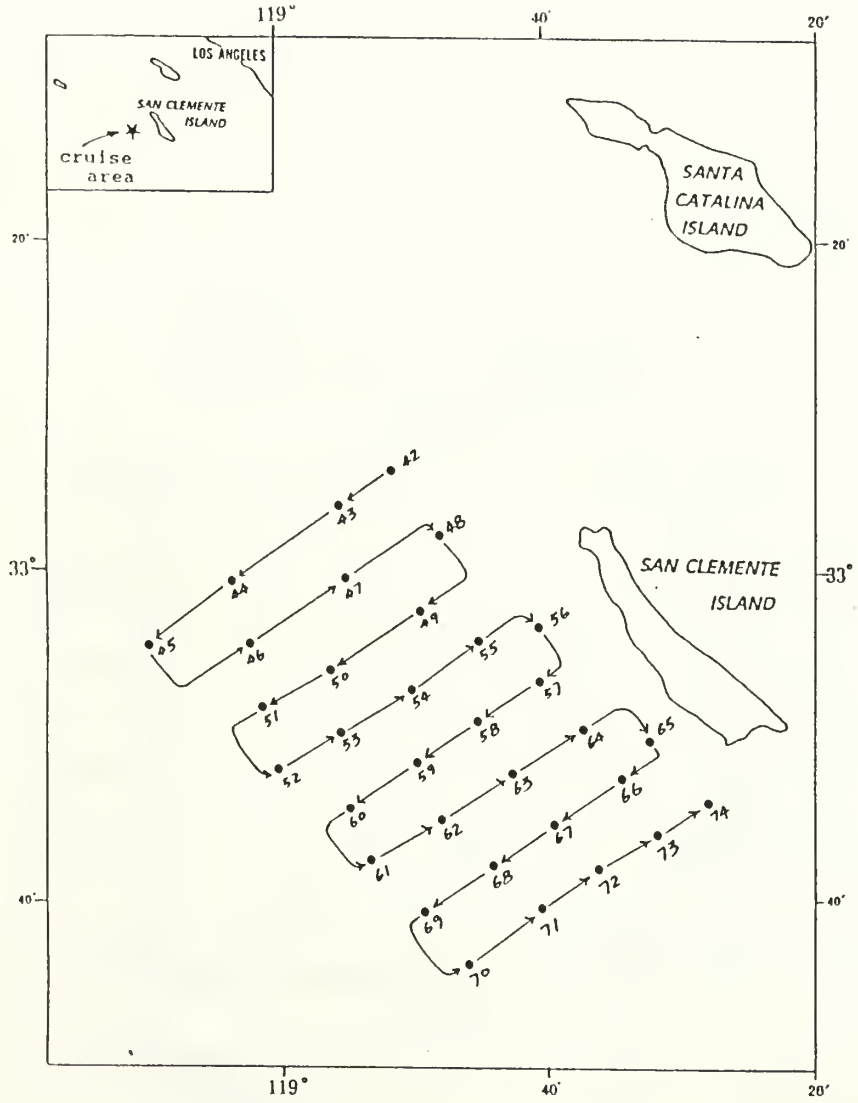

Figure 5. Cruise track followed during the second pass over the study area off San Clemente Island during the cruise SCBE-II 2-6 September, 1989. The solid circle . denotes location of XBT sounding.

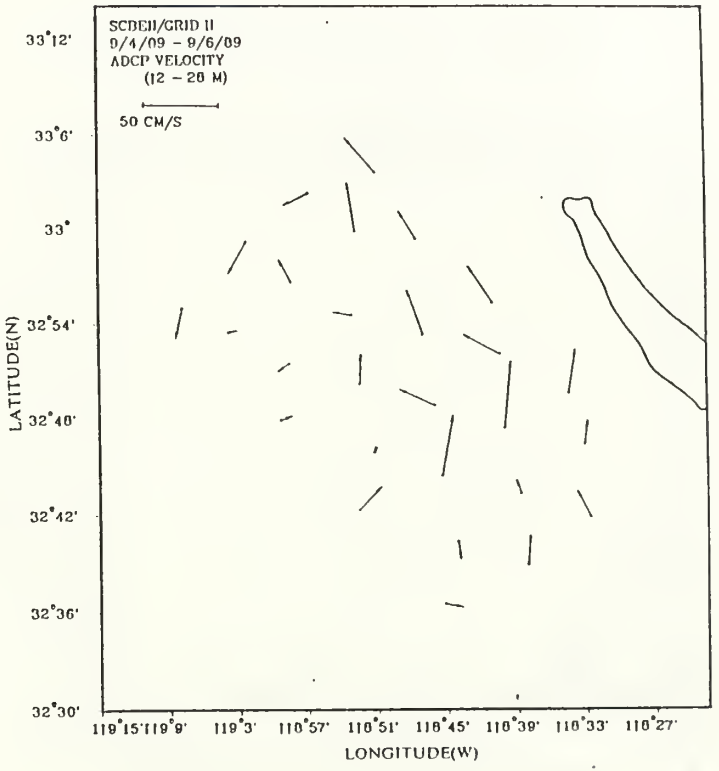

Figure 6a. Vertically averaged currents (12-28m) measured during the cruise SCBE-II (2240 UT, 4 September - 0640 UT, 6 September)

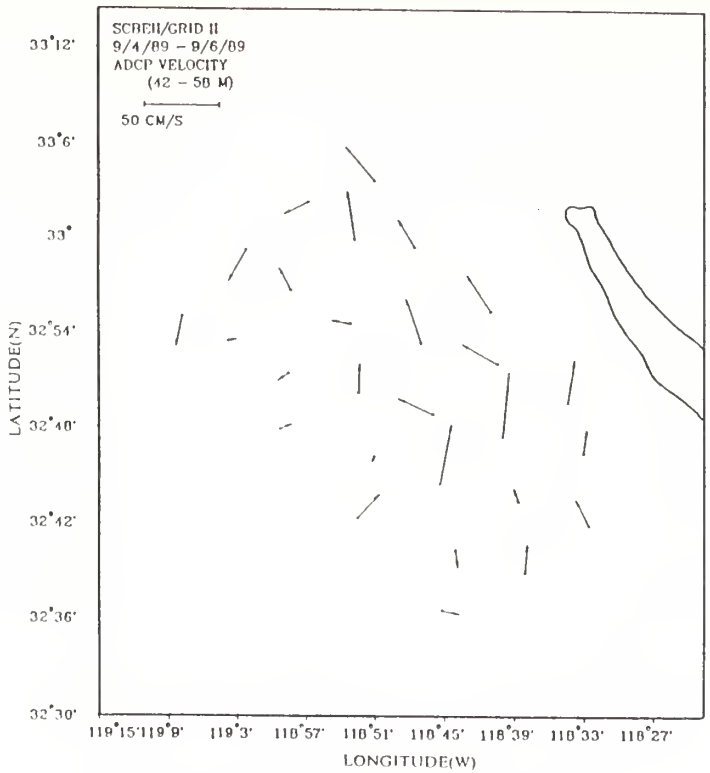

Figure 6b. Vertically averaged currents (42-58m) measured during the cruise SCBE-II (2240 UT, 4 September - 0640 UT, 6 September)

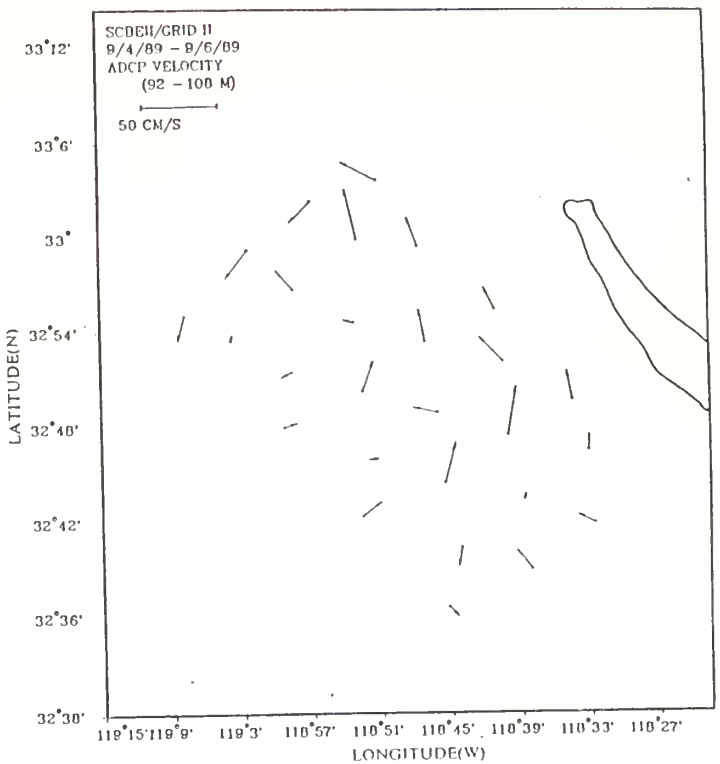

Figure 6c. Vertically averaged currents (92-108m) measured during the cruise SCBE-II (2240 UT, 4 September - 0640 UT, 6 September)

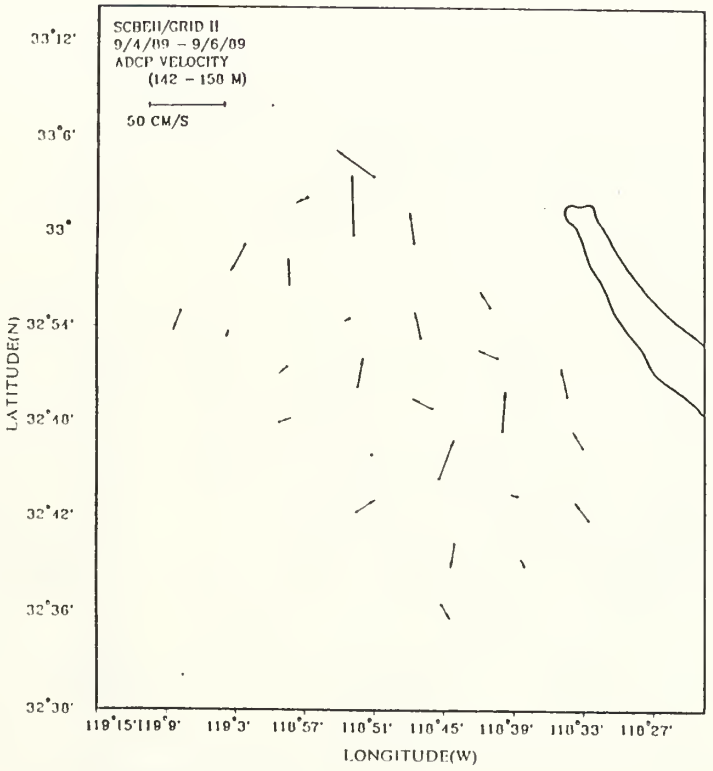

Figure 6d. Vertically averaged currents (142-158m) measured during the cruise SCBE-II (2240 UT, 4 September - 0640 UT, 6 September)

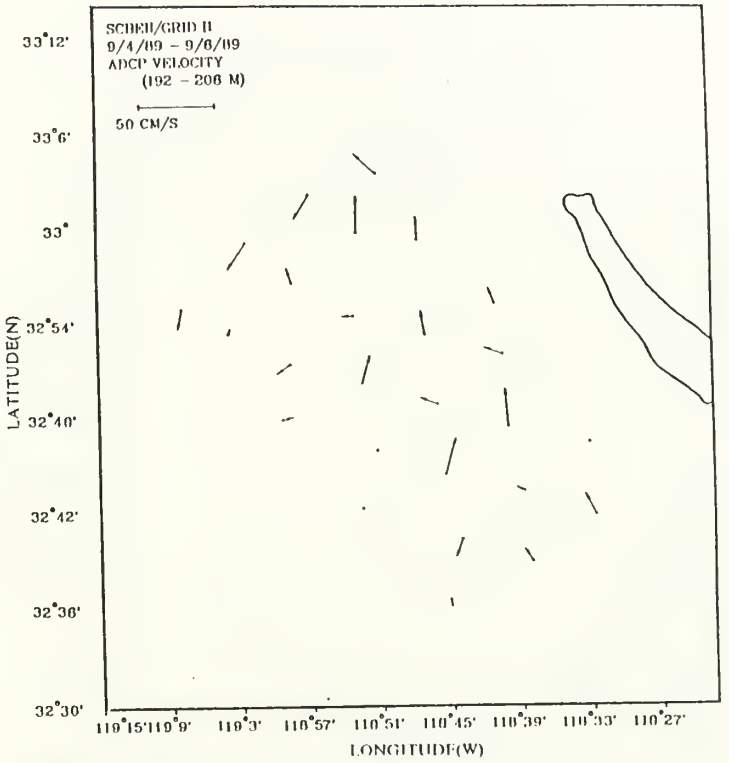

Figure 6e. Vertically averaged currents (192-208m) measured during the cruise SCBE-II (2240 UT, 4 September - 0640 UT, 6 September).

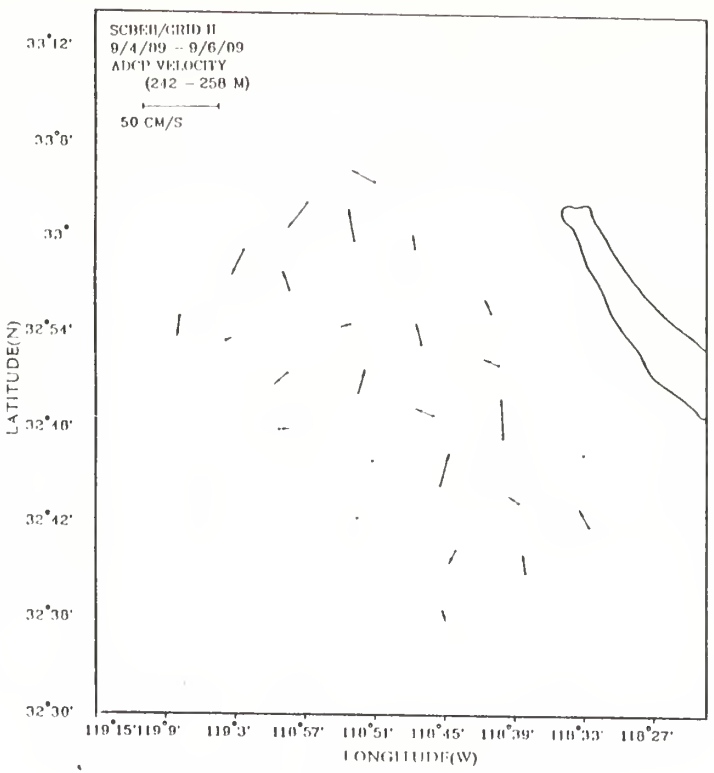

Figure 6f. Vertically averaged currents (242-258m) measured during the cruise SCBE-II (2240 UT, 4 September - 0640 UT, 6 September).

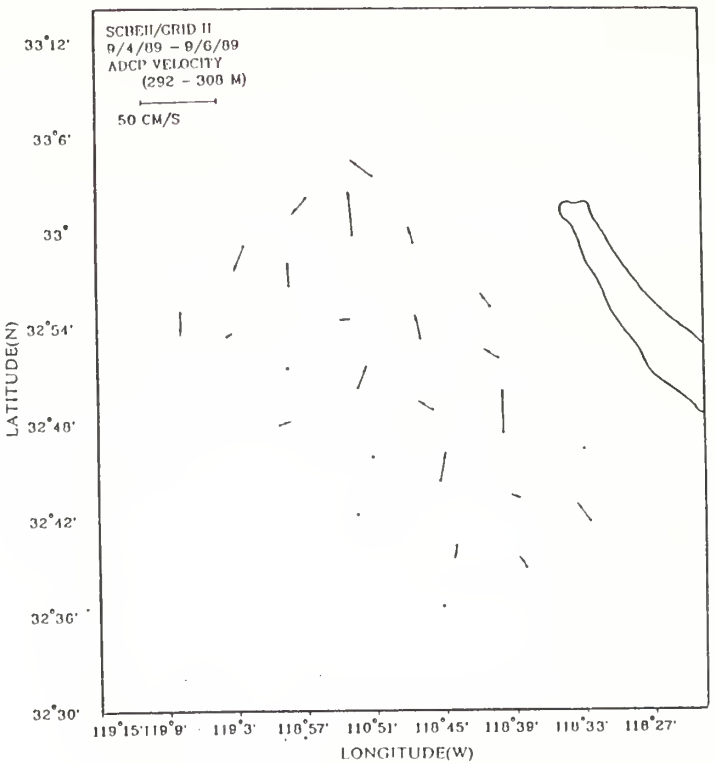

Figure 6g. Vertically averaged currents (292-308m) measured during the cruise SCBE-II (2240 UT, 4 September - 0640 UT, 6 September).

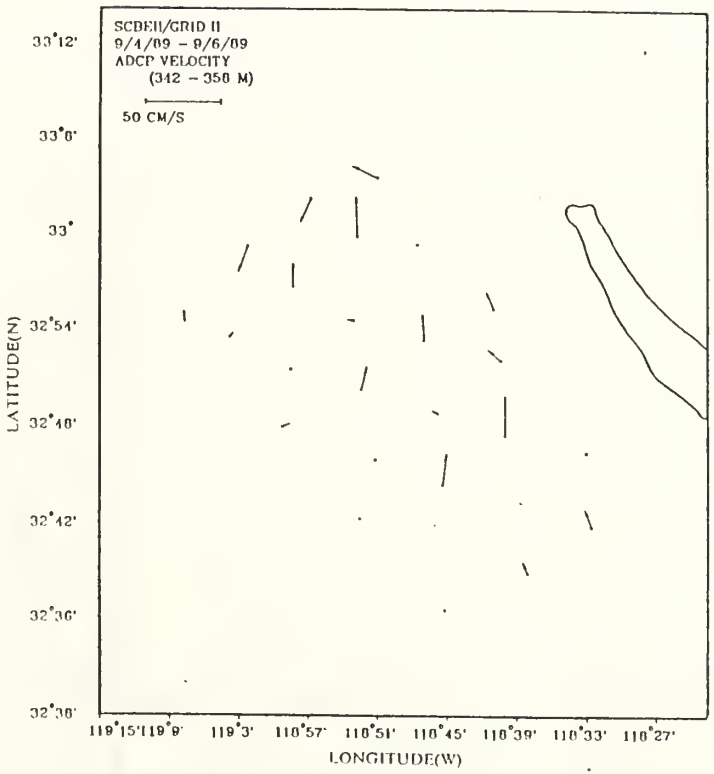

Figure 6h. Vertically averaged currents (342-358m) measured during the cruise SCBE-II (2240 UT, 4 September - 0640 UT, 6 September).

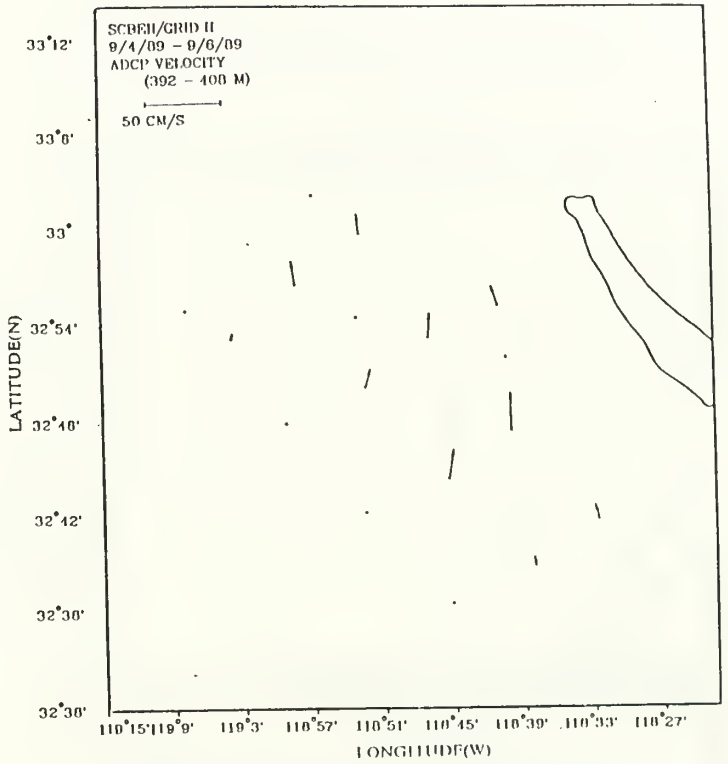

Figure 6i. Vertically averaged currents (392-408m) measured during the cruise SCBE-II (2240 UT, 4 September - 0640 UT, 6 September).

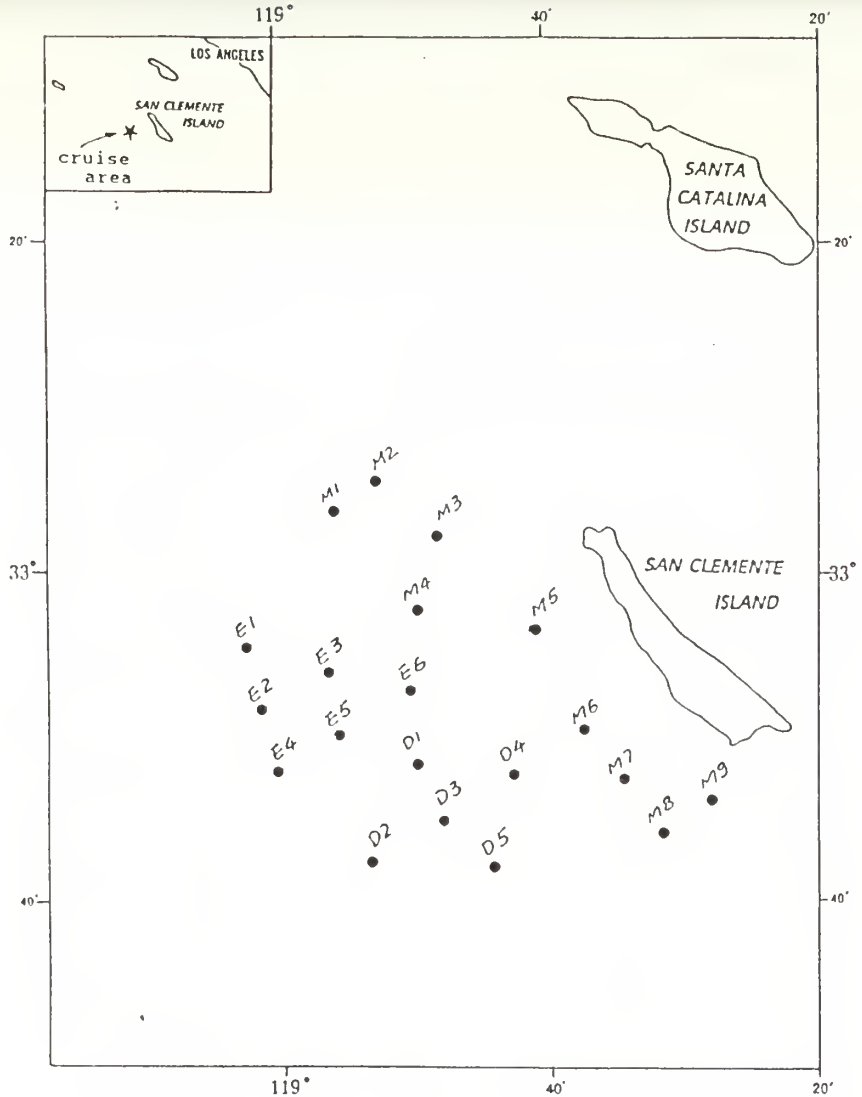

Figure 7. Distribution of locations at which a vertical profile of currents measured by the ADCP is presented in following figures.

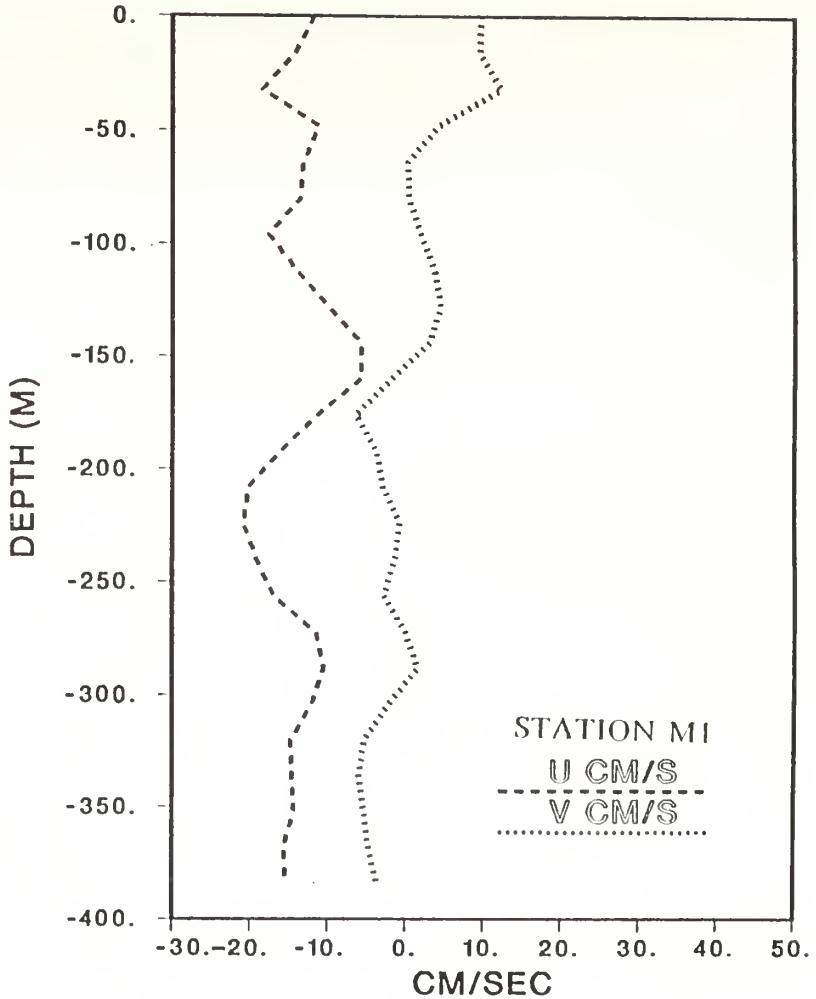

Figure 8a. Vertical profiles of currents (u,v) at M1 in figure 7.

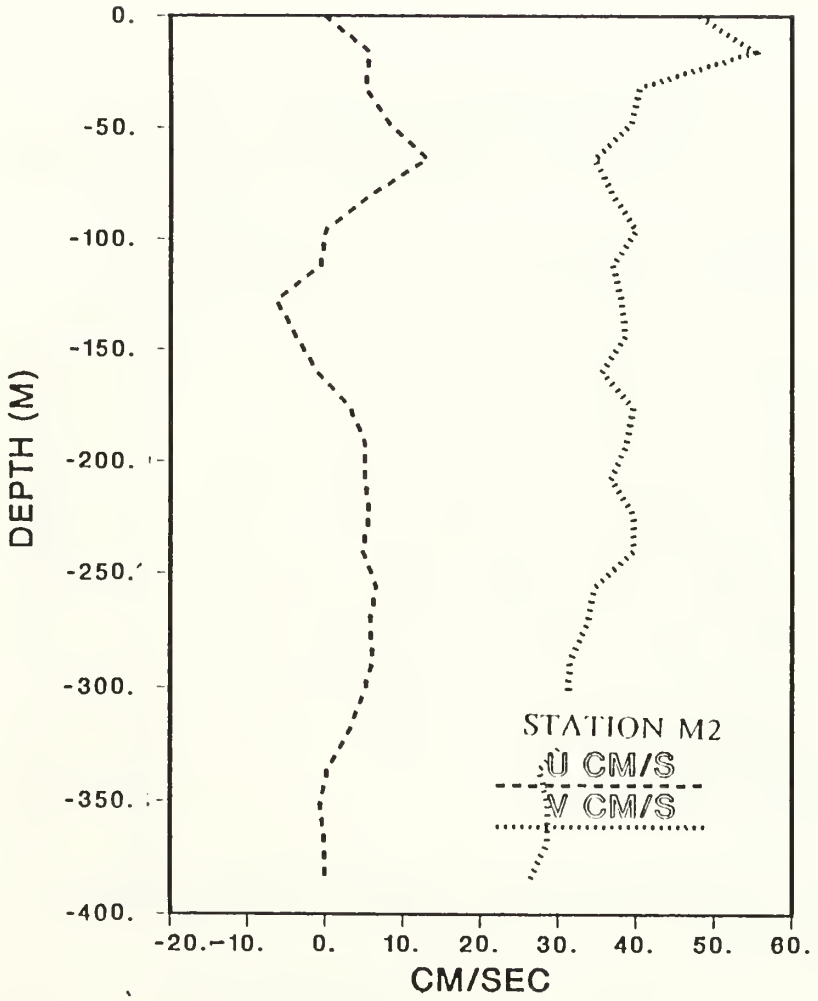

Figure 8b. Vertical profiles of currents (u,v) at M2 in figure 7.

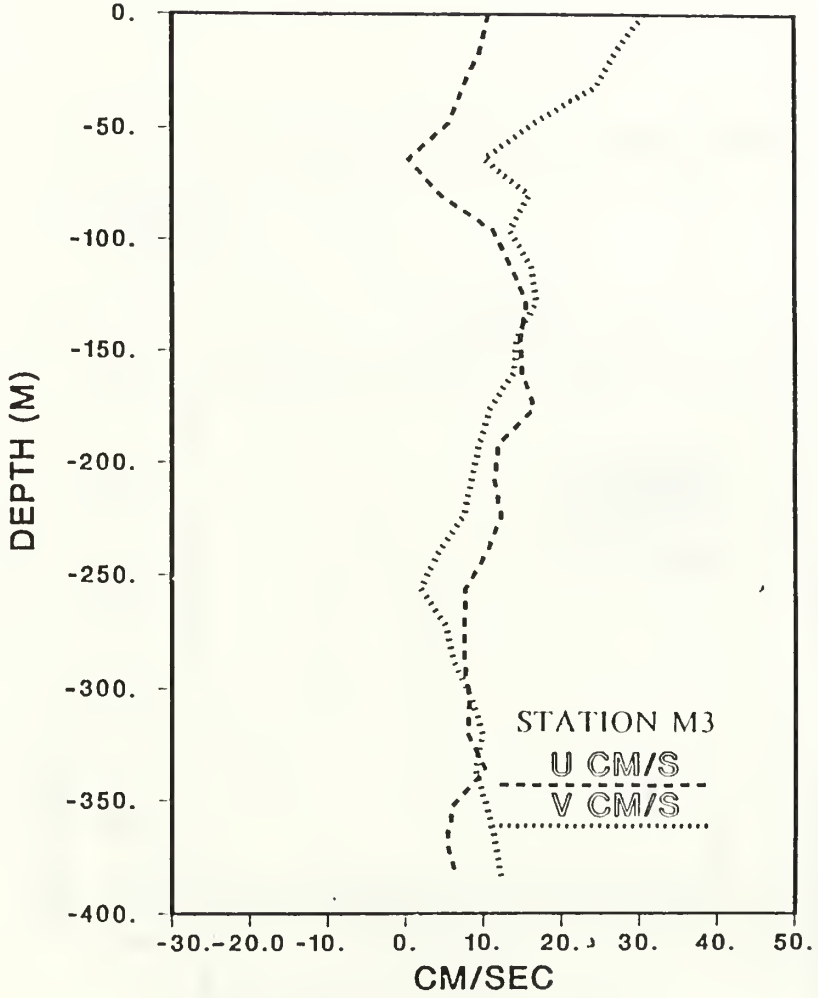

Figure 8c. Vertical profiles of currents (u,v) at M3 in figure 7.

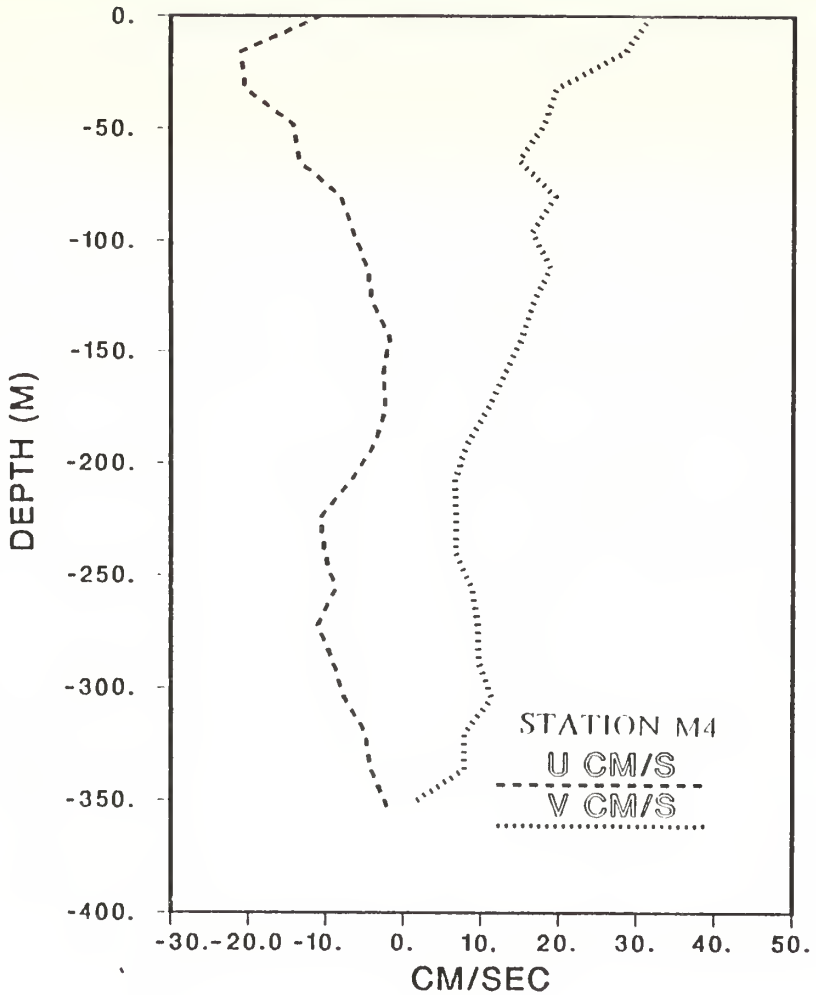

Figure 8d. Vertical profiles of currents (u,v) at M4 in figure 7.

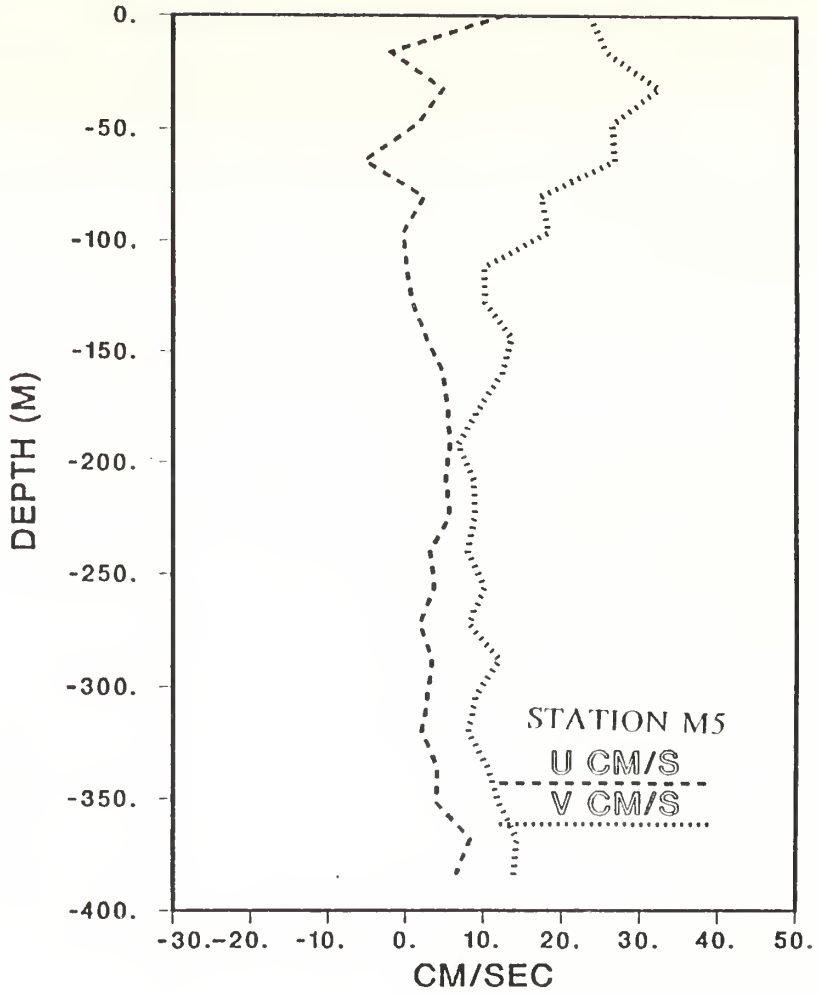

Figure 8e. Vertical profiles of currents (u,v) at M5 in figure 7.

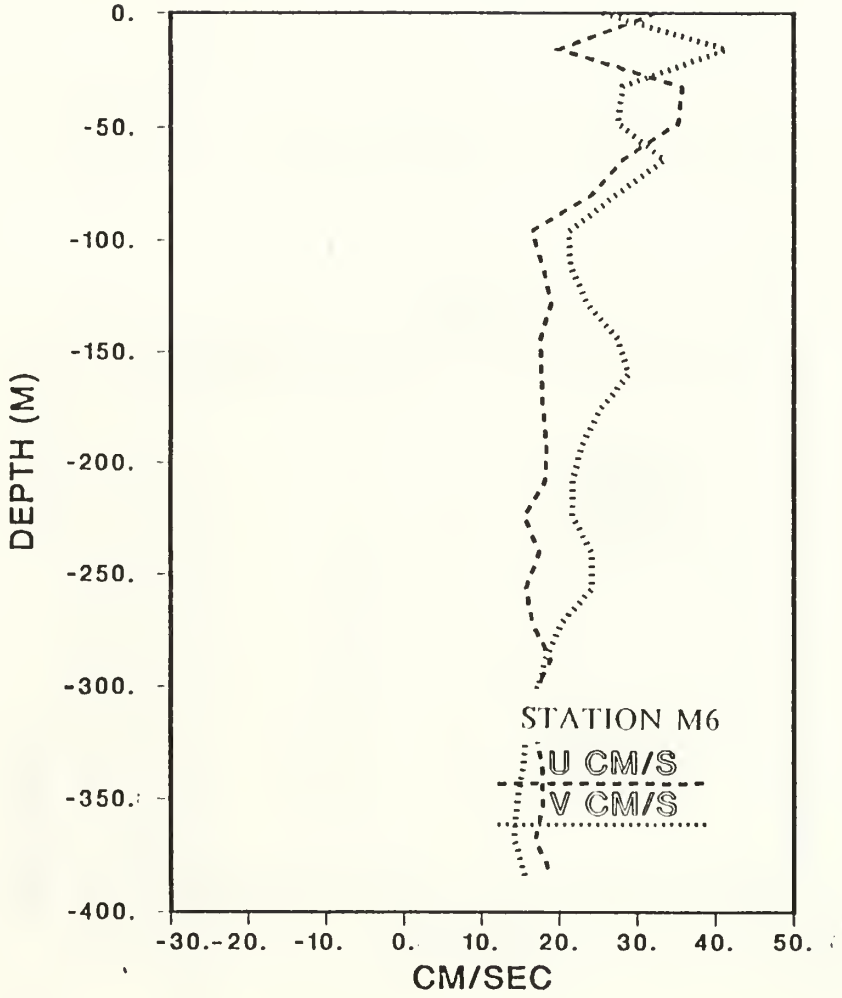

Figure 8f. Vertical profiles of currents (u,v) at M6 in figure 7.

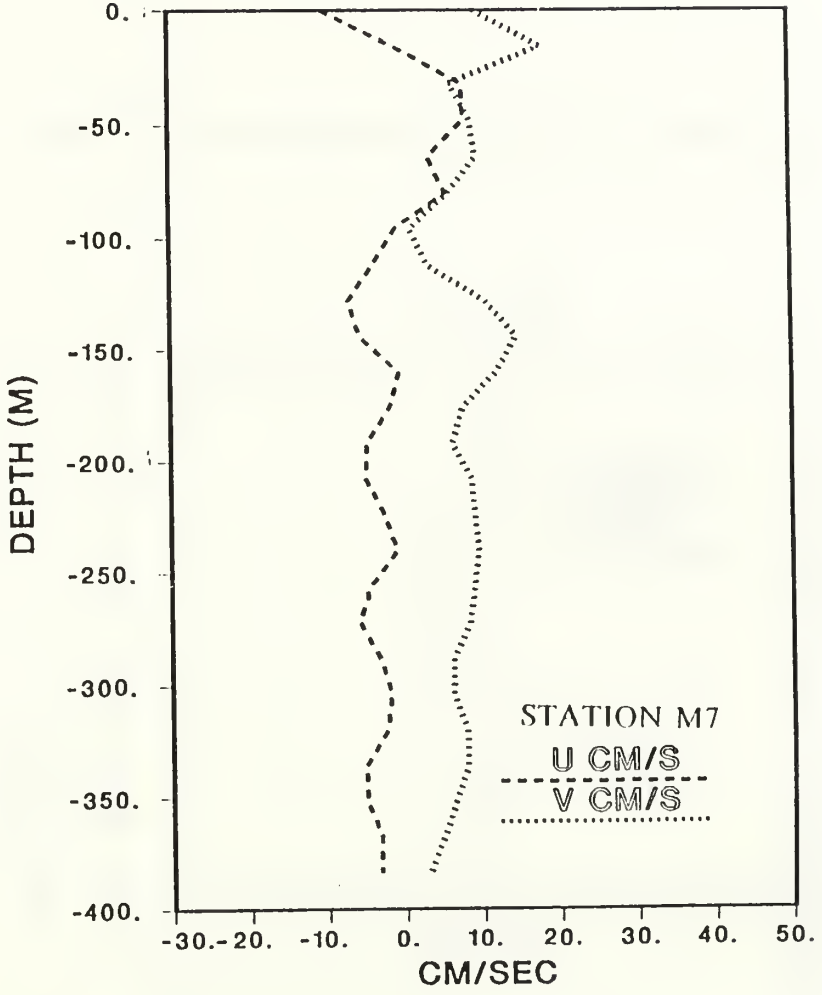

Figure 8g. Vertical profiles of currents (u,v) at M7 in figure 7.

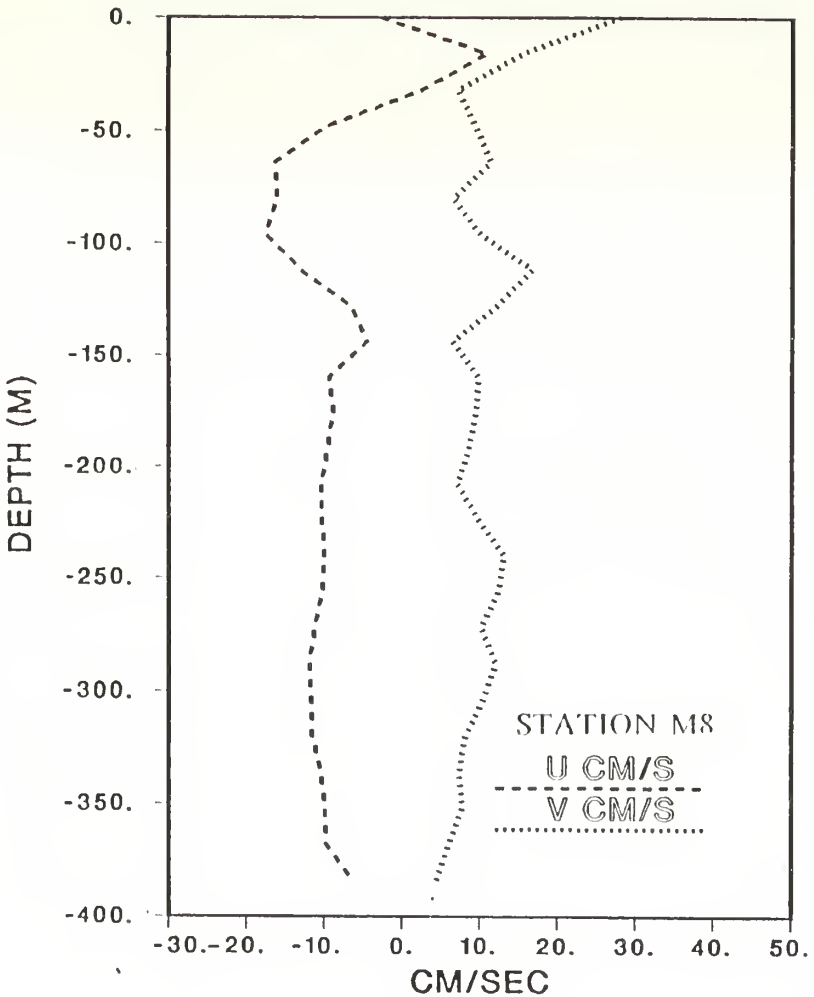

Figure 8h. Vertical profiles of currents (u,v) at M8 in figure 7.

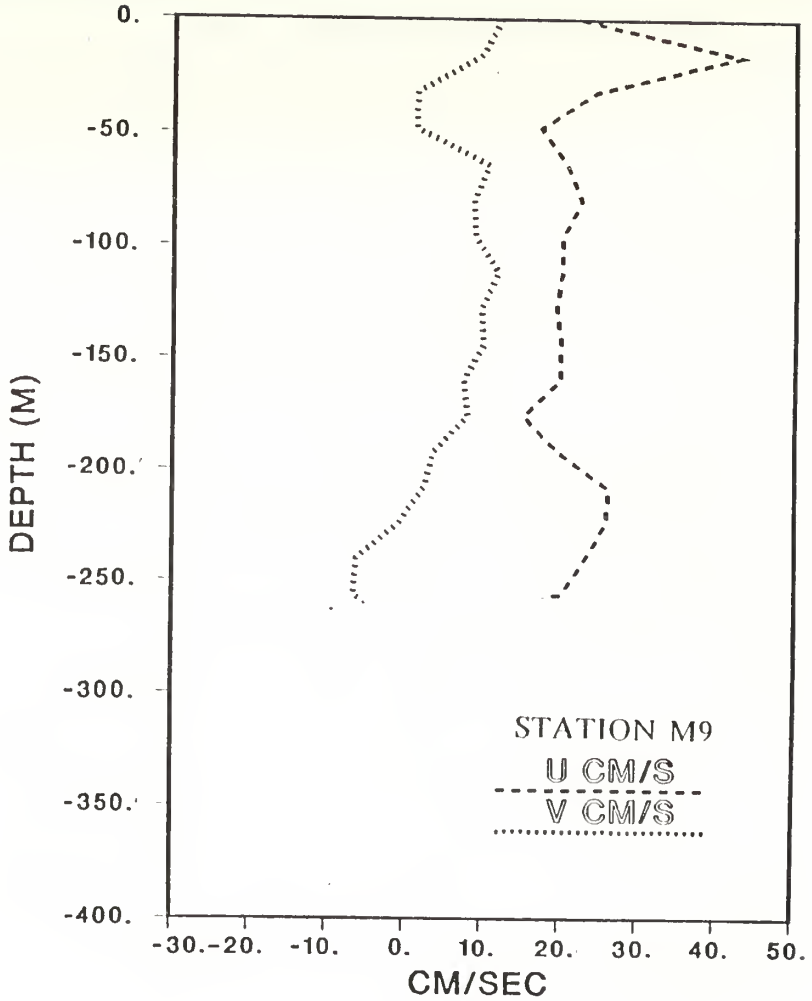

Figure 8i. Vertical profiles of currents (u,v) at M9 in figure 7.

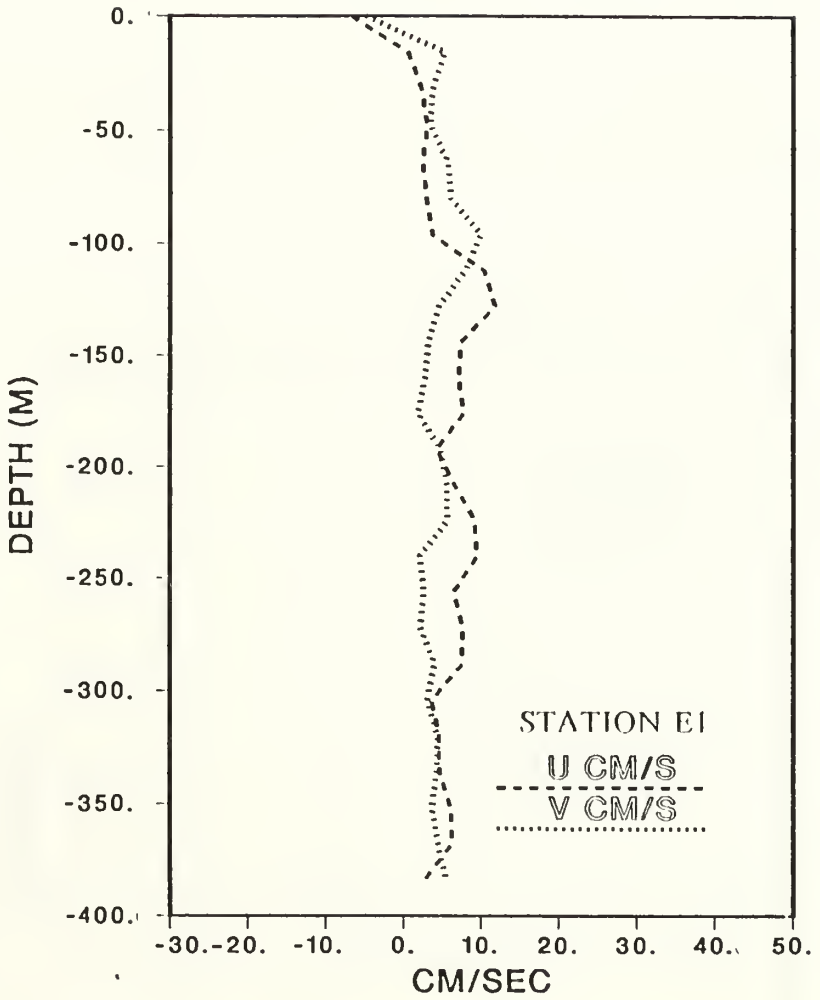

Figure 8j. Vertical profiles of currents (u,v) at E1 in figure 7.

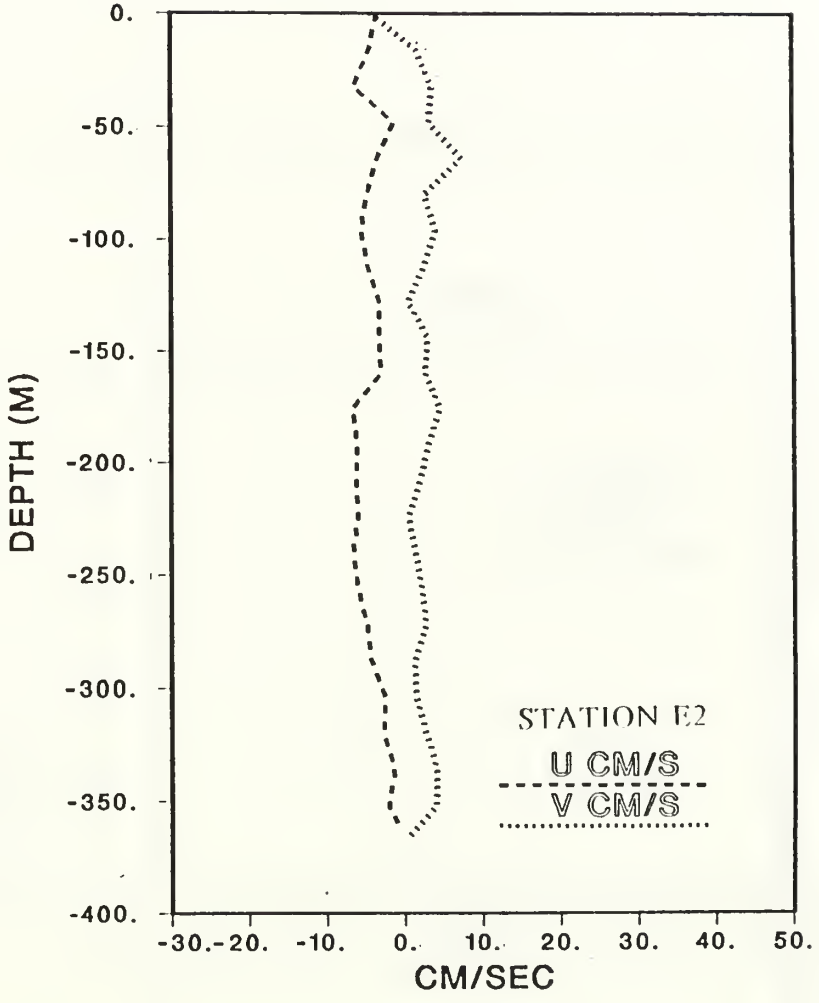

Figure 8k. Vertical profiles of currents (u,v) at E2 in figure 7.

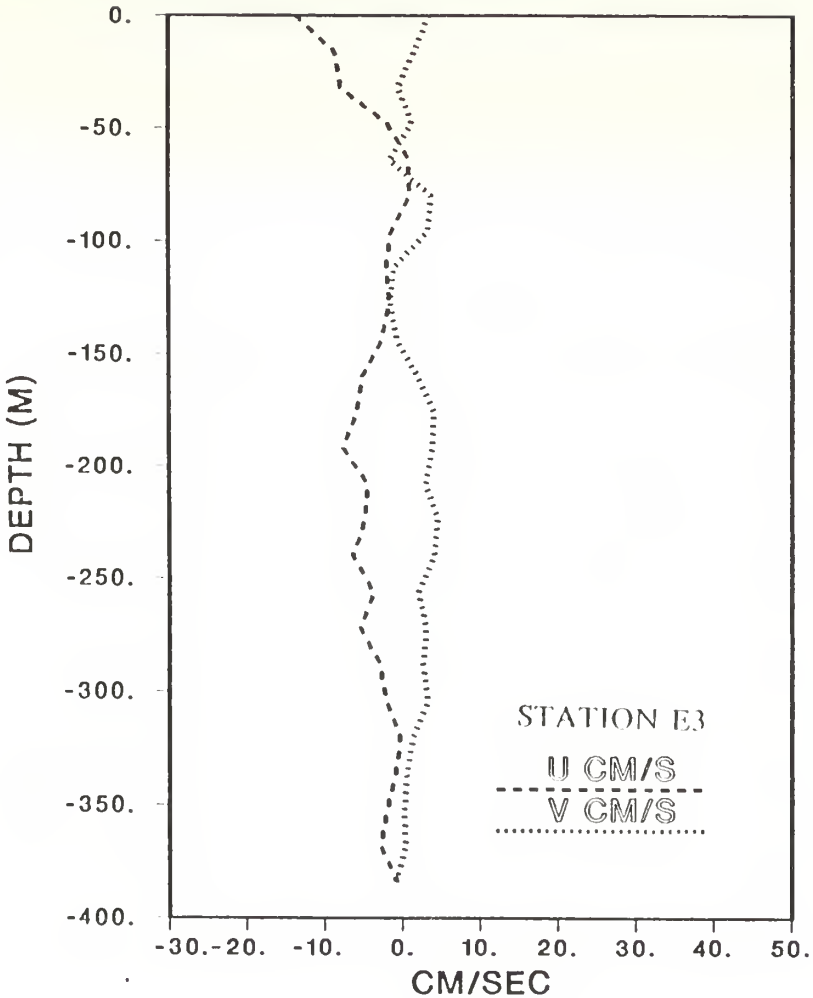

Figure 8l. Vertical profiles of currents (u,v) at E3 in figure 7.

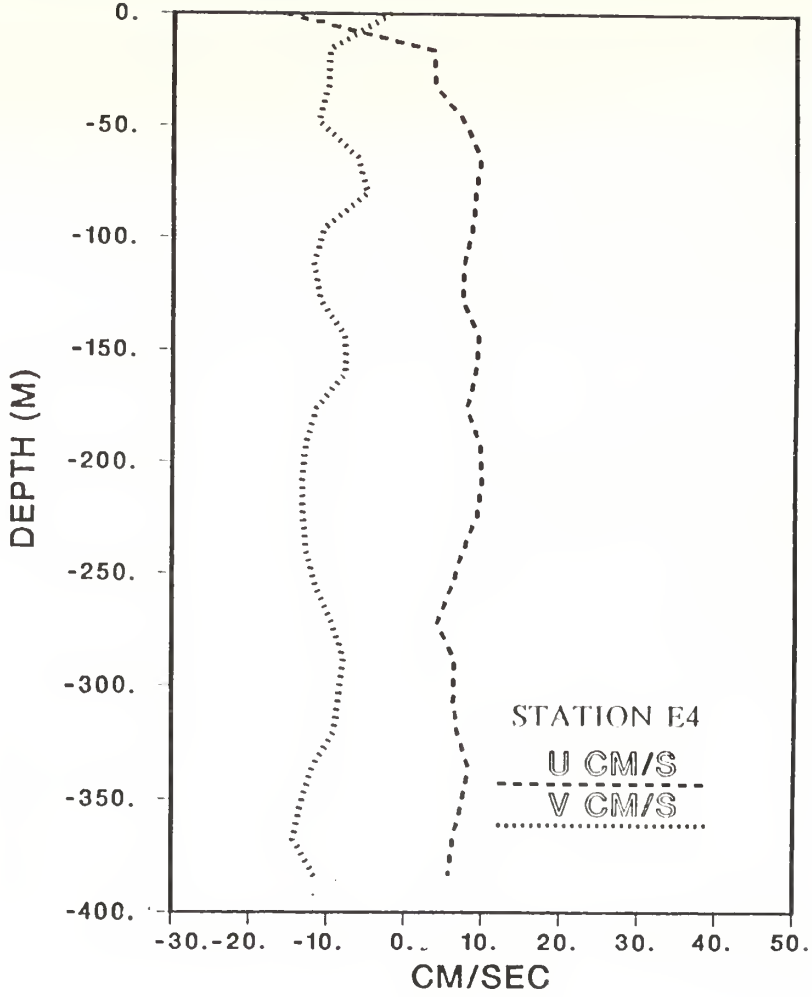

Figure 8m. Vertical profiles of currents (u,v) at E4 in figure 7.

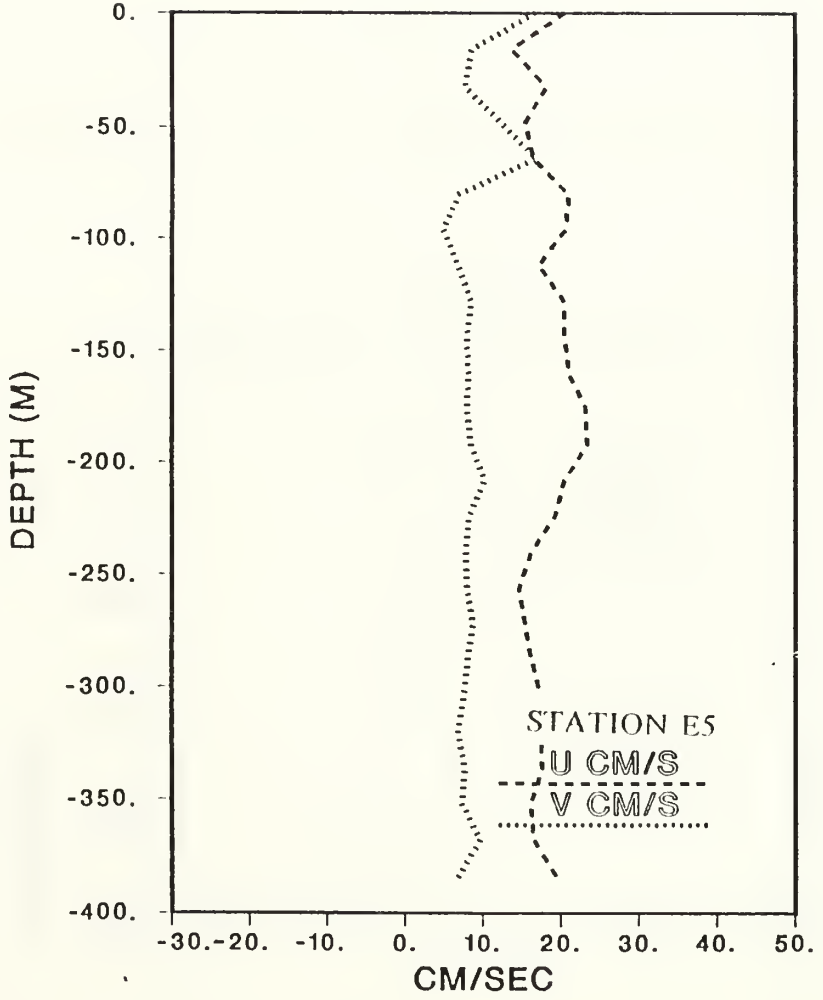

Figure 8n. Vertical profiles of currents (u,v) at E5 in figure 7.

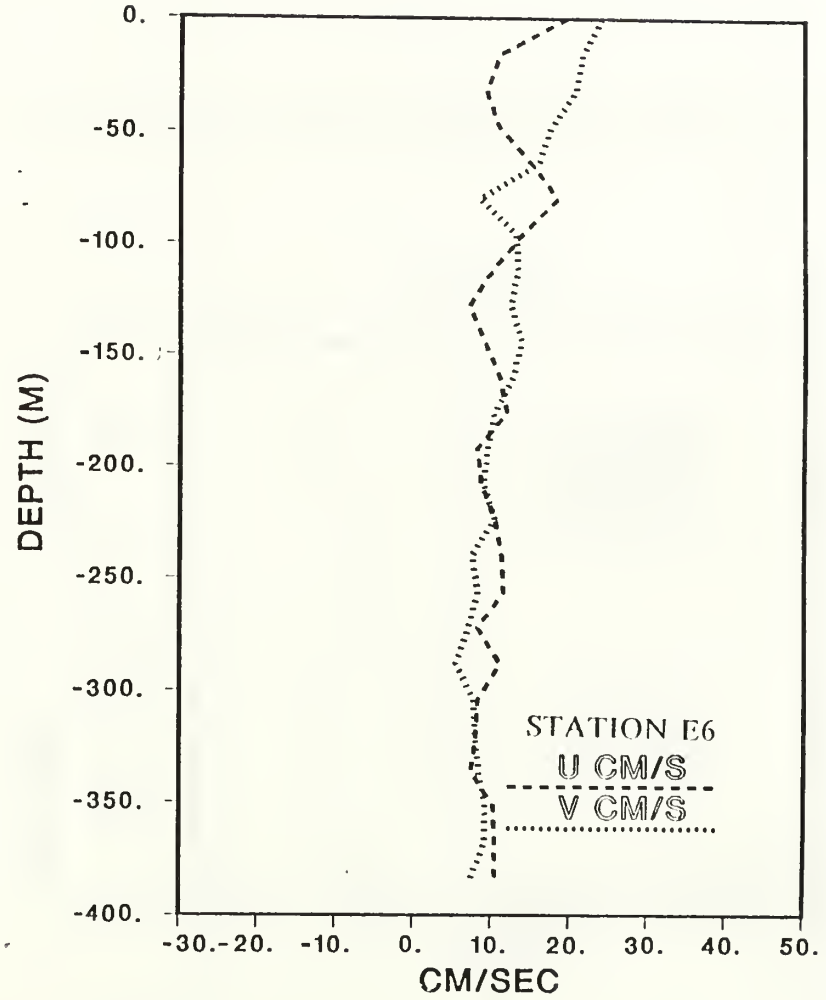

Figure 8o. Vertical profiles of currents (u,v) at E6 in figure 7.

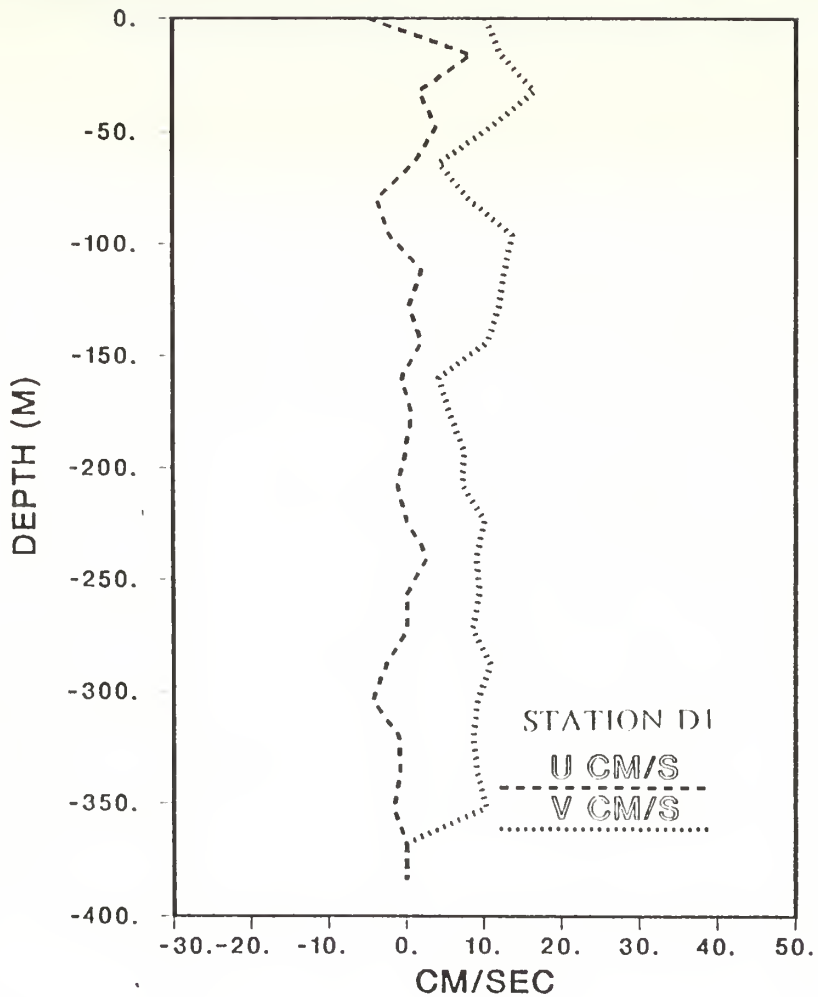

Figure 8p. Vertical profiles of currents (u,v) at D1 in figure 7.

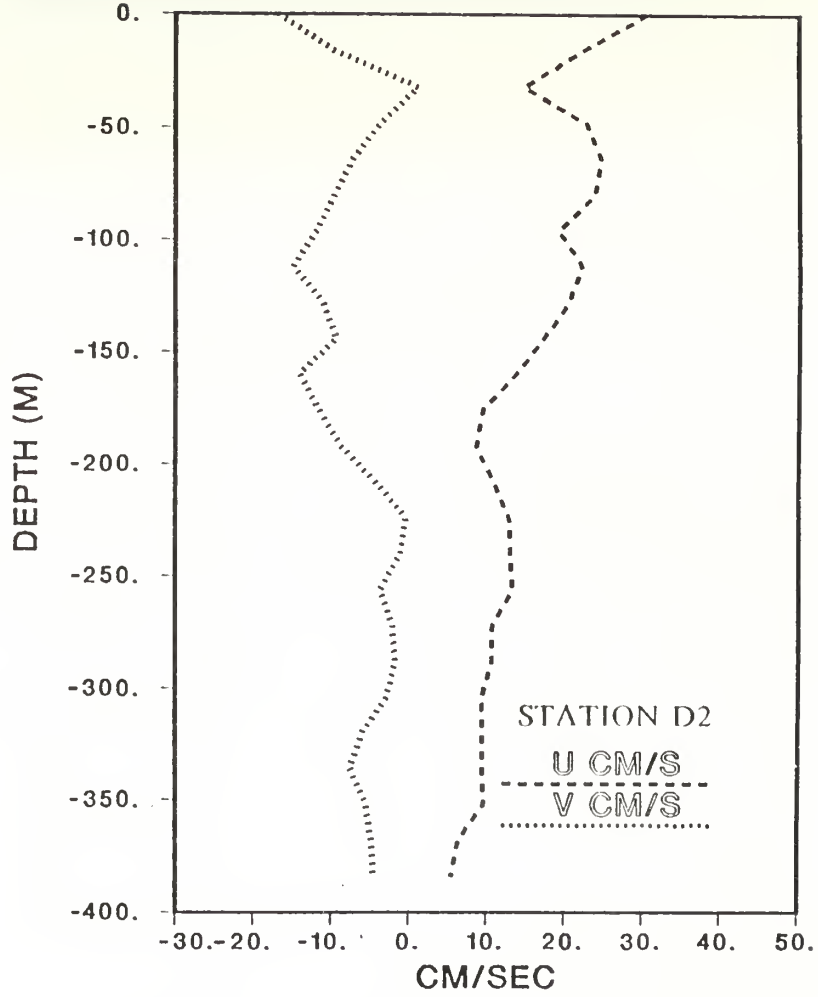

Figure 8q. Vertical profiles of currents (u,v) at D2 in figure 7.

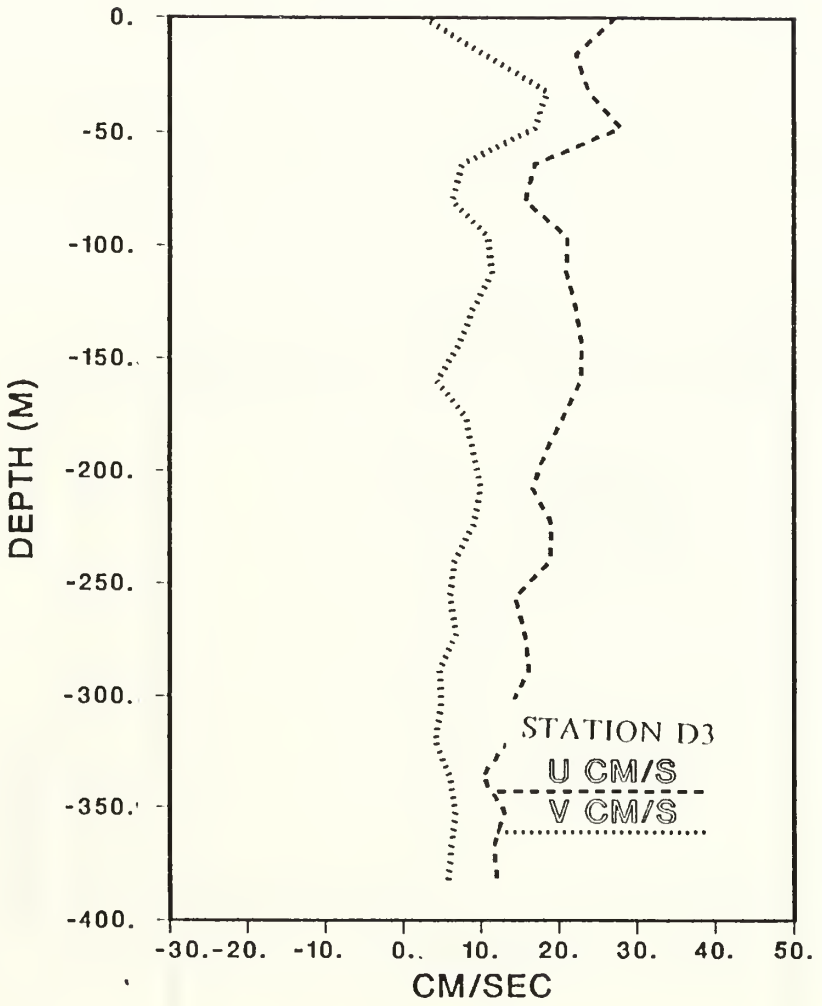

Figure 8r. Vertical profiles of currents (u,v) at D3 in figure 7.

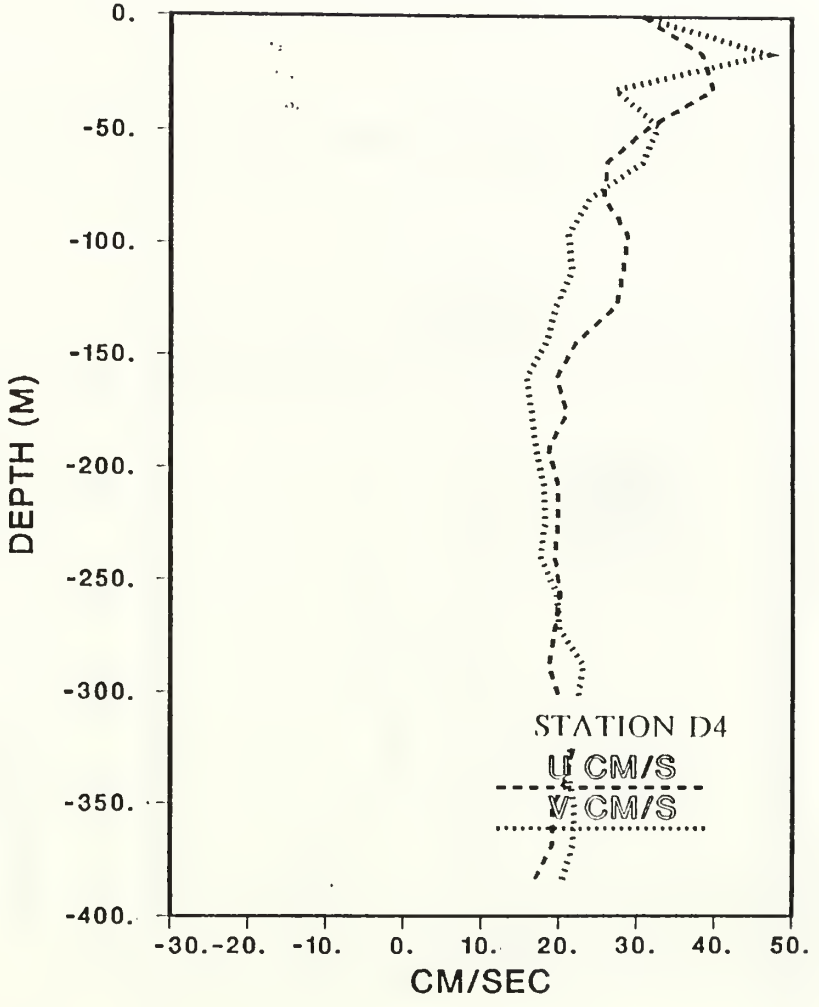

Figure 8s. Vertical profiles of currents (u,v) at D4 in figure 7.

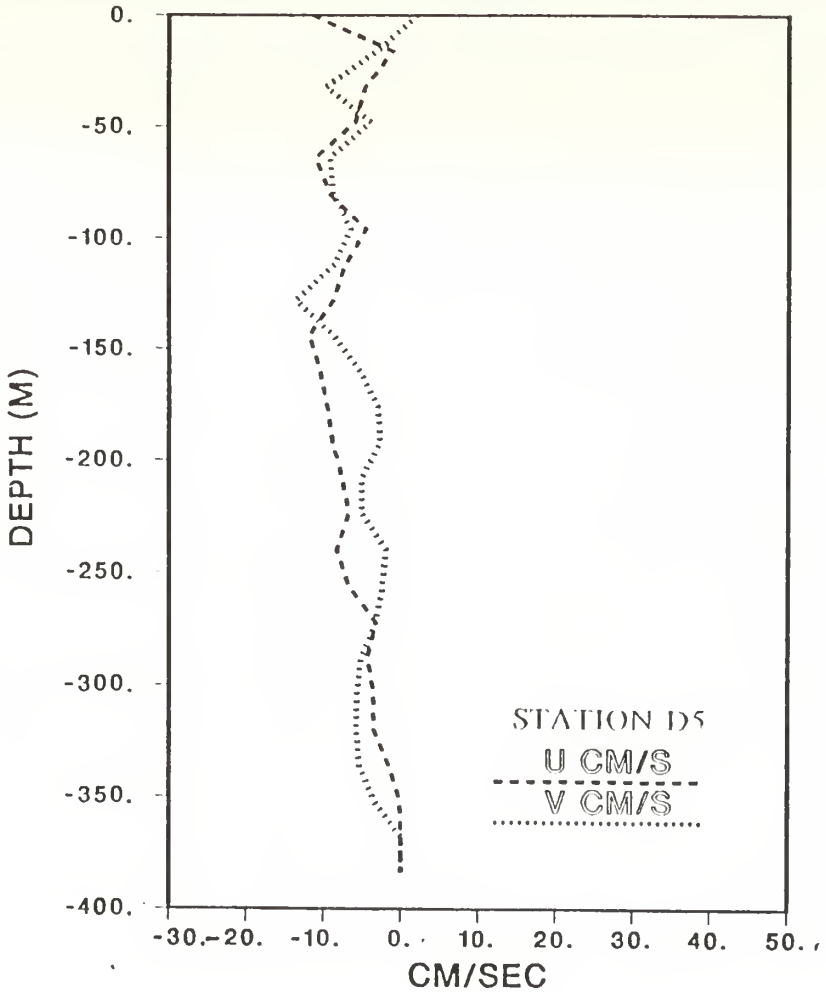

Figure 8t. Vertical profiles of currents (u,v) at D5 in figure 7.

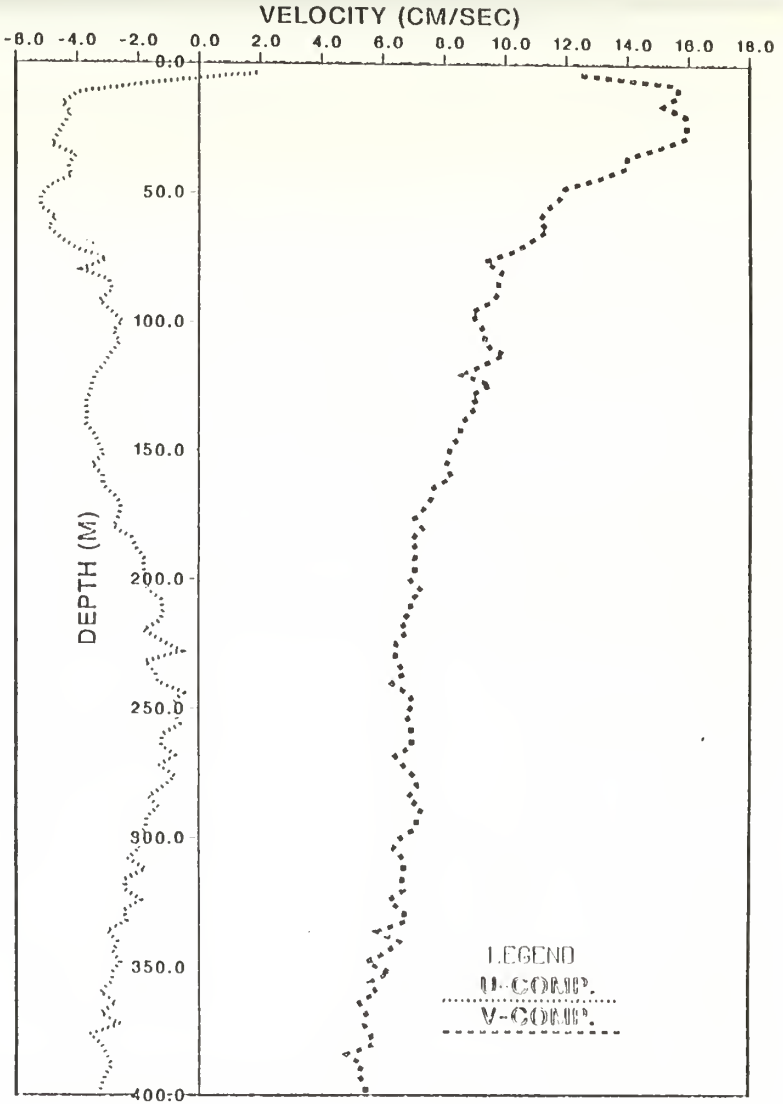

Figure 8u. Mean vertical profiles of currents (u,v) at study area given in figure 5.

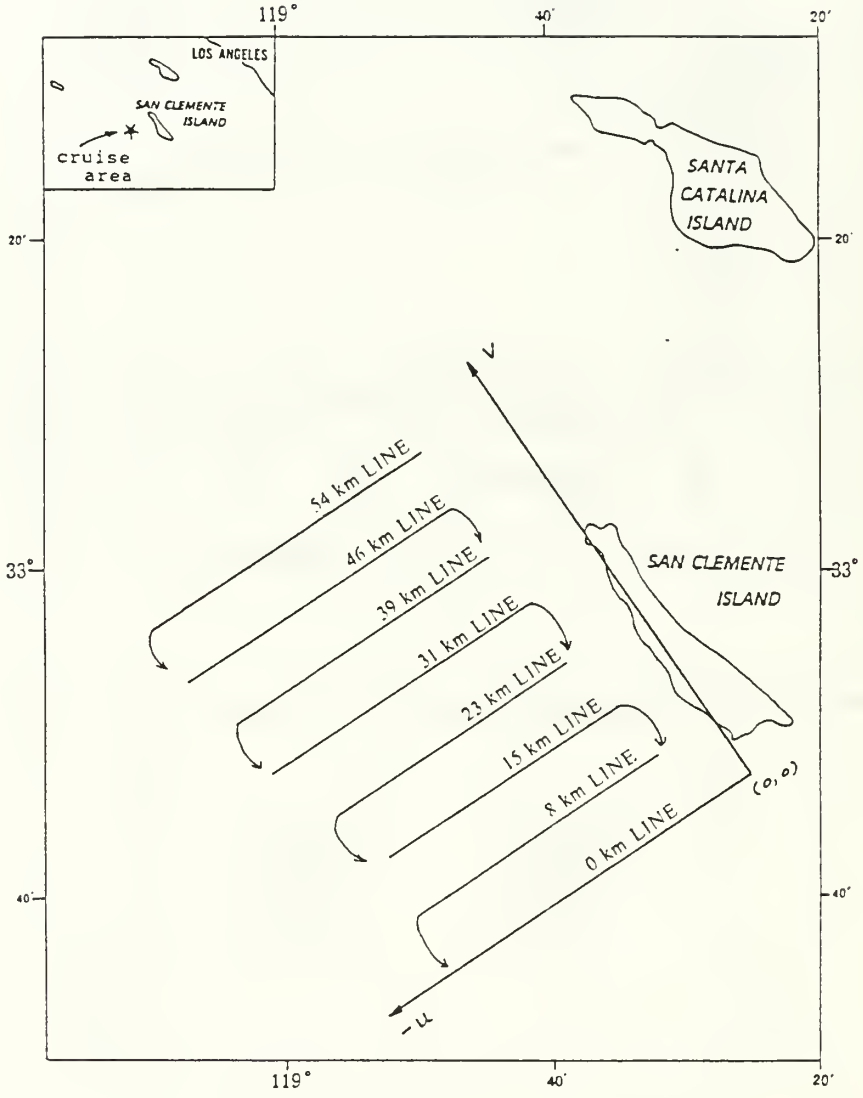

Figure 9. Coordinate system and primary cruise lines along which most shipboard current measurements were made.

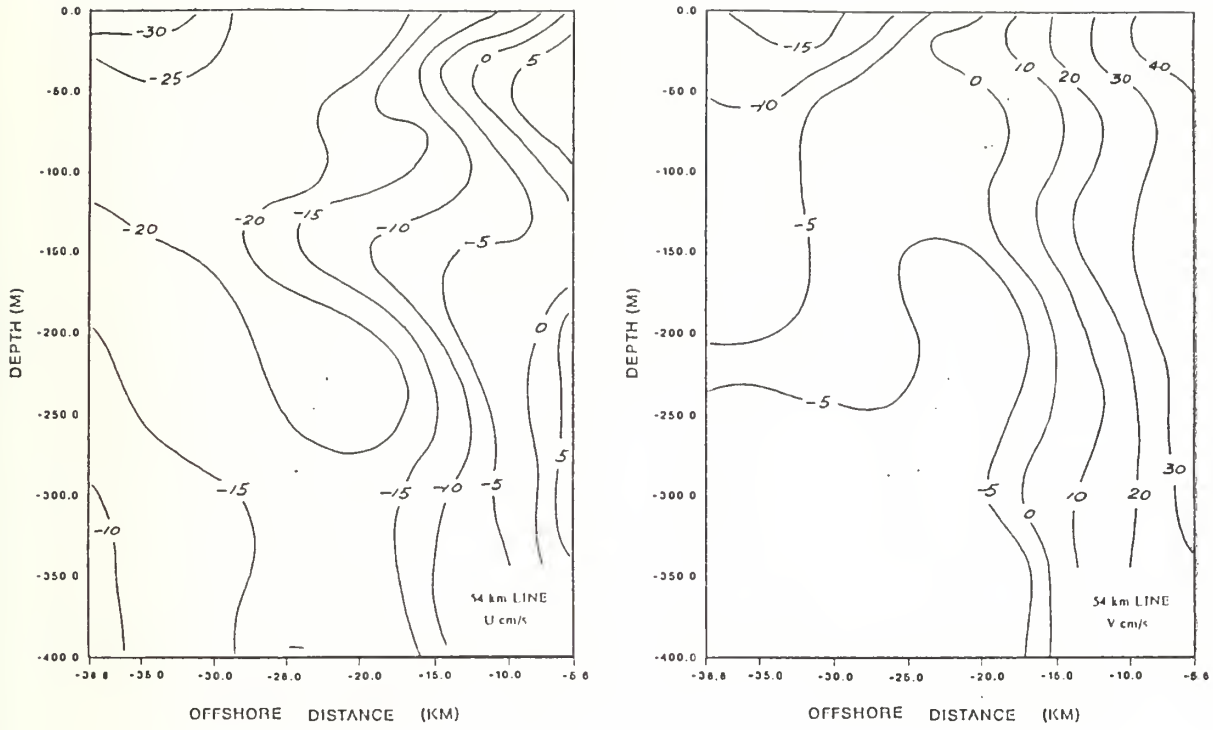

Figure 10a. Vertical cross-section of onshore and alongshore current components at the 54 km line in figure 9.

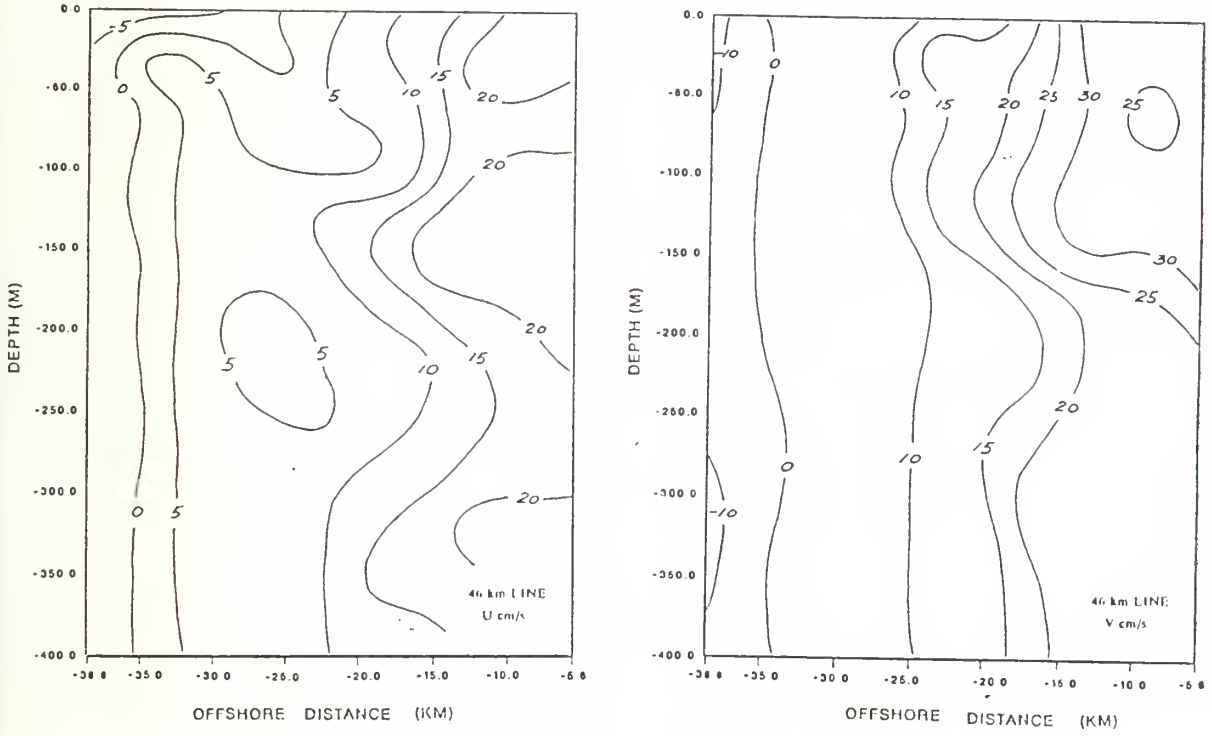

Figure 10b. Vertical cross-section of onshore and alongshore current components at the 46 km line in figure 9

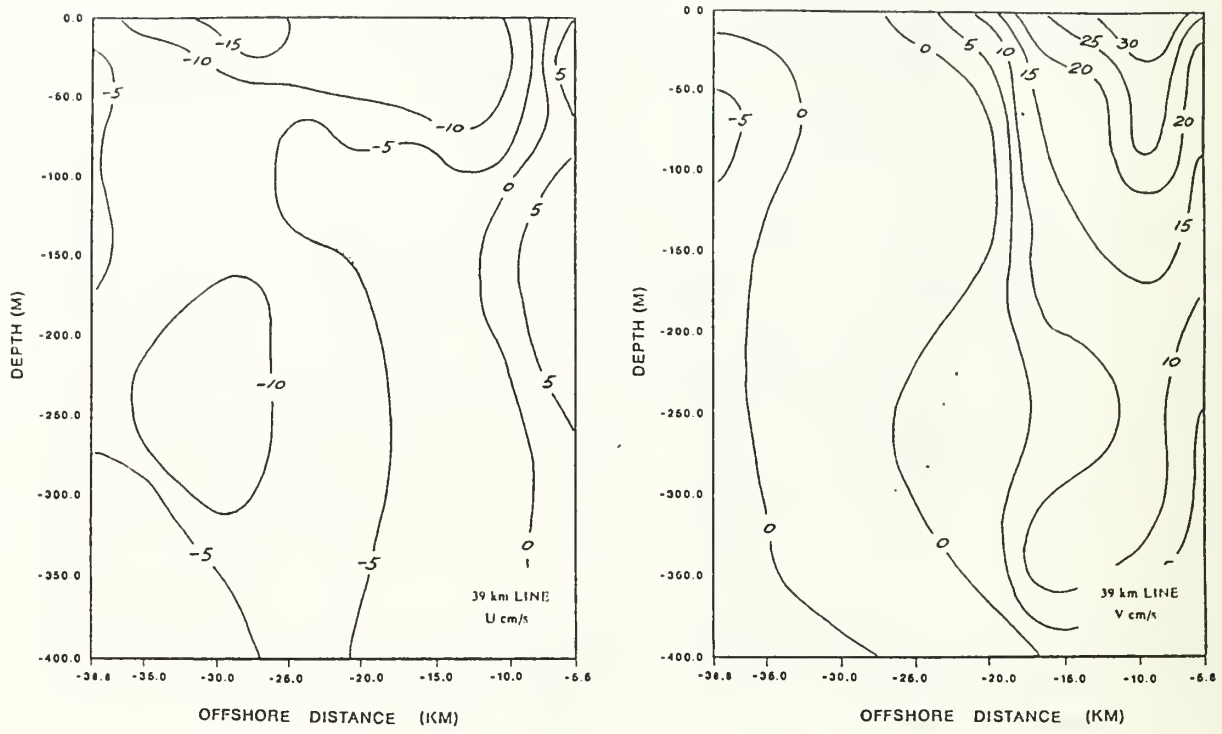

Figure 10c. Vertical cross-section of onshore and alongshore current components at the 39 km line in figure 9.

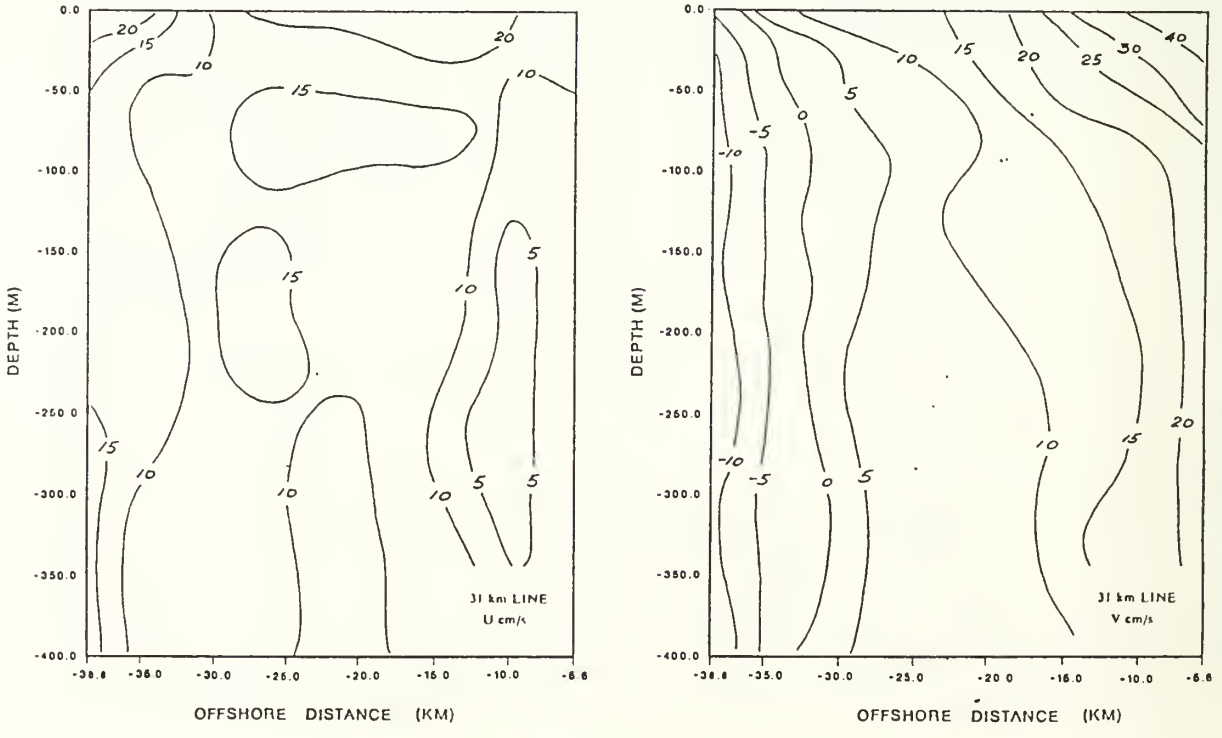

Figure 10d. Vertical cross-section of onshore and alongshore current components at the 31 km line in figure 9.

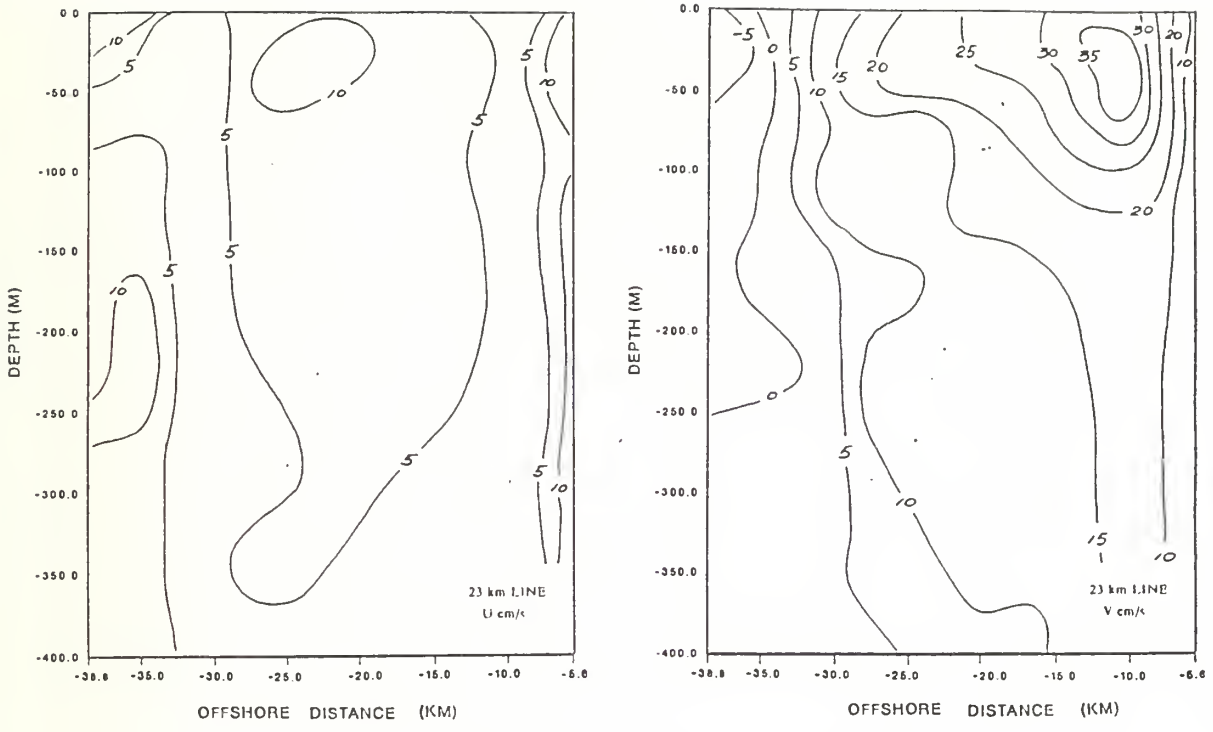

Figure 10e. Vertical cross-section of onshore and alongshore current components at the 23 km line in figure 9.

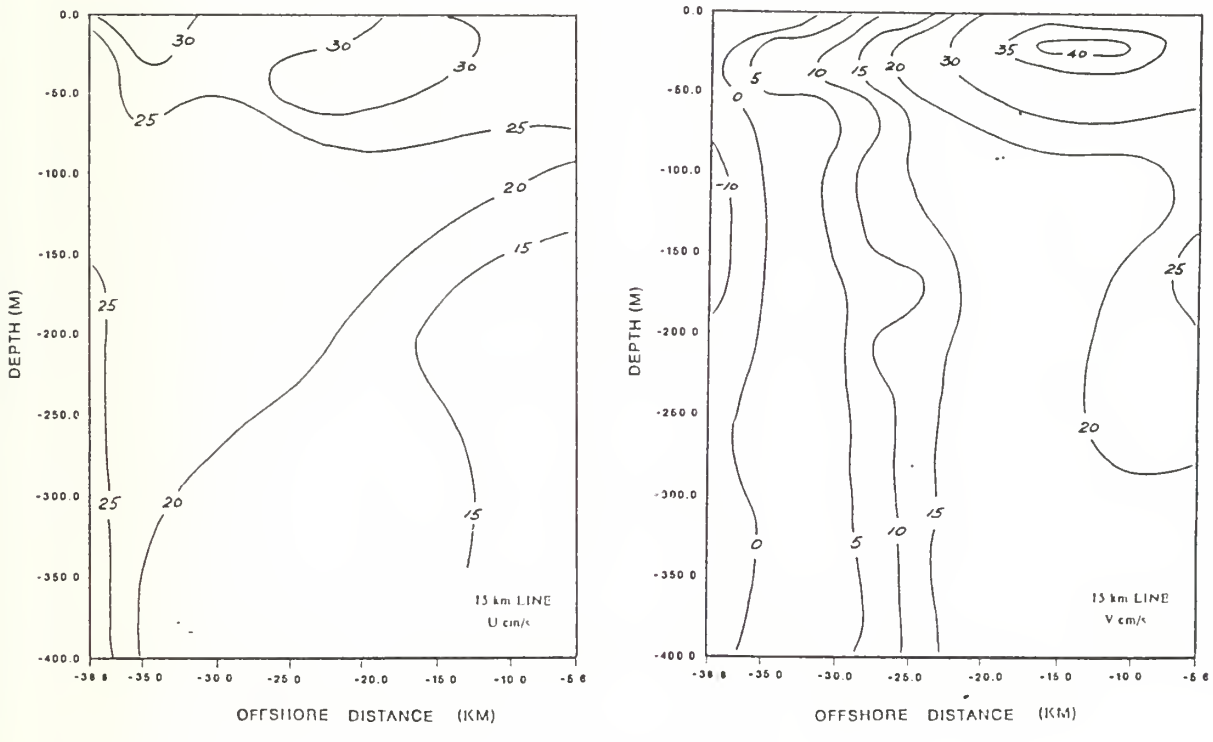

Figure 10f. Vertical cross-section of onshore and alongshore current components at the 15 km line in figure 9.

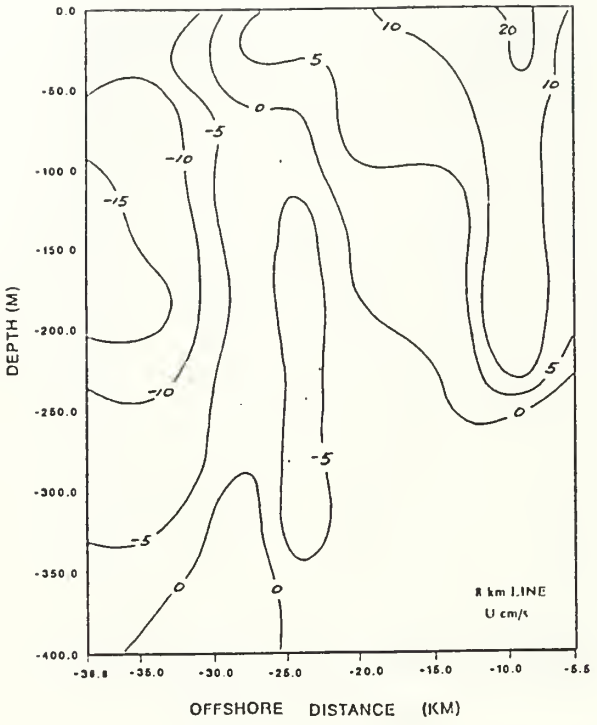

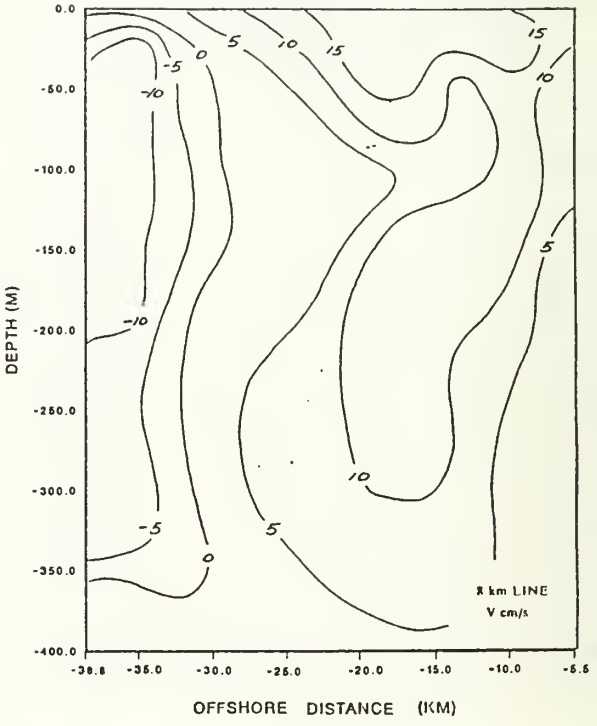

Figure 10g. Vertical cross-section of onshore and alongshore current components at the 8 km line in figure 9.

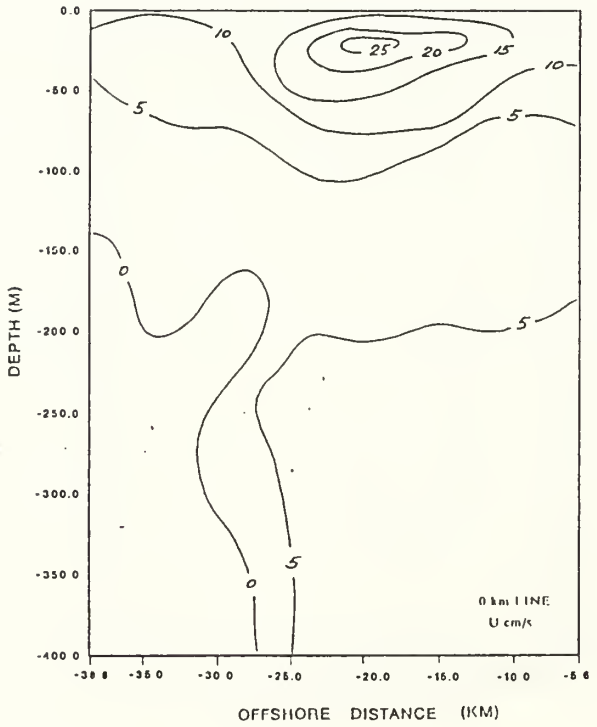

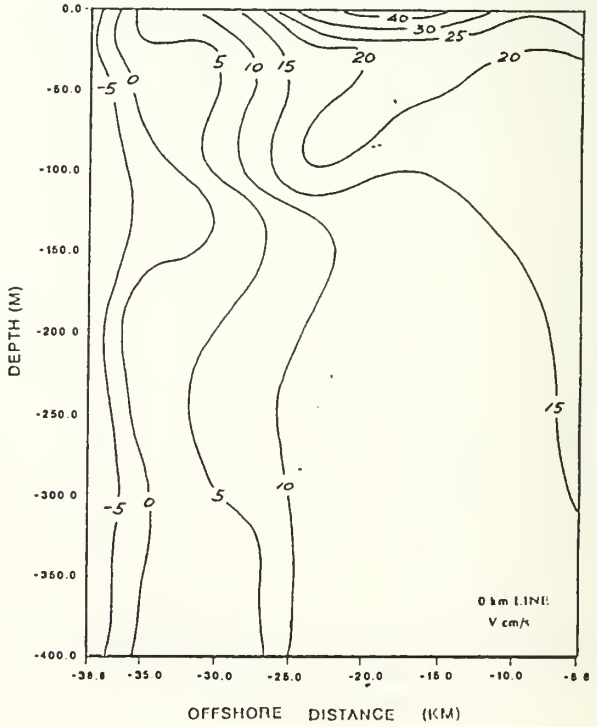

Figure 10h. Vertical cross-section of onshore and alongshore current components at the 0 km line in figure 9.

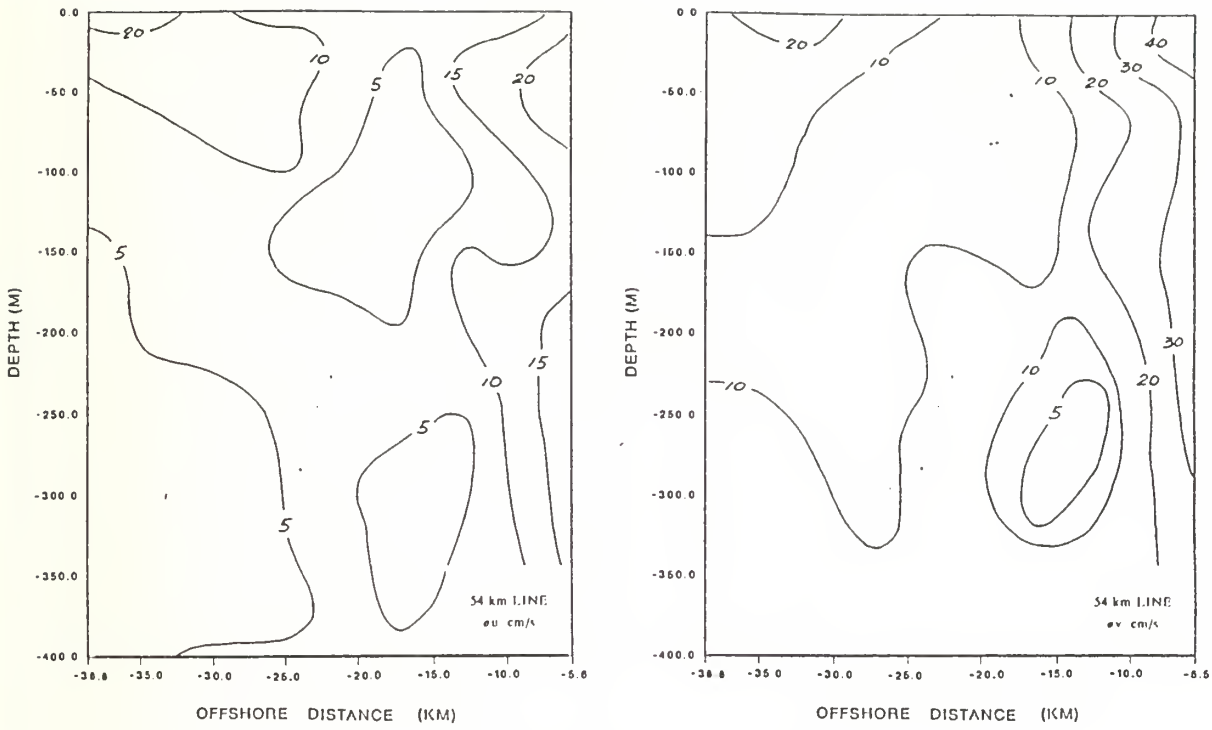

Figure 11a. Vertical cross-section of standard deviation of onshore and alongshore current components at the 54 km line in figure 9.

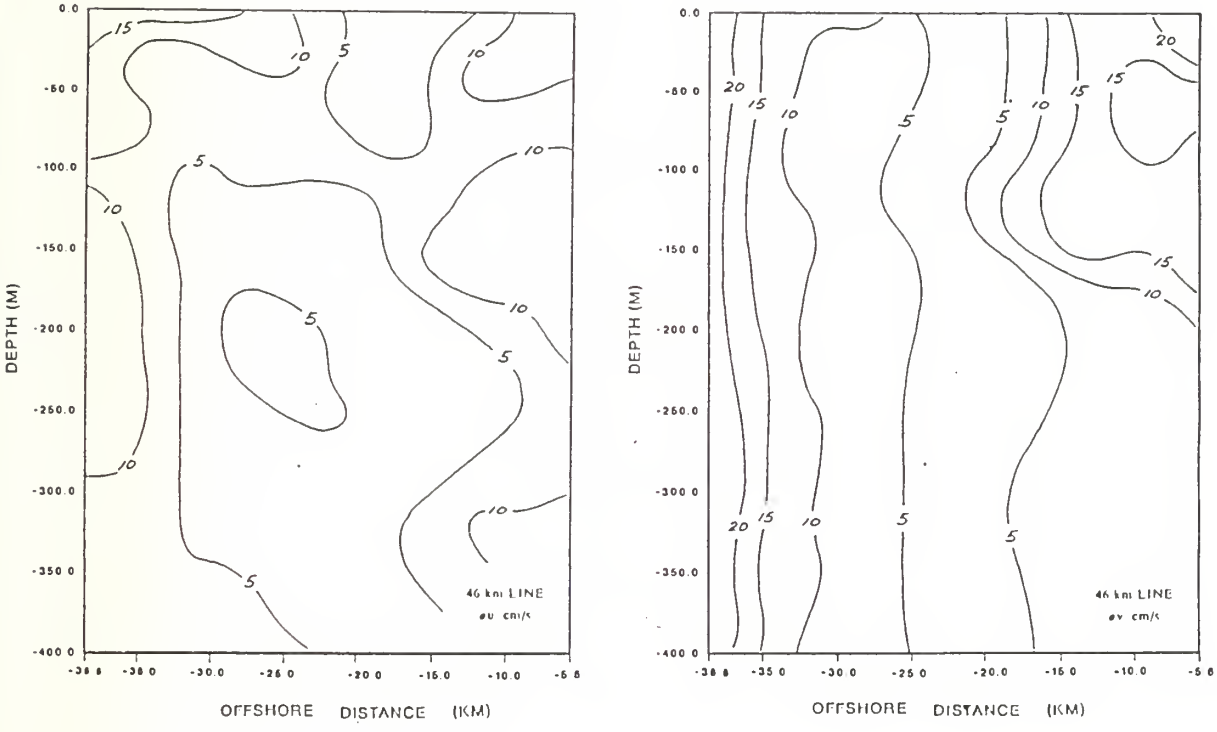

Figure 11b. Vertical cross-section of standard deviation of onshore and alongshore current components at the 46 km line in figure 9.

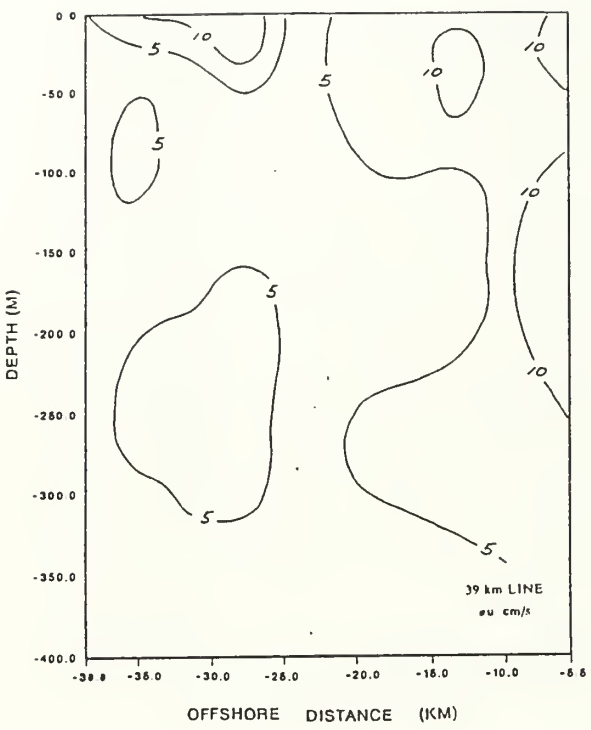

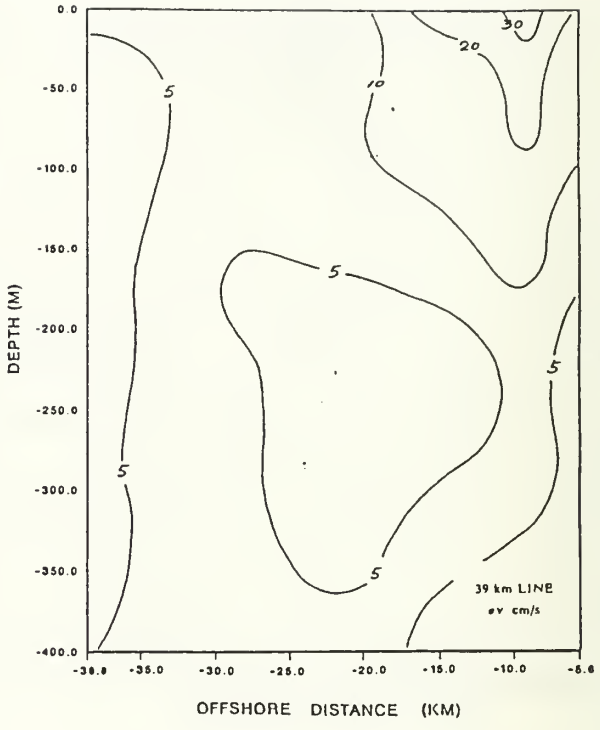

Figure 11c. Vertical cross-section of standard deviation of onshore and alongshore current components at the 39 km line in figure 9.

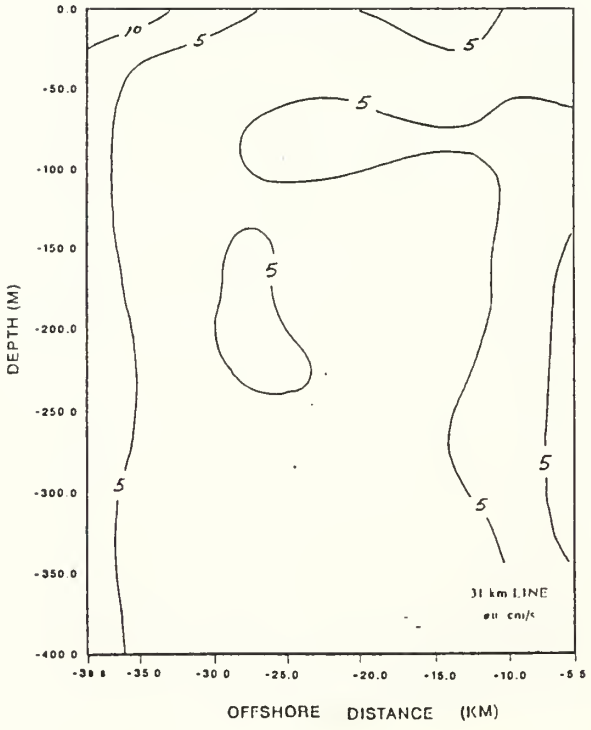

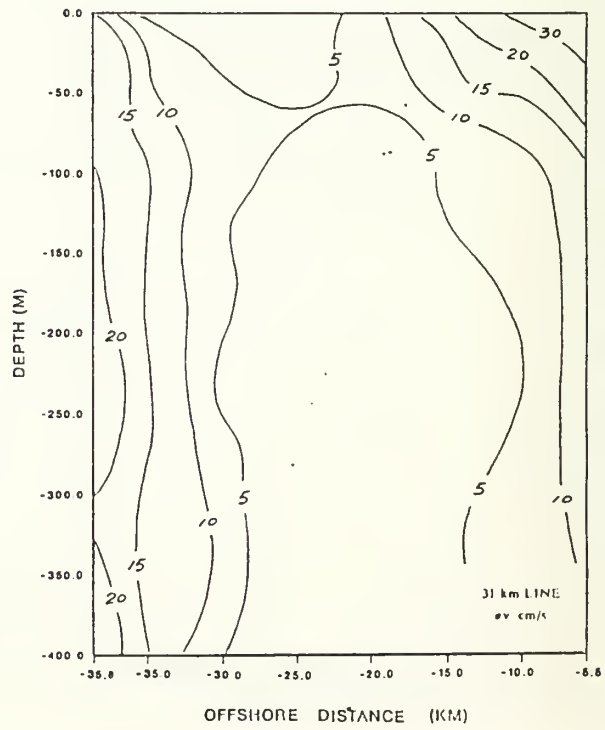

Figure 11d. Vertical cross-section of standard deviation of onshore and alongshore current components at the 31 km line in figure 9.

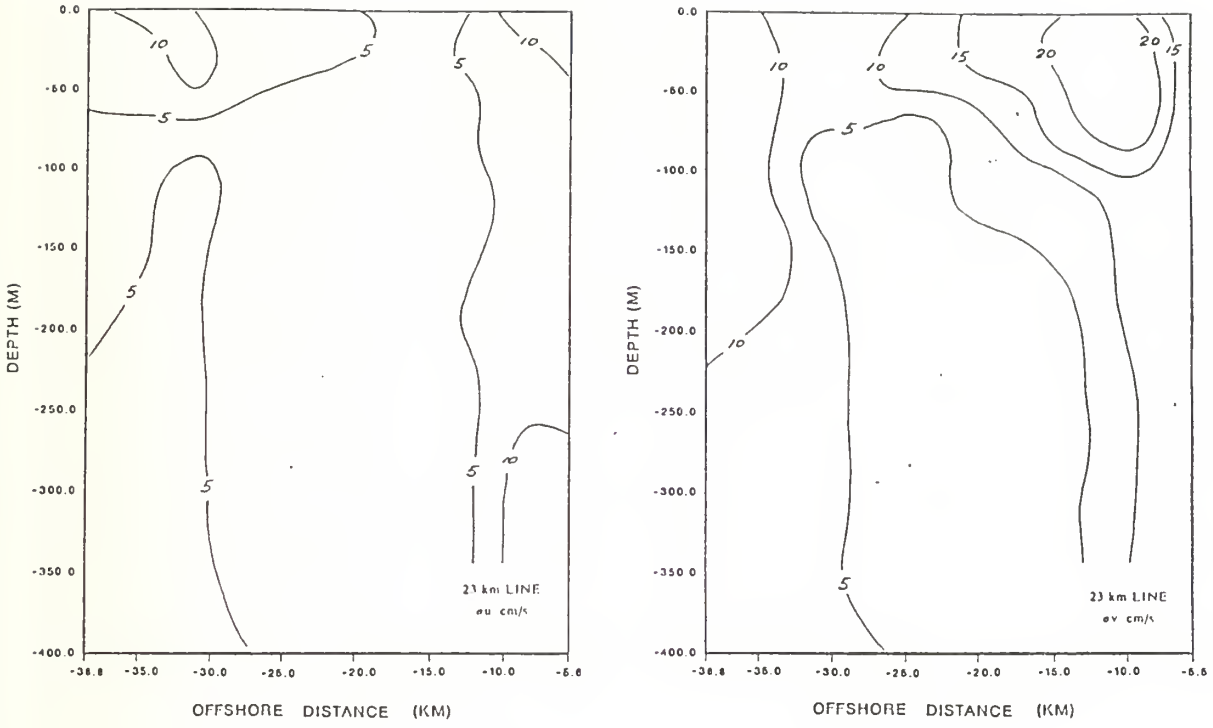

Figure 11e. Vertical cross-section of standard deviation of onshore and alongshore current components at the 23 km line in figure 9.

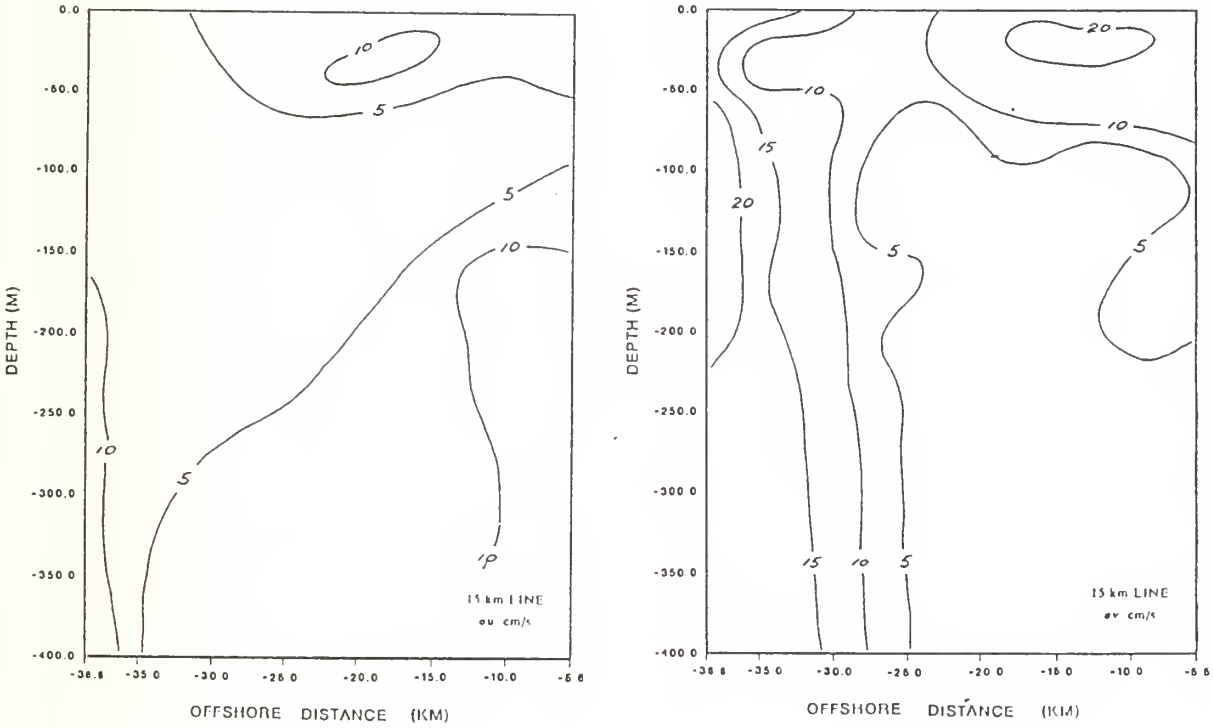

Figure 11f. Vertical cross-section of standard deviation of onshore and alongshore current components at the 15 km line in figure 9.

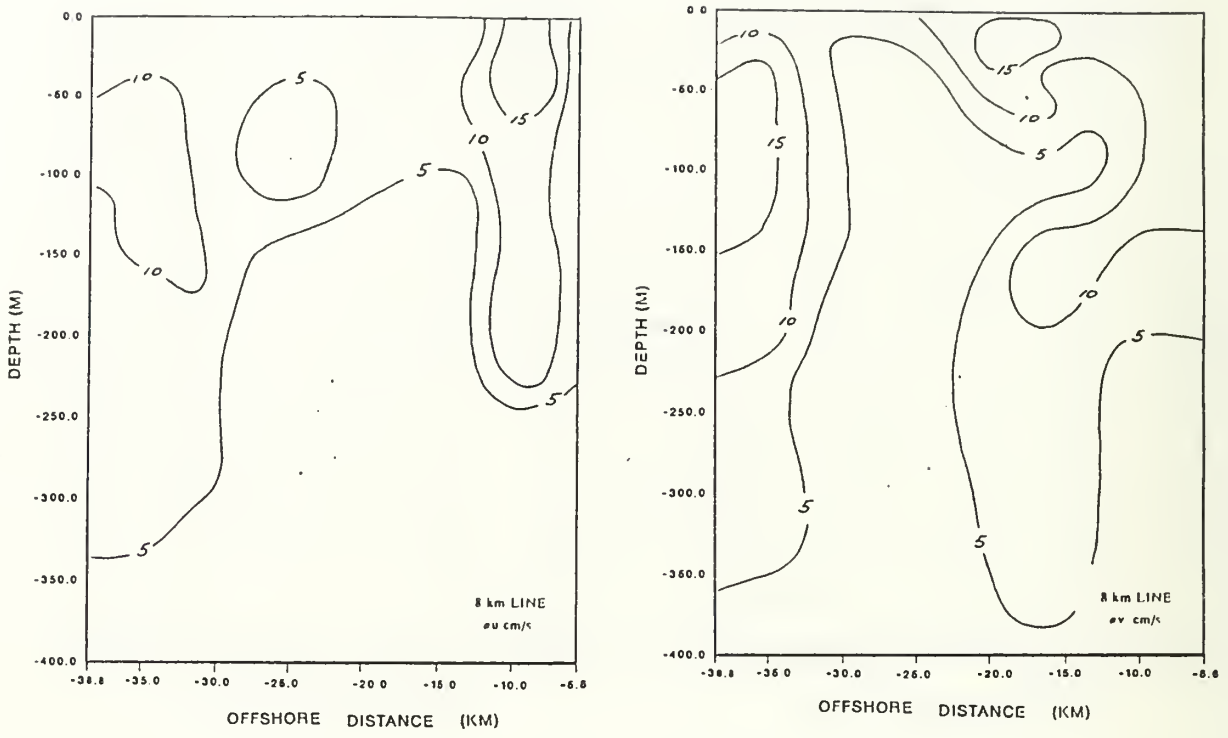

Figure 11g. Vertical cross-section of standard deviation of onshore and alongshore current components at the 8 km line in figure 9.

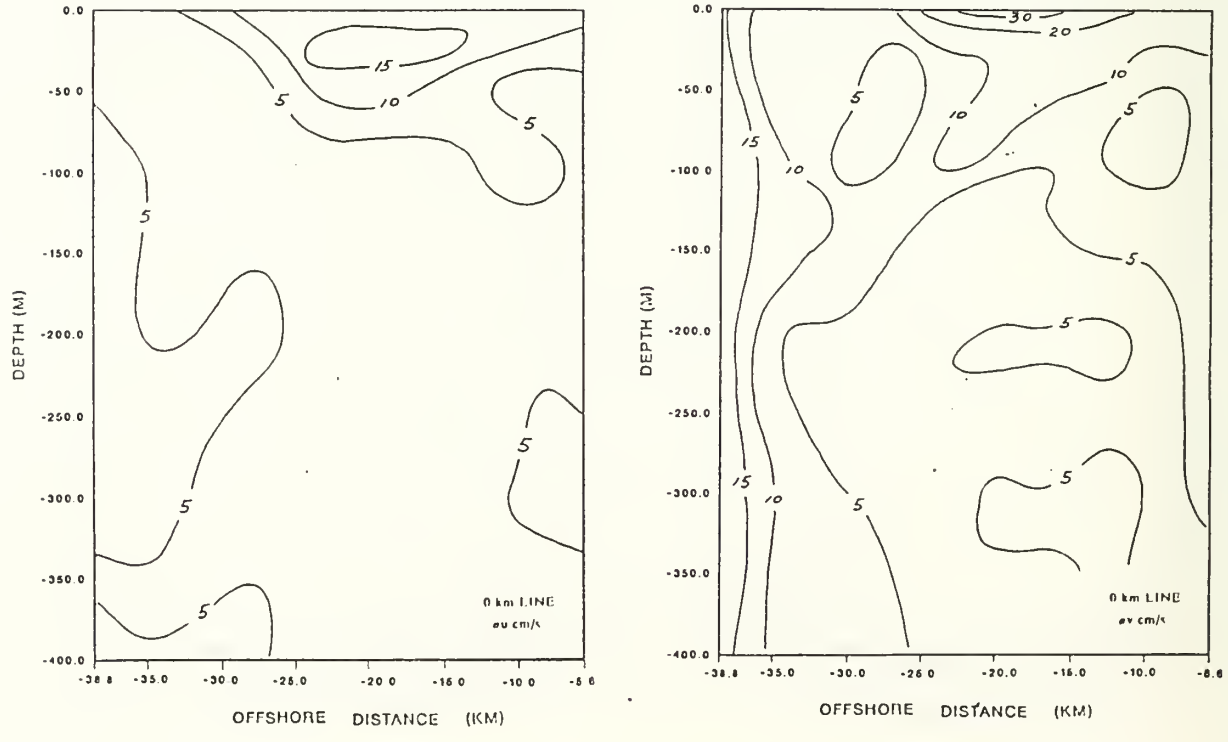

Figure 11h. Vertical cross-section of standard deviation of onshore and alongshore current components at the 0 km line in figure 9.

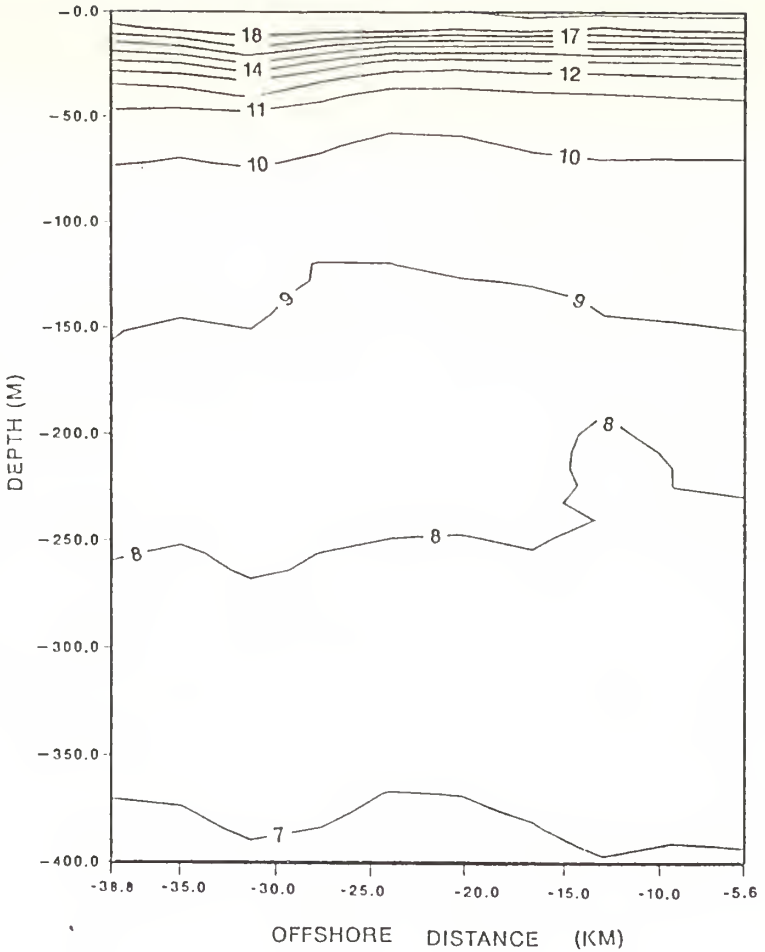

Figure 12a. Vertical cross-section of temperature at the 54 km line in figure 9

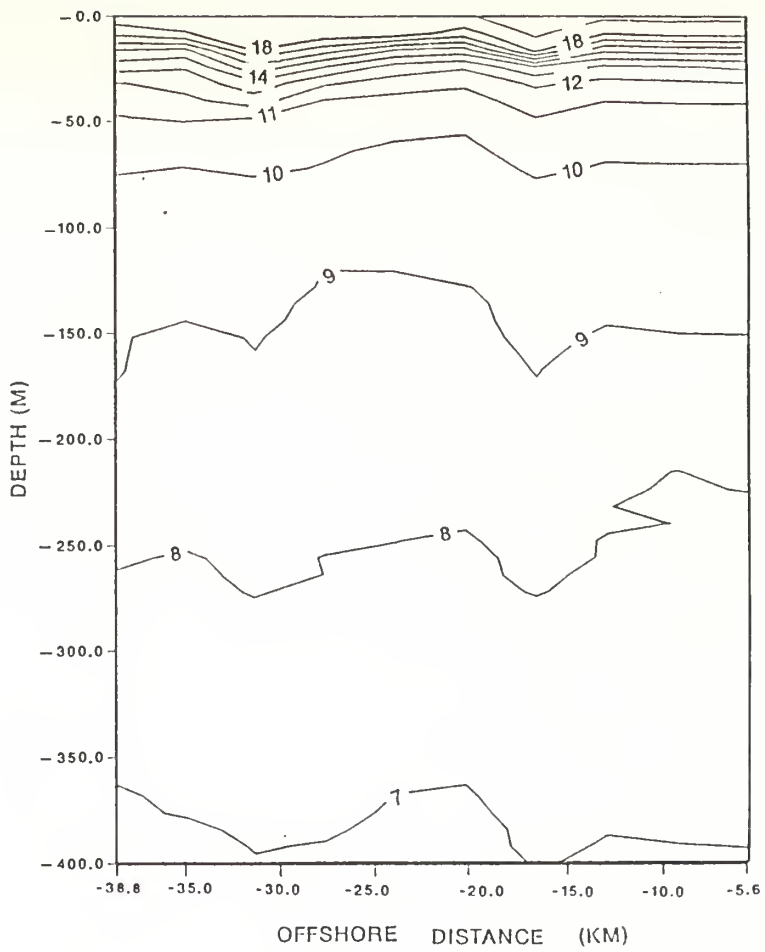

Figure 12b. Vertical cross-section of temperature at the 46 km line in figure 9.

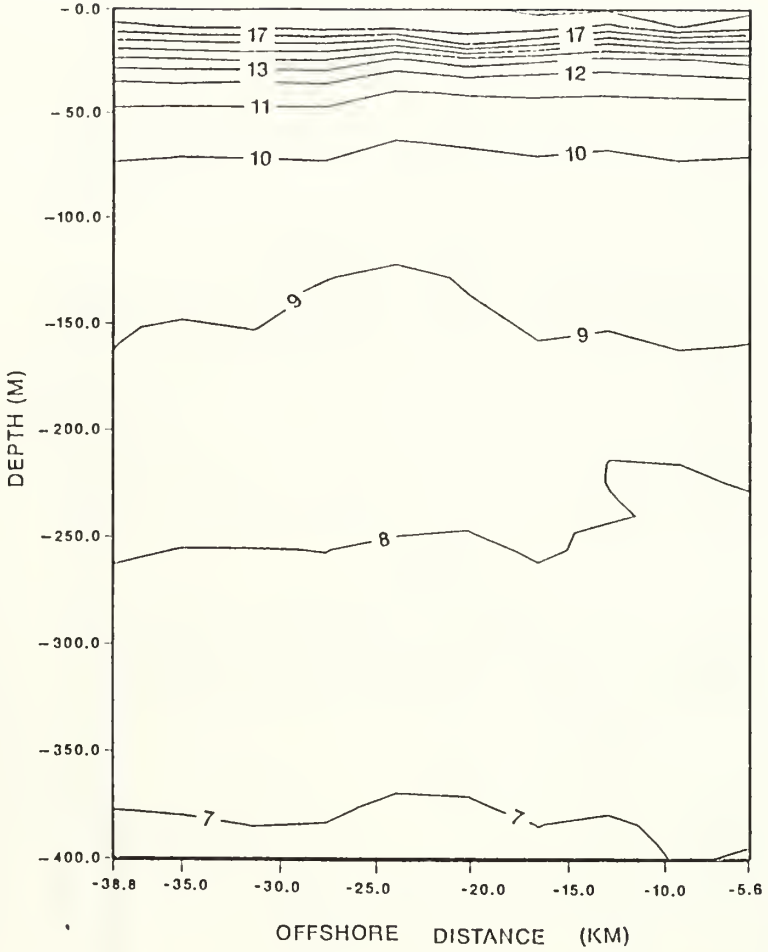

Figure 12c. Vertical cross-section of temperature at the 39 km line in figure 9.

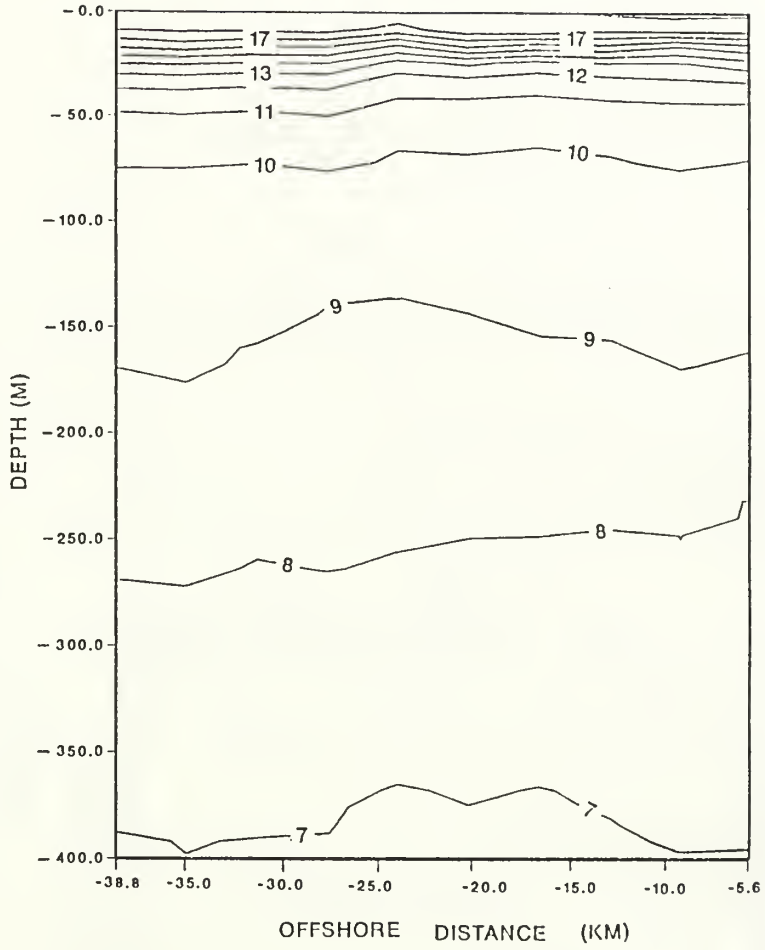

Figure 12d. Vertical cross-section of temperature at the 31 km line in figure 9.

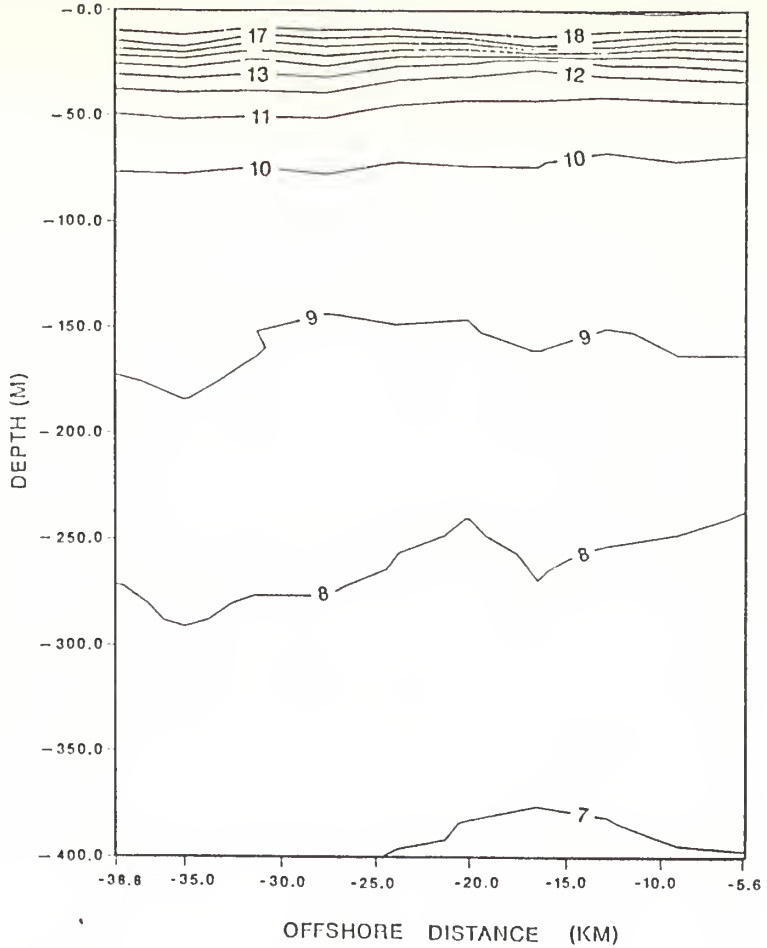

Figure 12e. Vertical cross-section of temperature at the 23 km line in figure 9.

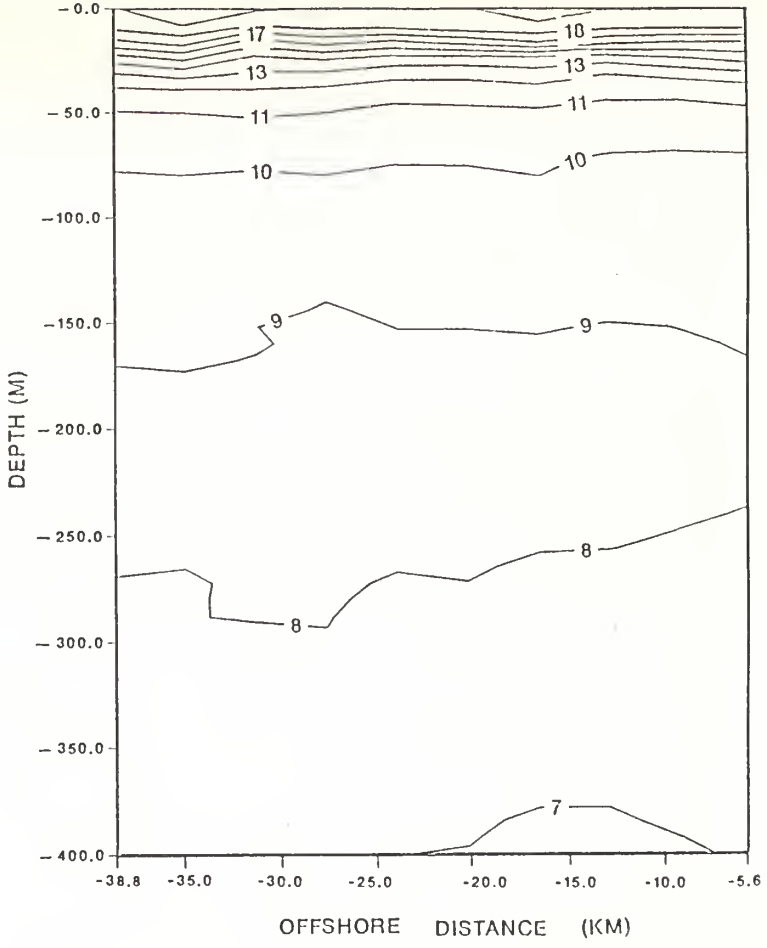

Figure 12f. Vertical cross-section of temperature at the 15 km line in figure 9.

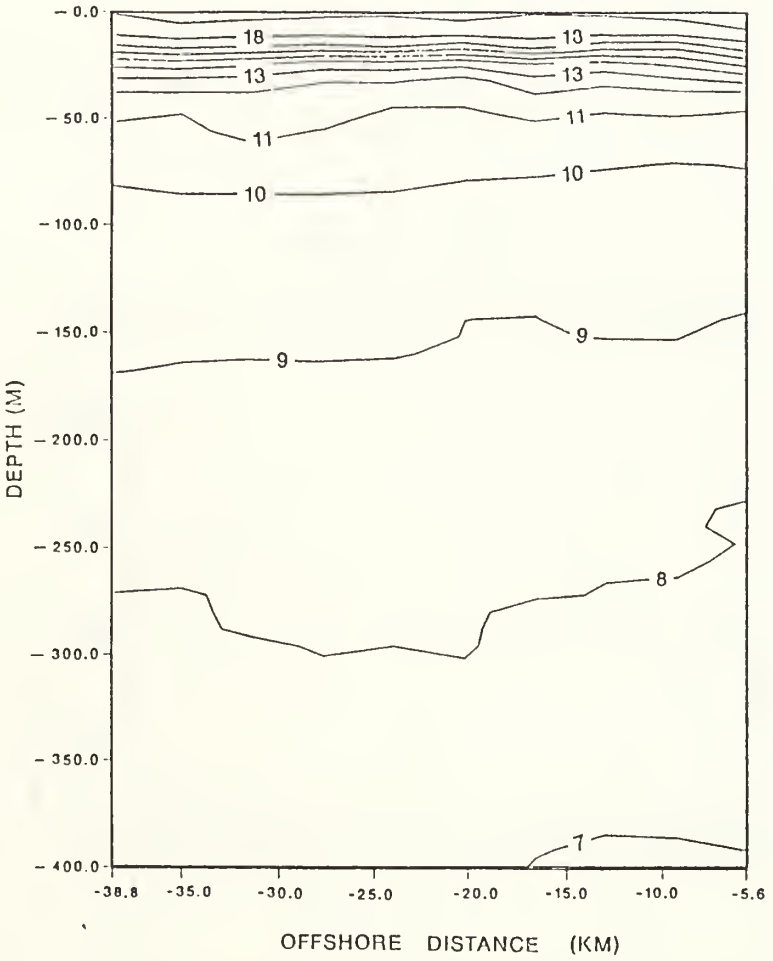

Figure 12g. Vertical cross-section of temperature at the 8 km line in figure 9.

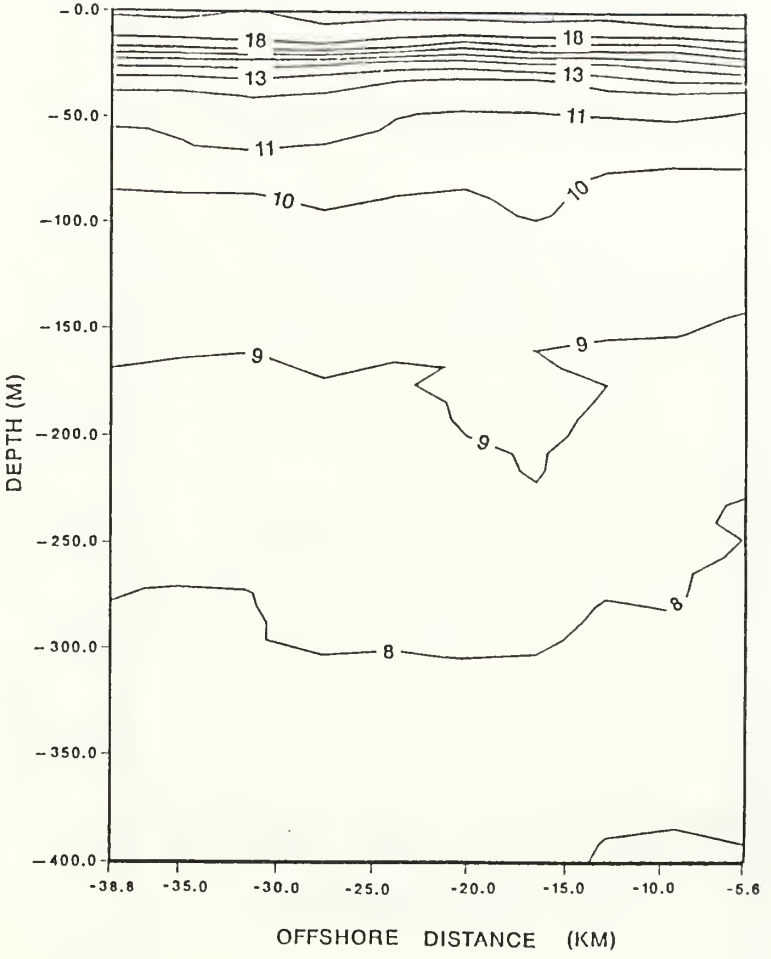

Figure 12h. Vertical cross-section of temperature at the 0 km line in figure 9.

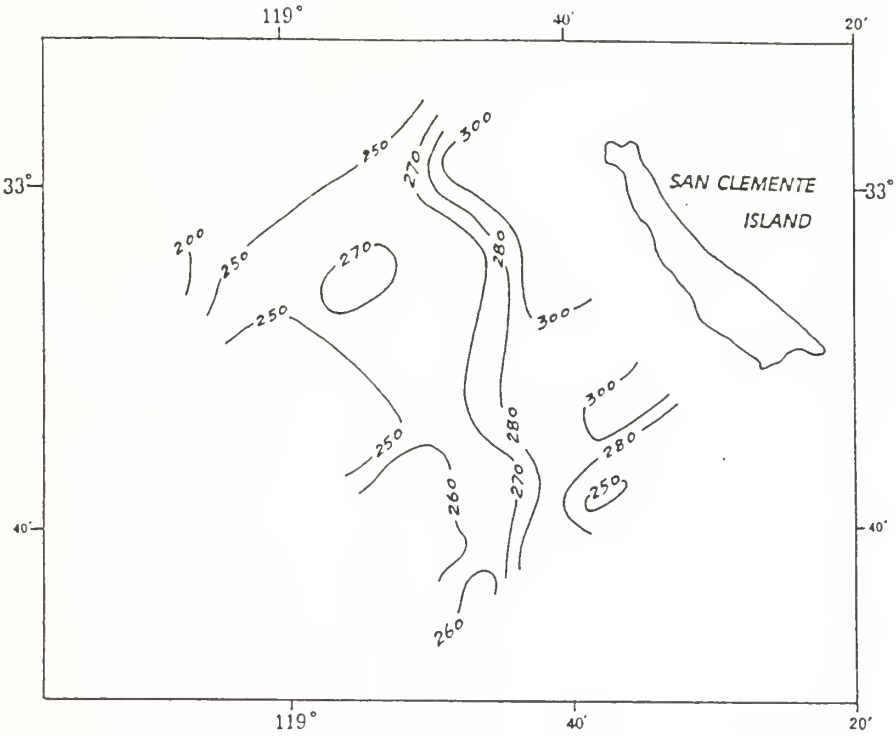

Figure 13a. The depth of 8° C isotherm at study area.

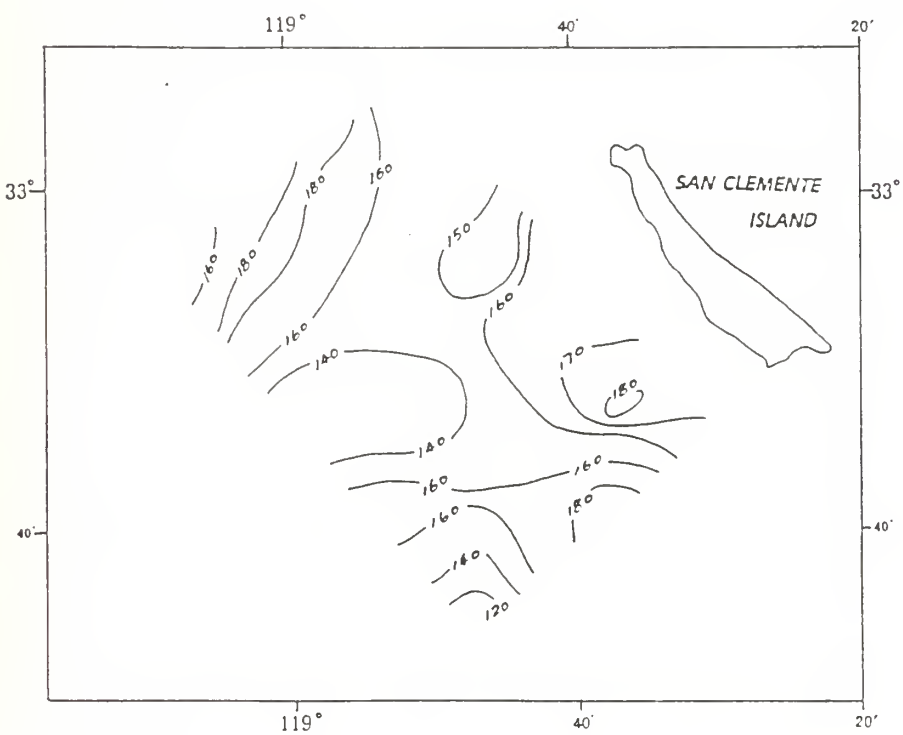

Figure 13b. The depth of 9° C isotherm at study area.

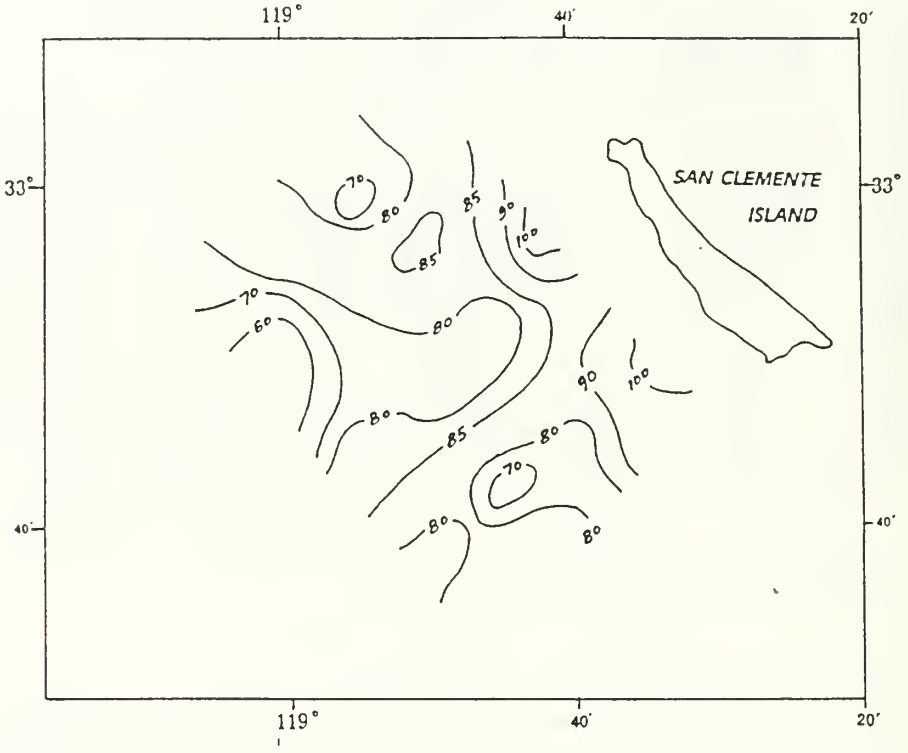

Figure 13c. The depth of 10° C isotherm at study area.

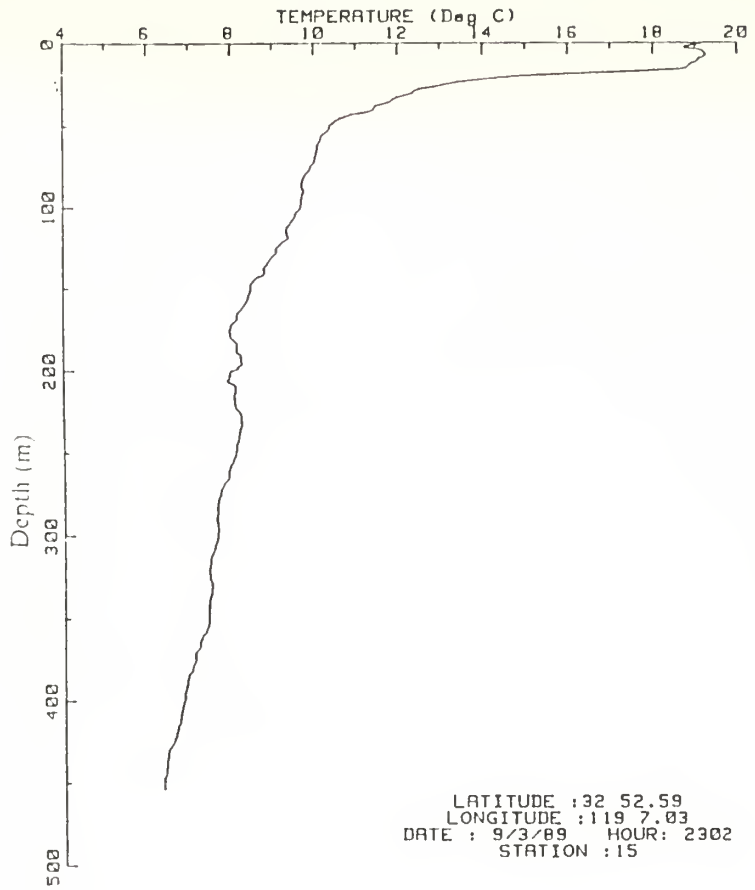

Figure 14.1 Vertical profile of temperature measured by XBT at station No. 15 in figure 3.

Figure 14.2 Vertical profile of temperature measured by XBT at station No. 16 in figure 3.

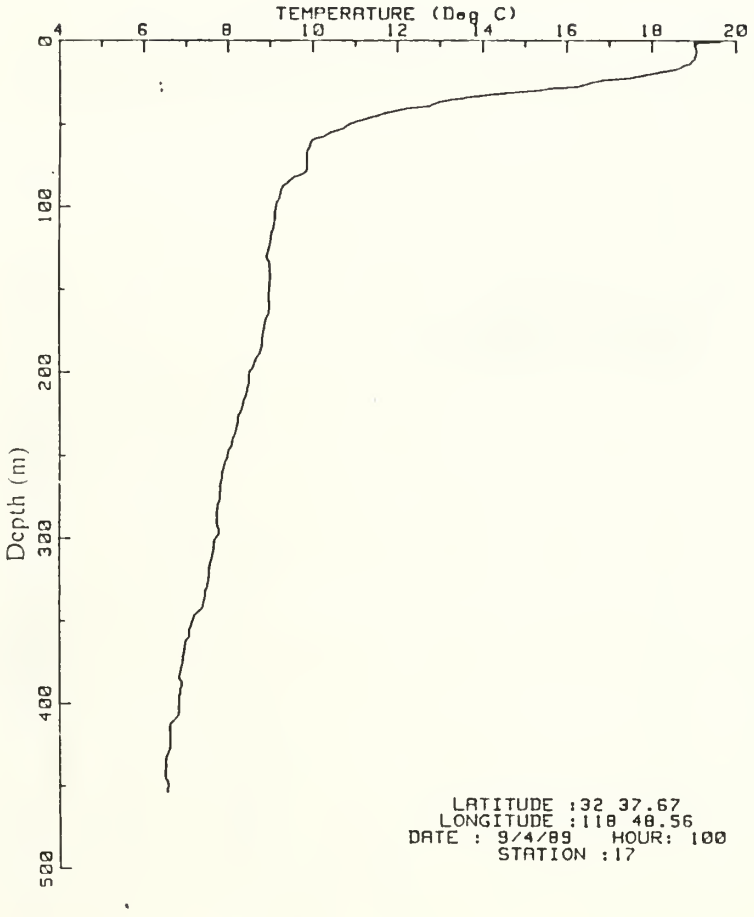

Figure 14.3 Vertical profile of temperature measured by XBT at station No. 17 in figure 3.

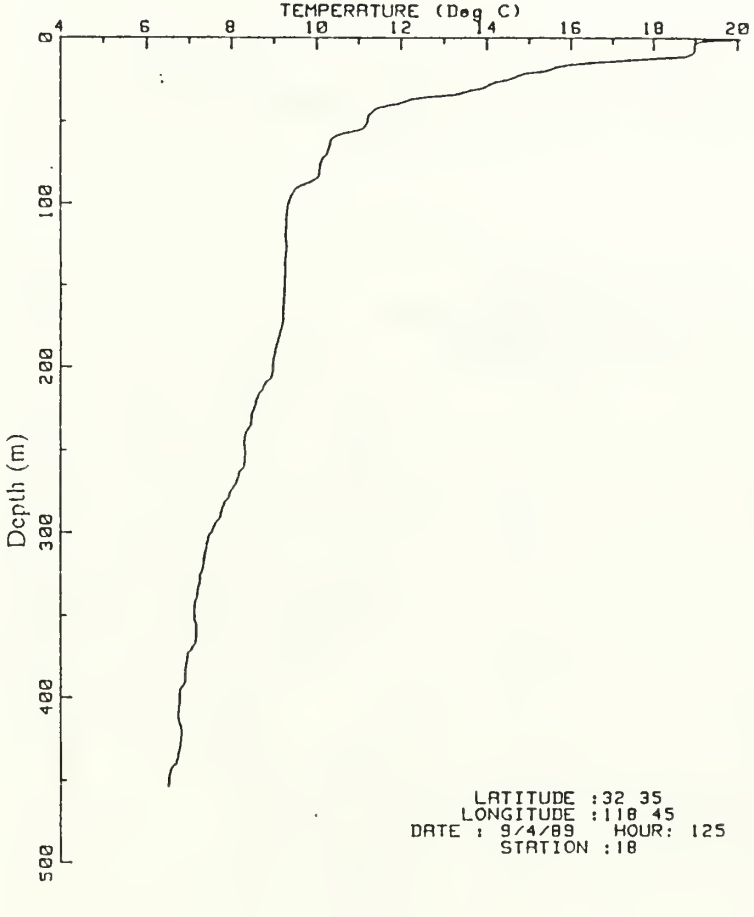

Figure 14.4 Vertical profile of temperature measured by XBT at station No. 18 in figure 3.

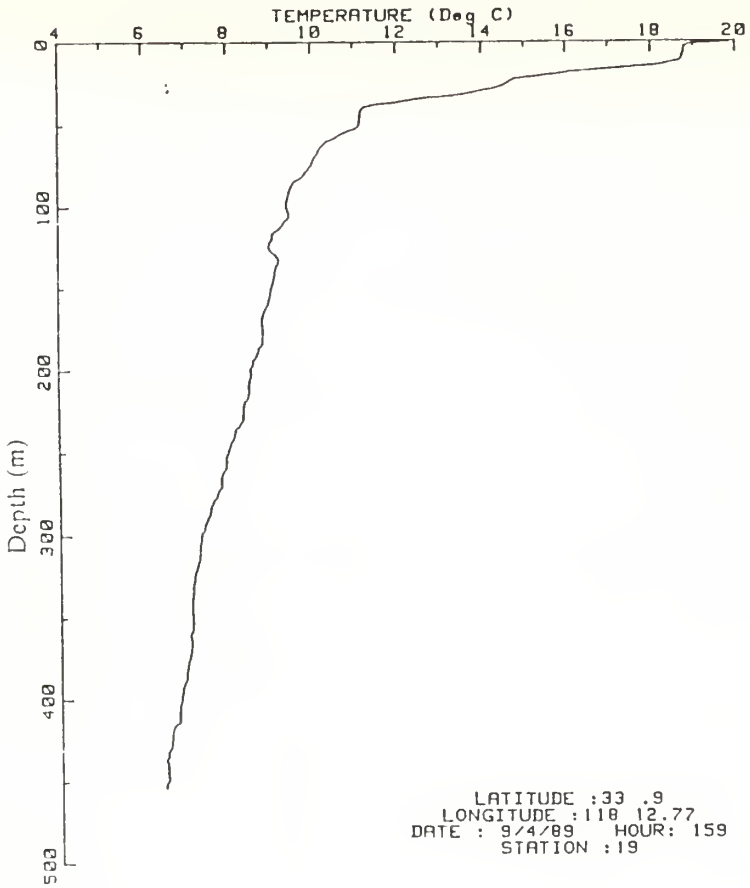

Figure 14.5 Vertical profile of temperature measured by XBT at station No. 19 in figure 3.

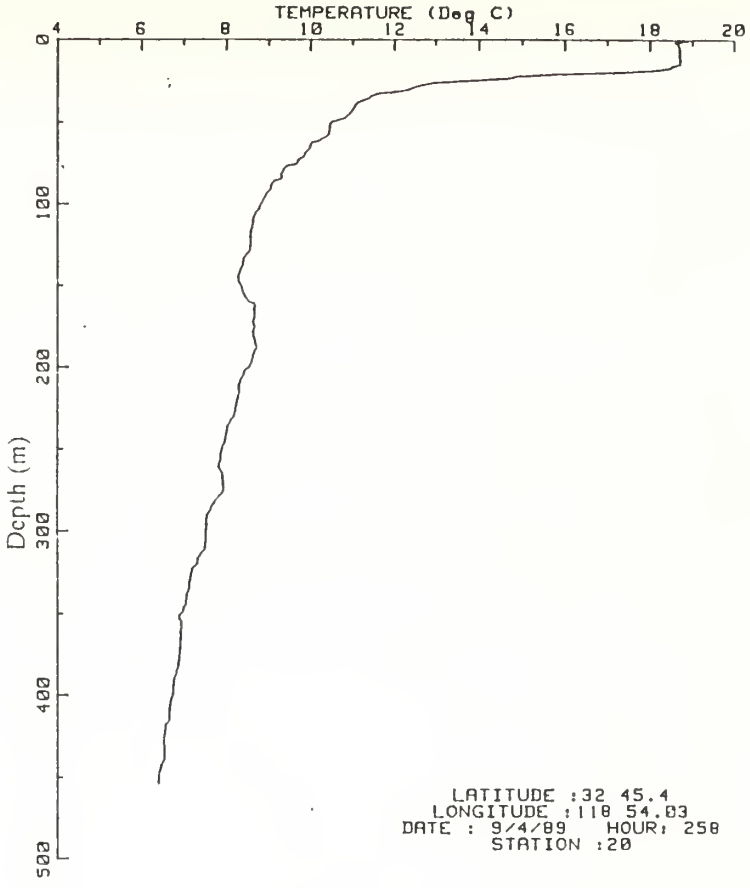

Figure 14.6 Vertical profile of temperature measured by XBT at station No. 20 in figure 3.

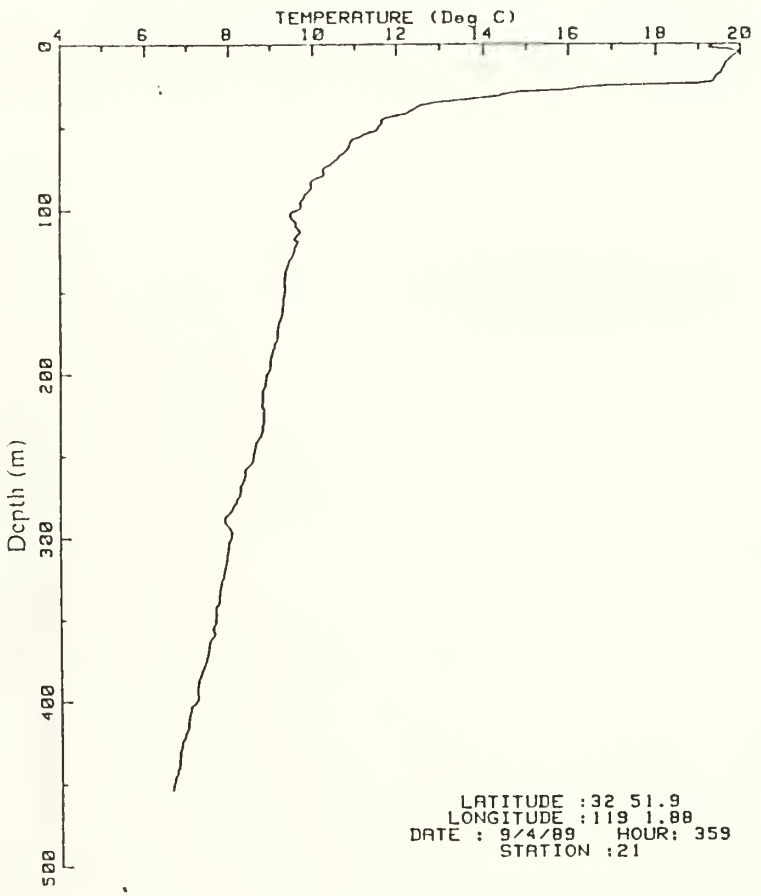

Figure 14.7 Vertical profile of temperature measured by XBT at station No. 21 in figure 3.

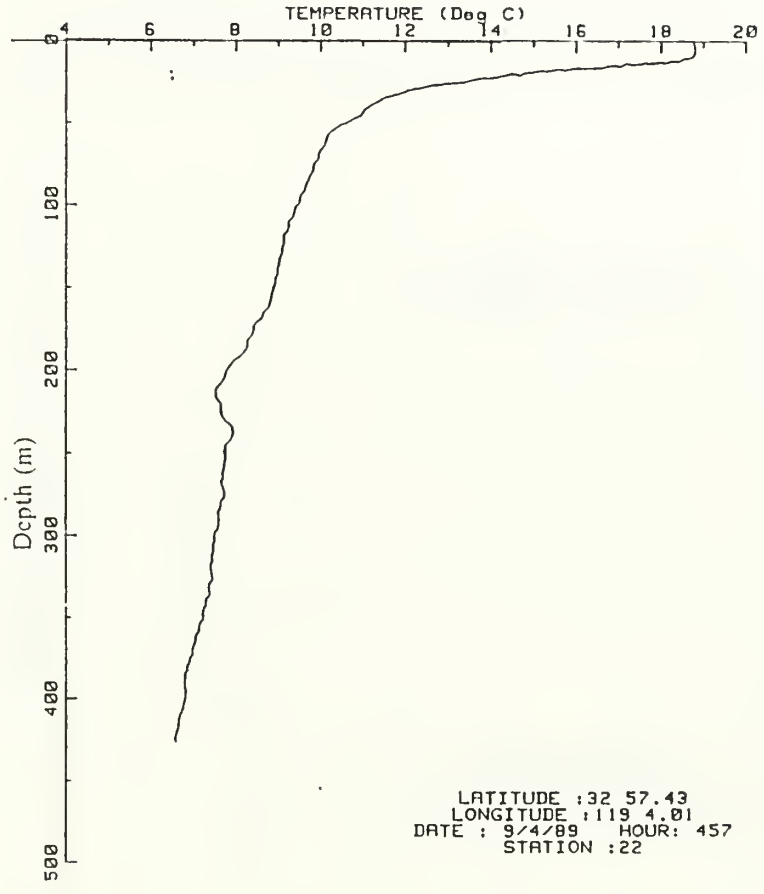

Figure 14.8 Vertical profile of temperature measured by XBT at station No. 22 in figure 3.

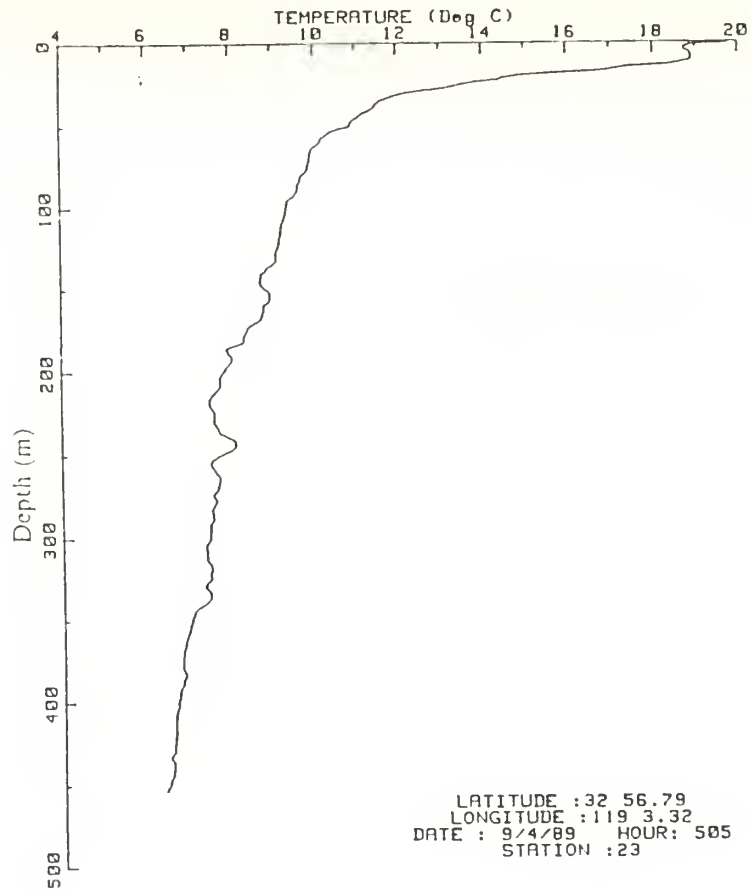

Figure 14.9 Vertical profile of temperature measured by XBT at station No. 23 in figure 3.

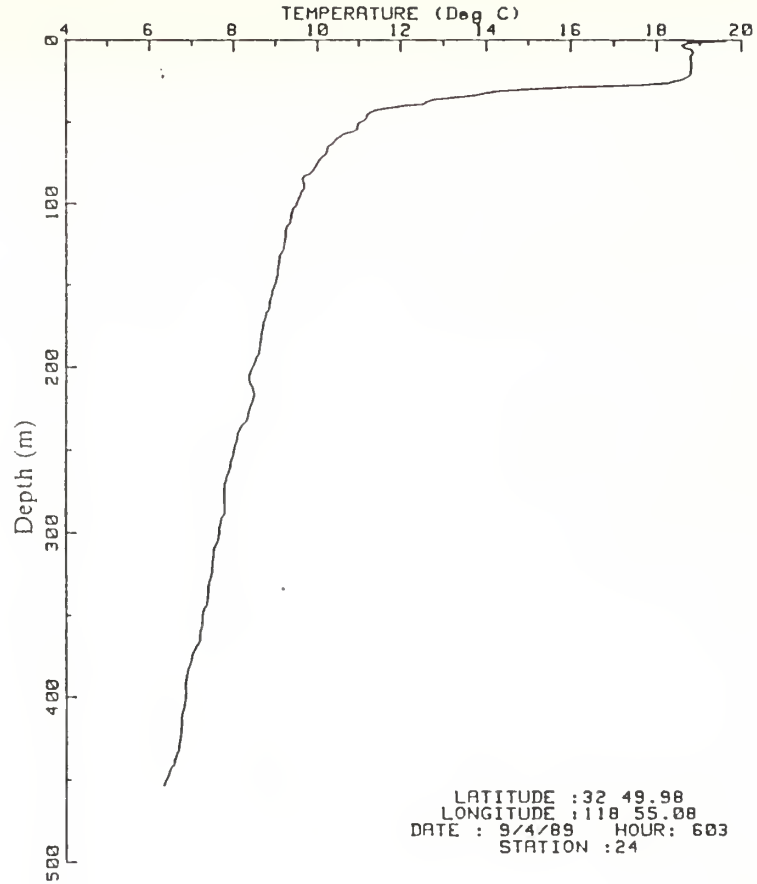

Figure 14.10 Vertical profile of temperature measured by XBT at station No. 24 in figure 3.

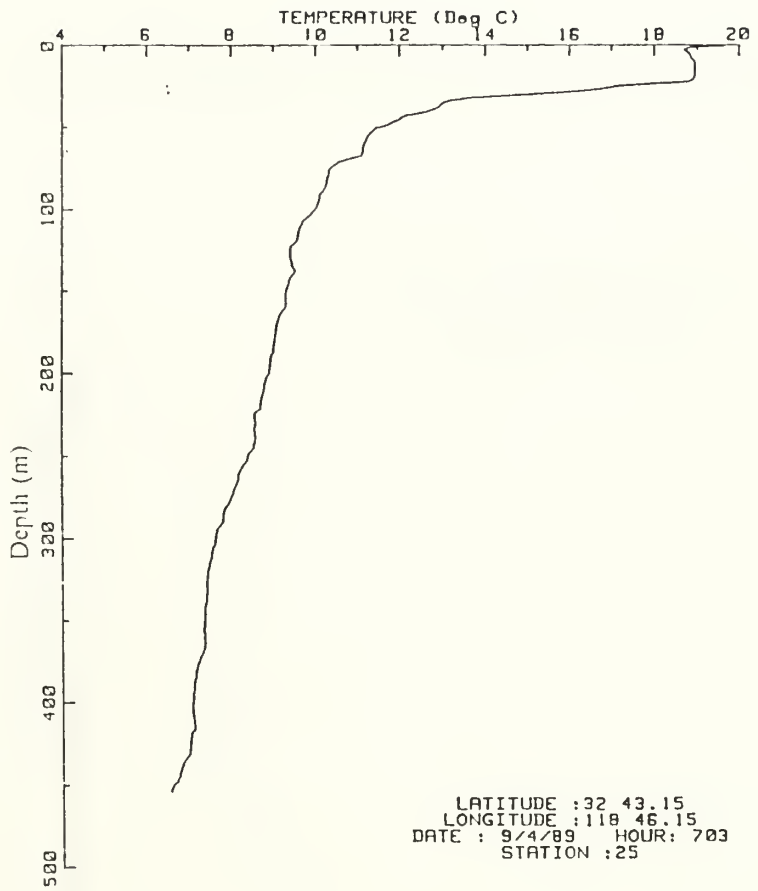

Figure 14.11 Vertical profile of temperature measured by XBT at station No. 25 in figure 3.

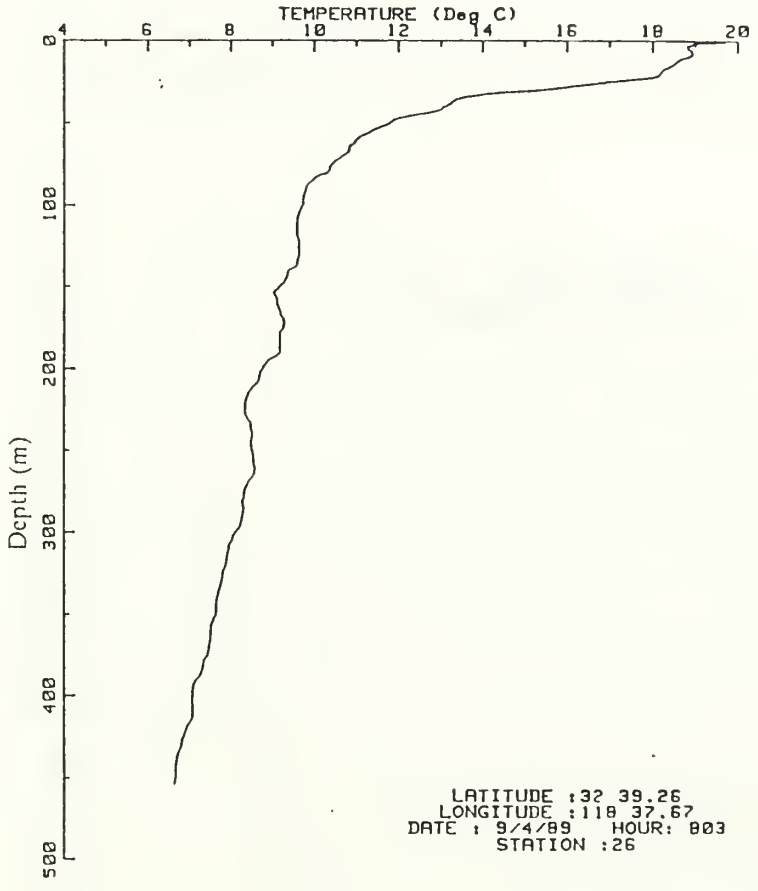

Figure 14.12 Vertical profile of temperature measured by XBT at station No. 26 in figure 3.

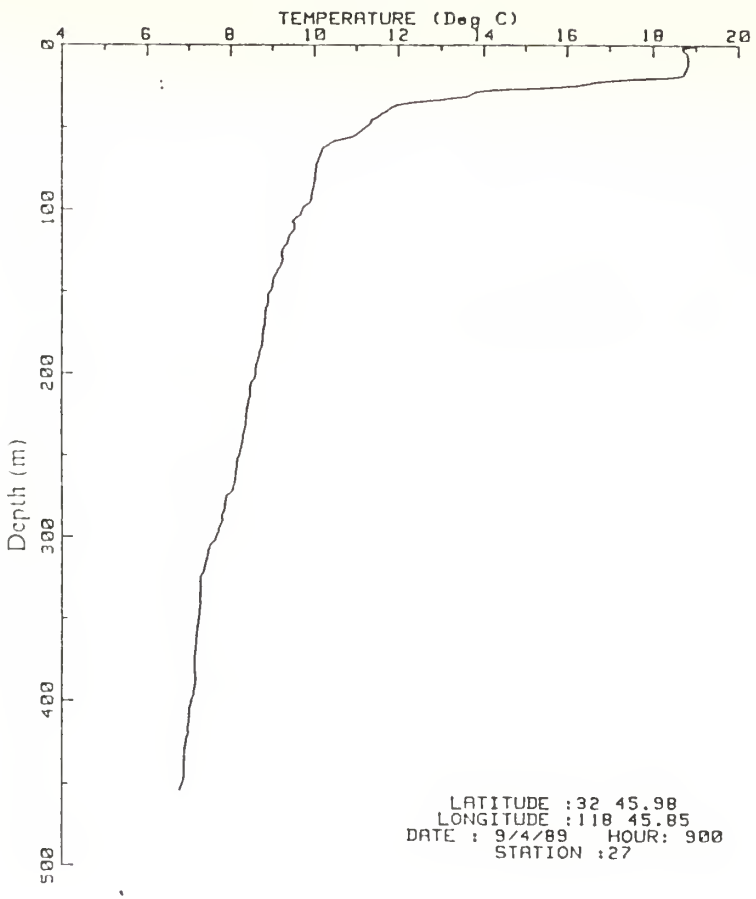

Figure 14.13 Vertical profile of temperature measured by XBT at station No. 27 in figure 3.

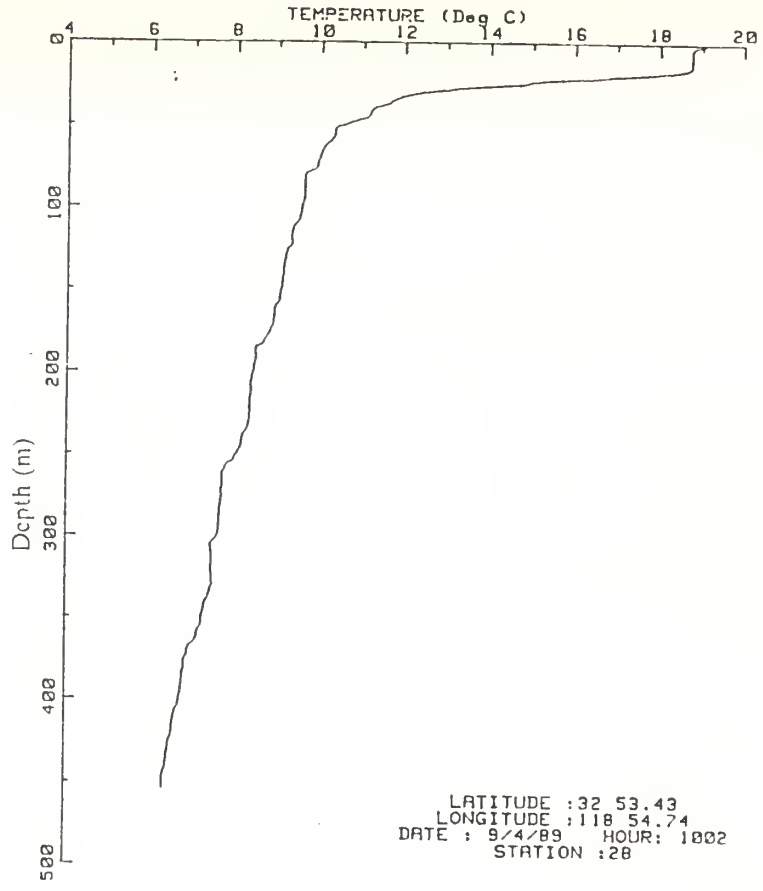

Figure 14.14 Vertical profile of temperature measured by XBT at station No. 28 in figure 3.

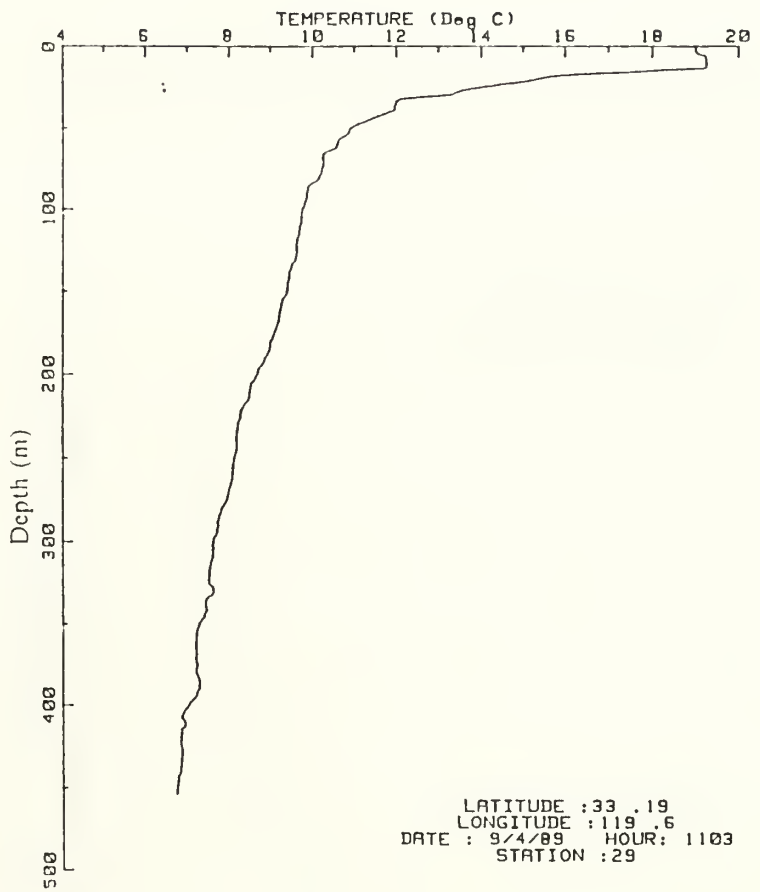

Figure 14.15 Vertical profile of temperature measured by XBT at station No. 29 in figure 3.

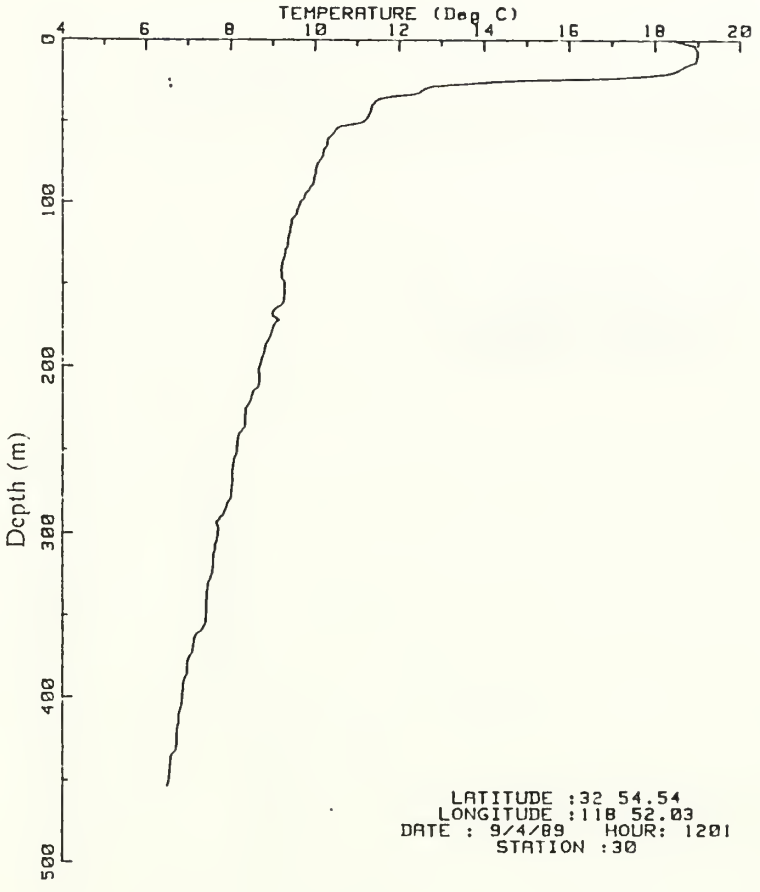

Figure 14.16 Vertical profile of temperature measured by XBT at station No. 30 in figure 3.

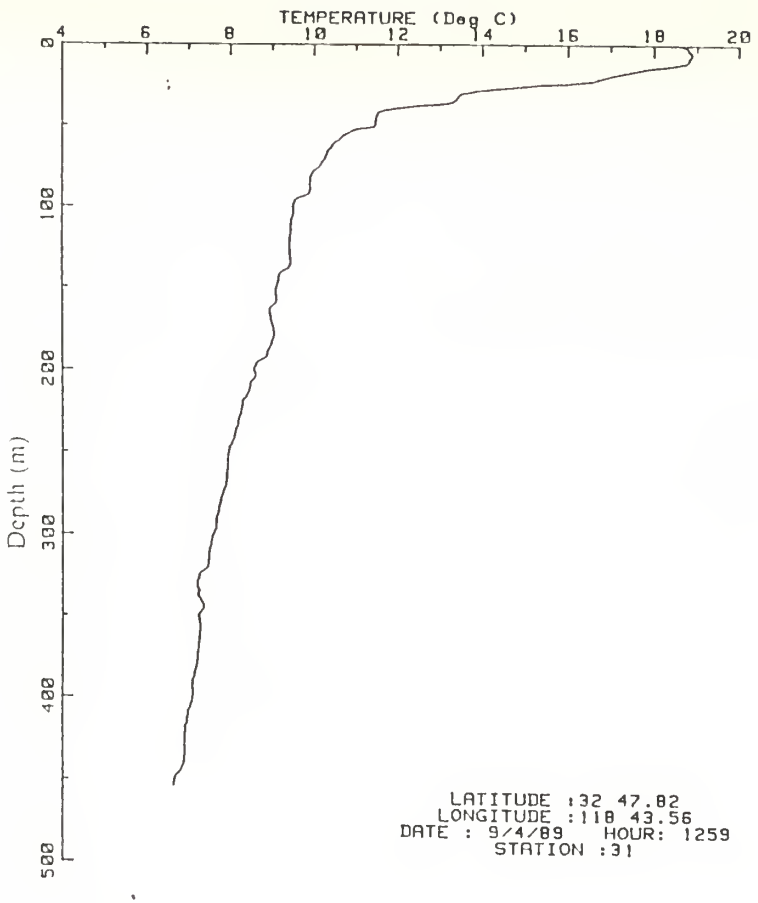

Figure 14.17 Vertical profile of temperature measured by XBT at station No. 31 in figure 3.

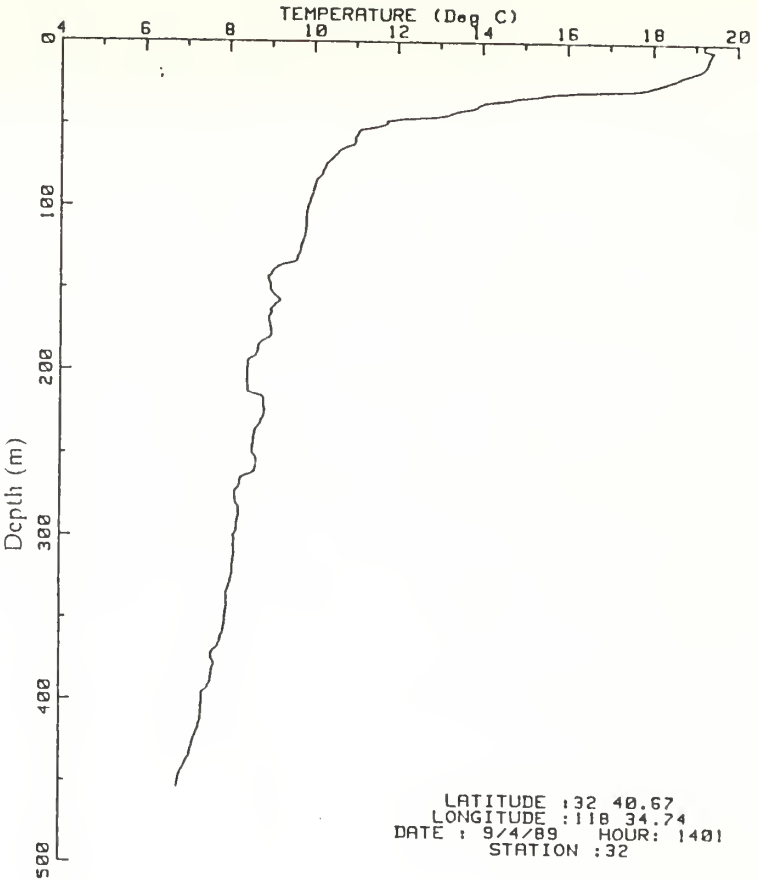

Figure 14.18 Vertical profile of temperature measured by XBT at station No. 32 in figure 3.

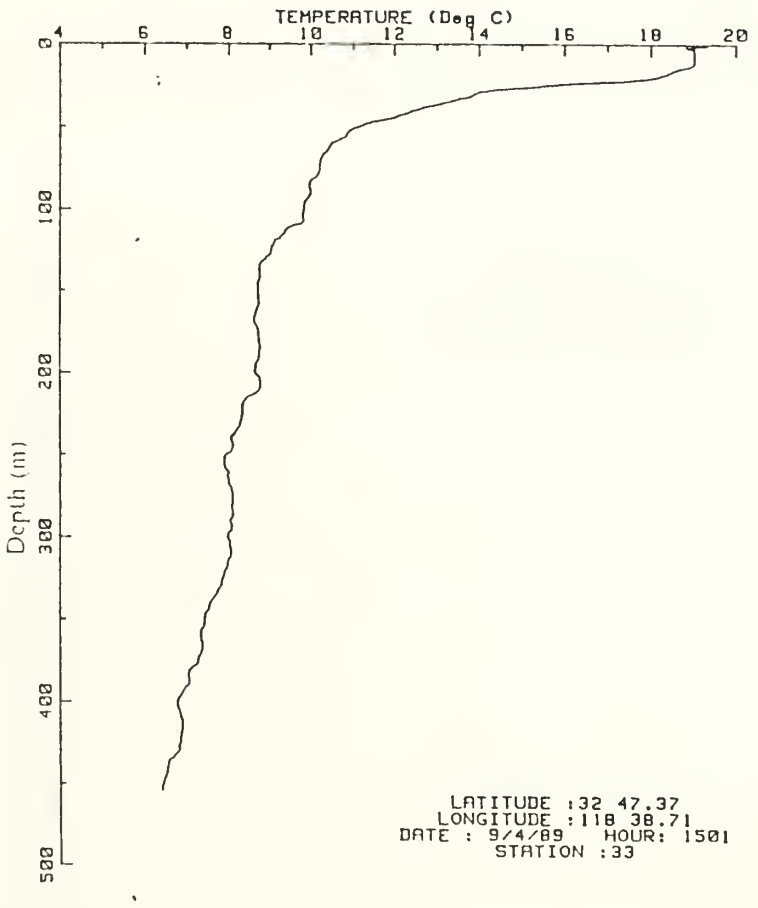

Figure 14.19 Vertical profile of temperature measured by XBT at station No. 33 in figure 3.

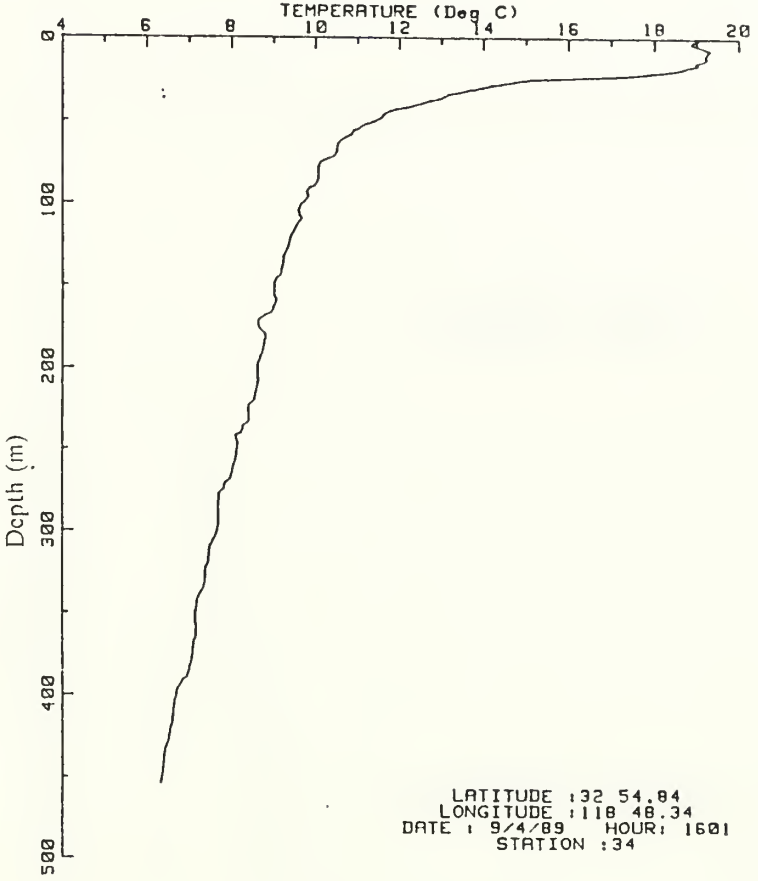

Figure 14.20 Vertical profile of temperature measured by XBT at station No. 34 in figure 3.

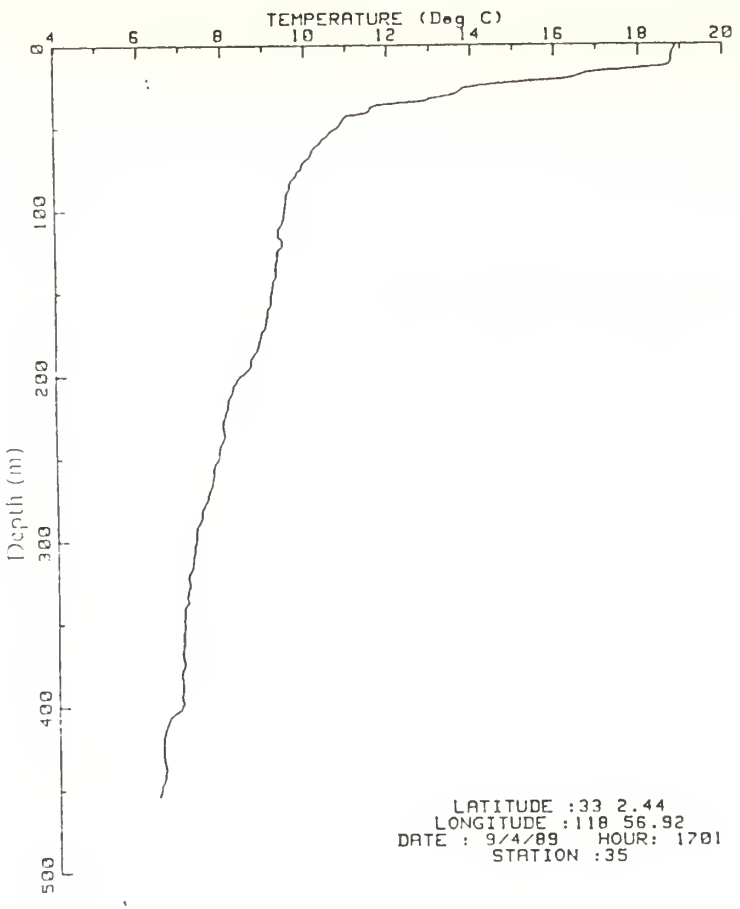

Figure 14.21 Vertical profile of temperature measured by XBT at station No. 35 in figure 3.

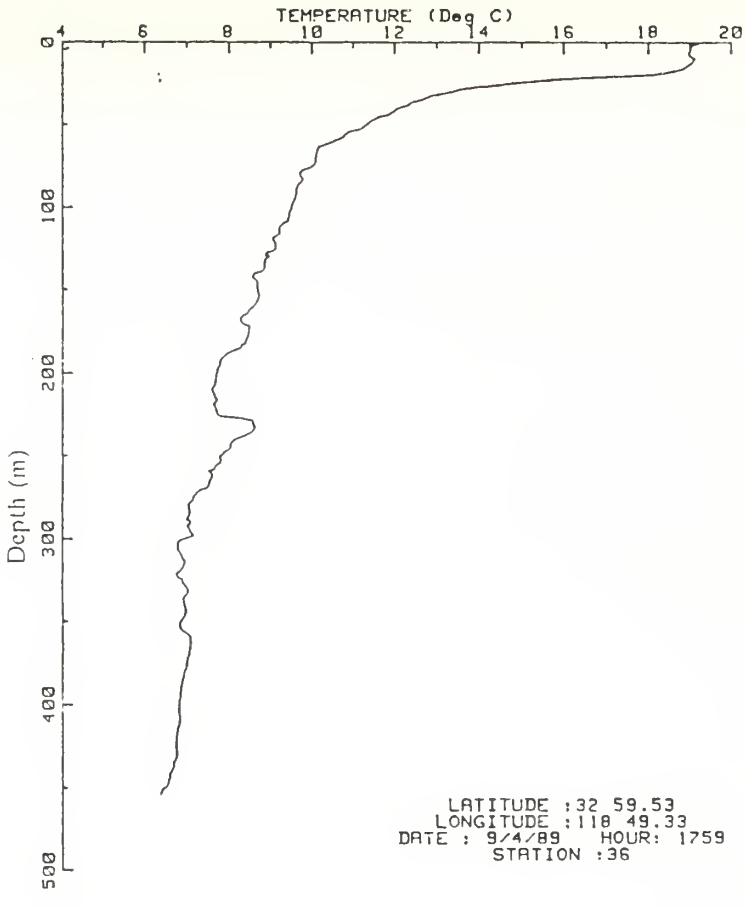

Figure 14.22 Vertical profile of temperature measured by XBT at station No. 36 in figure 3.

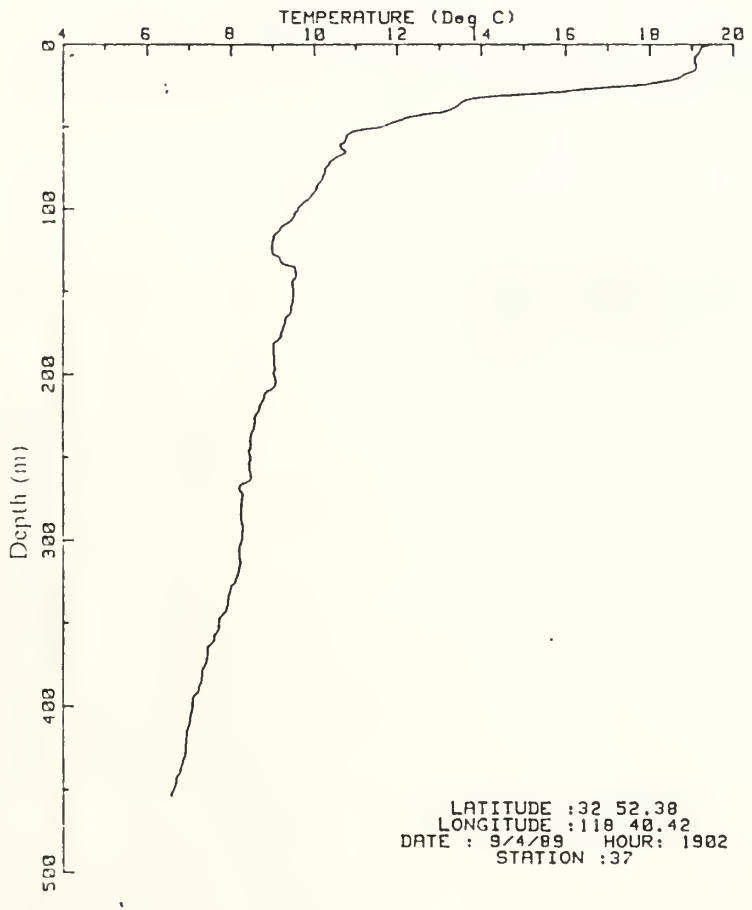

Figure 14.23 Vertical profile of temperature measured by XBT at station No. 37 in figure 3.

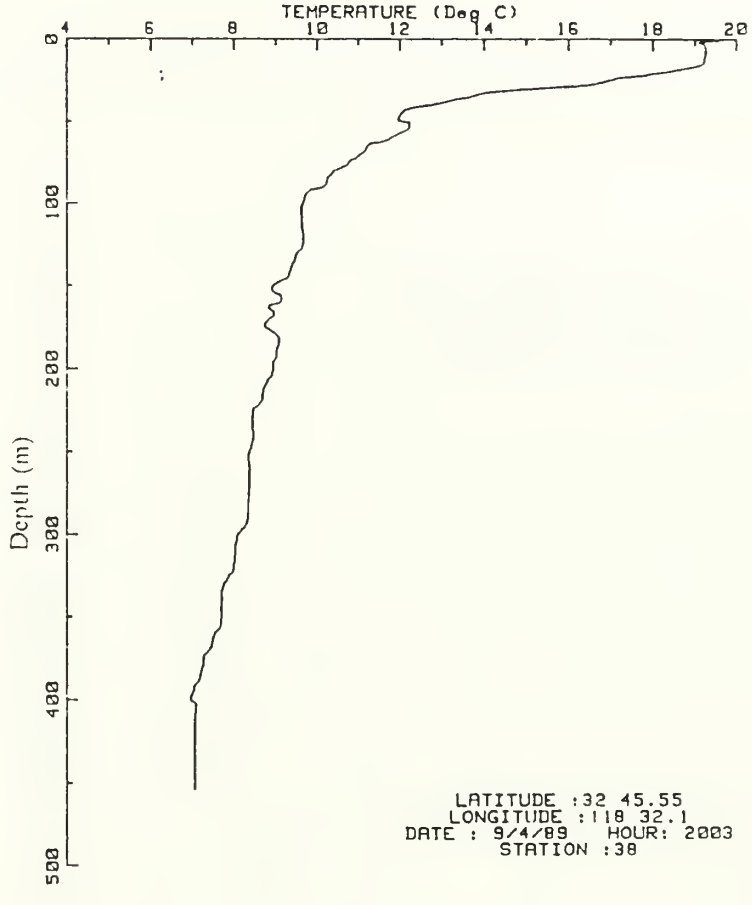

Figure 14.24 Vertical profile of temperature measured by XBT at station No. 38 in figure 3.

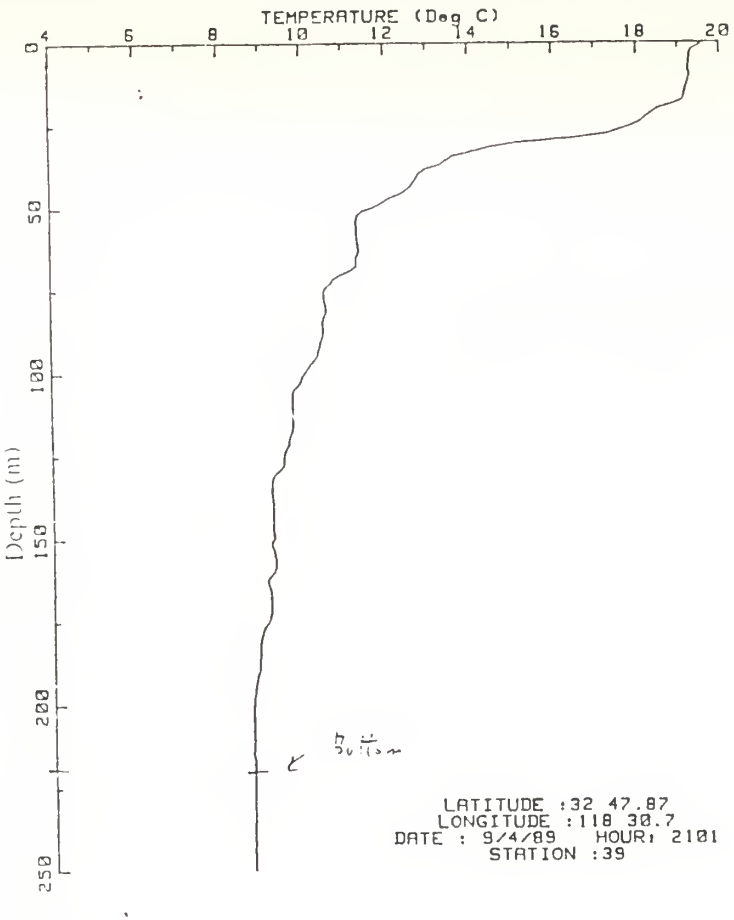

Figure 14.25 Vertical profile of temperature measured by XBT at station No. 39 in figure 3.

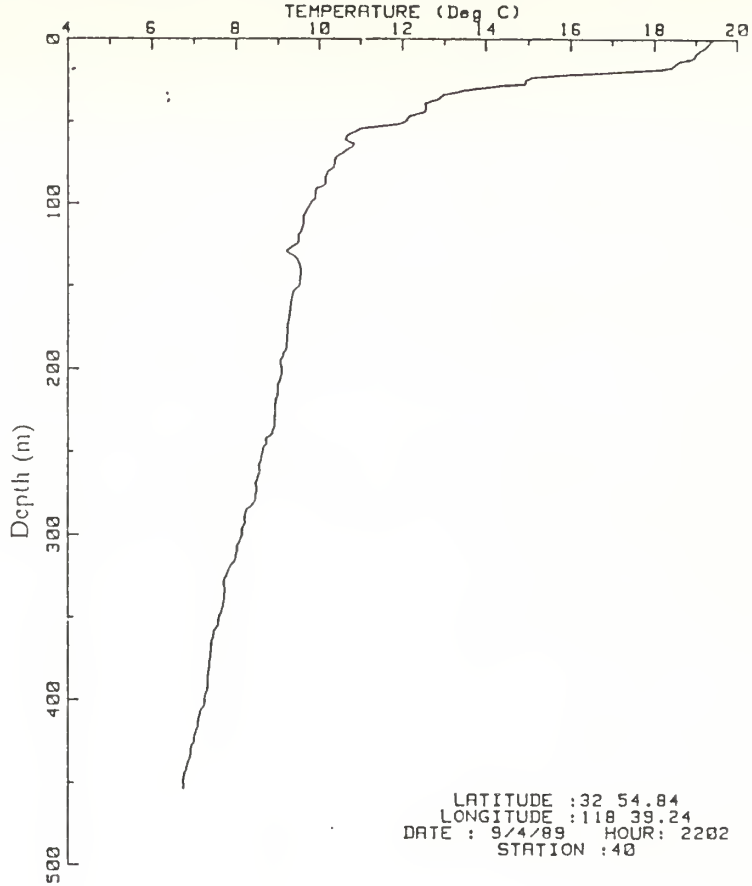

Figure 14.26 Vertical profile of temperature measured by XBT at station No. 40 in figure 3.

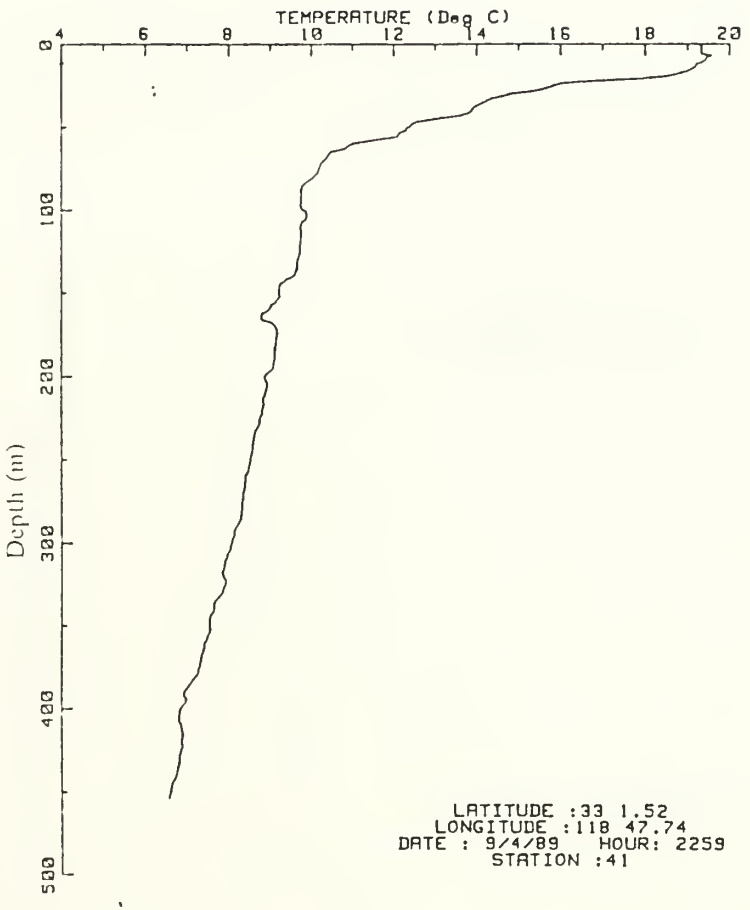

Figure 14.27 Vertical profile of temperature measured by XBT at station No. 41 in figure 3.

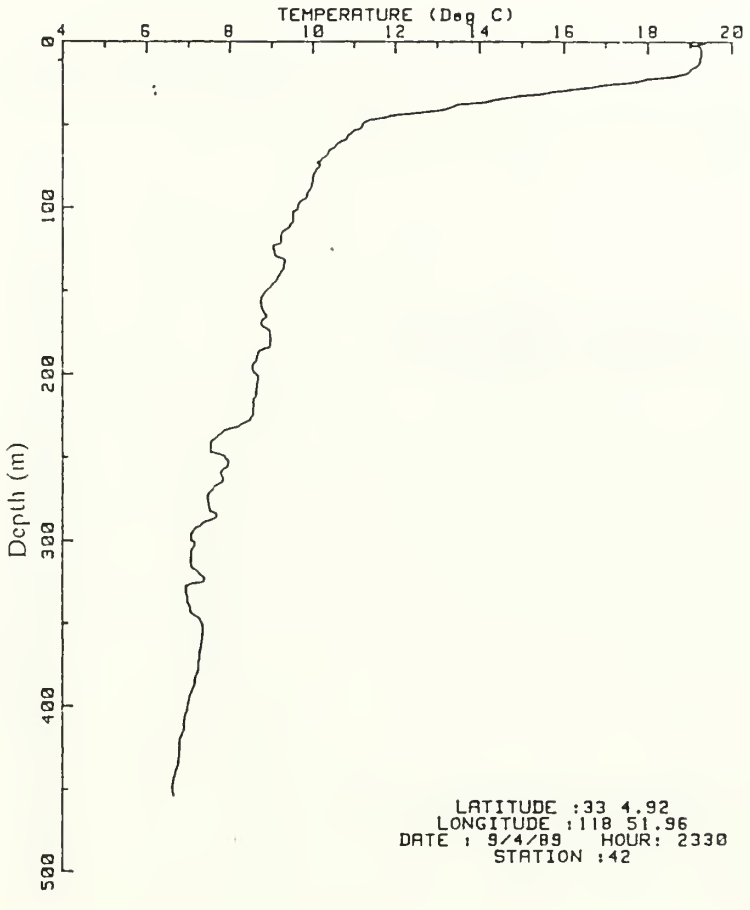

Figure 14.28 Vertical profile of temperature measured by XBT at station No. 42 in figure 3.

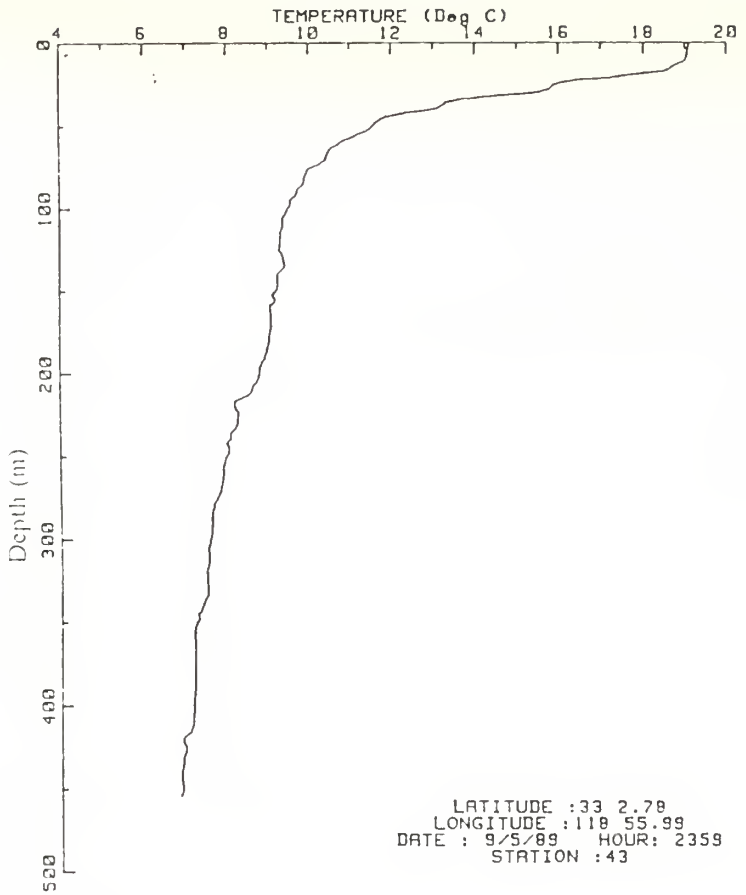

Figure 15.1 Vertical profile of temperature measured by XBT at station No. 43 in figure 5.

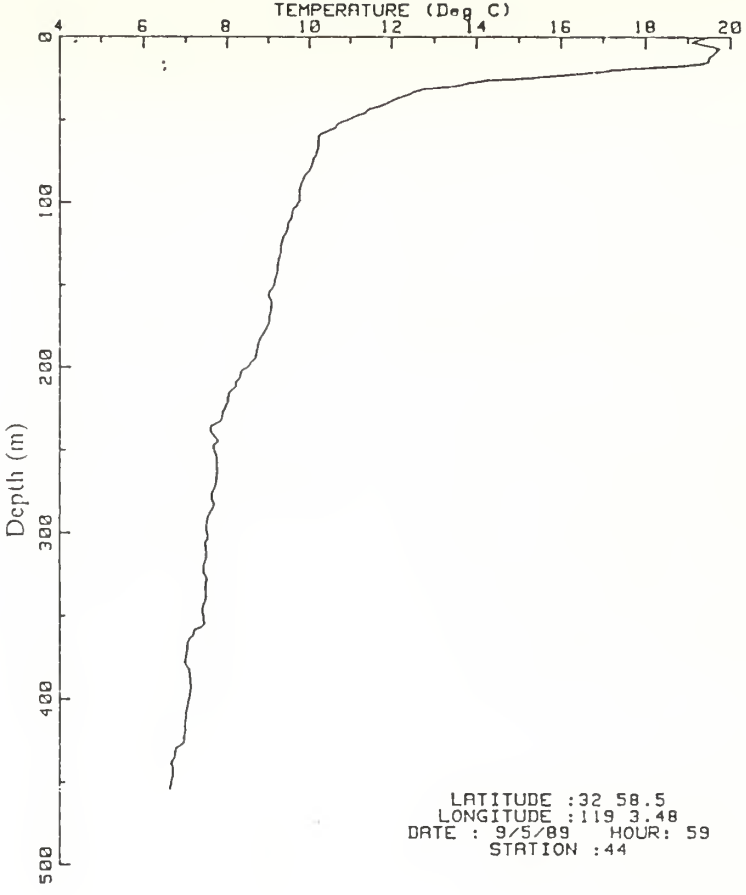

Figure 15.2 Vertical profile of temperature measured by XBT at station No. 44 in figure 5.

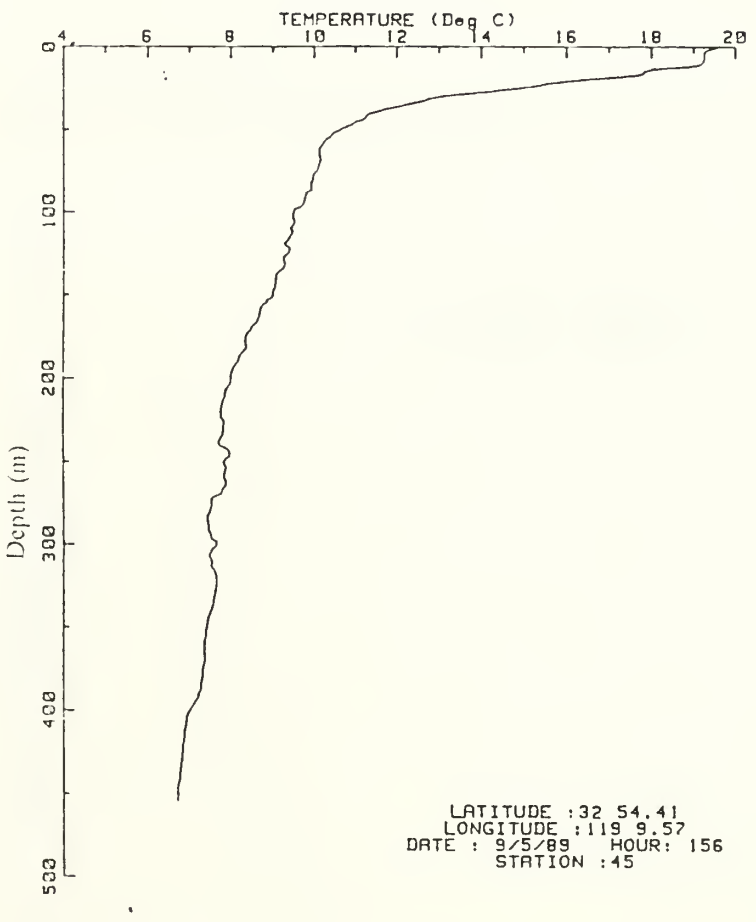

Figure 15.3 Vertical profile of temperature measured by XBT at station No. 45 in figure 5.

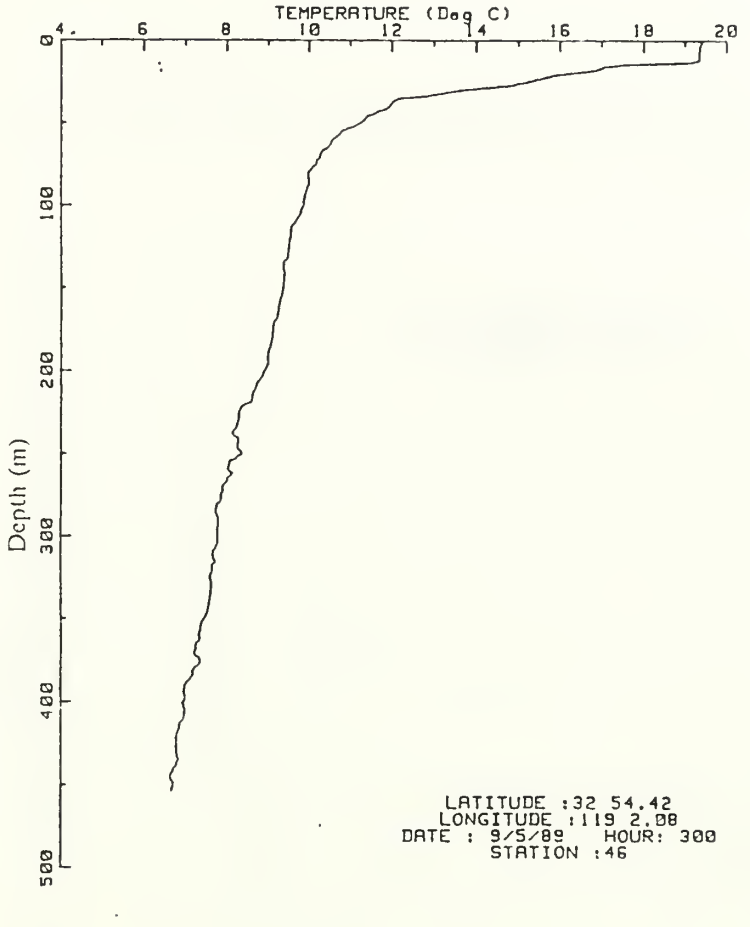

Figure 15.4 Vertical profile of temperature measured by XBT at station No. 46 in figure 5.

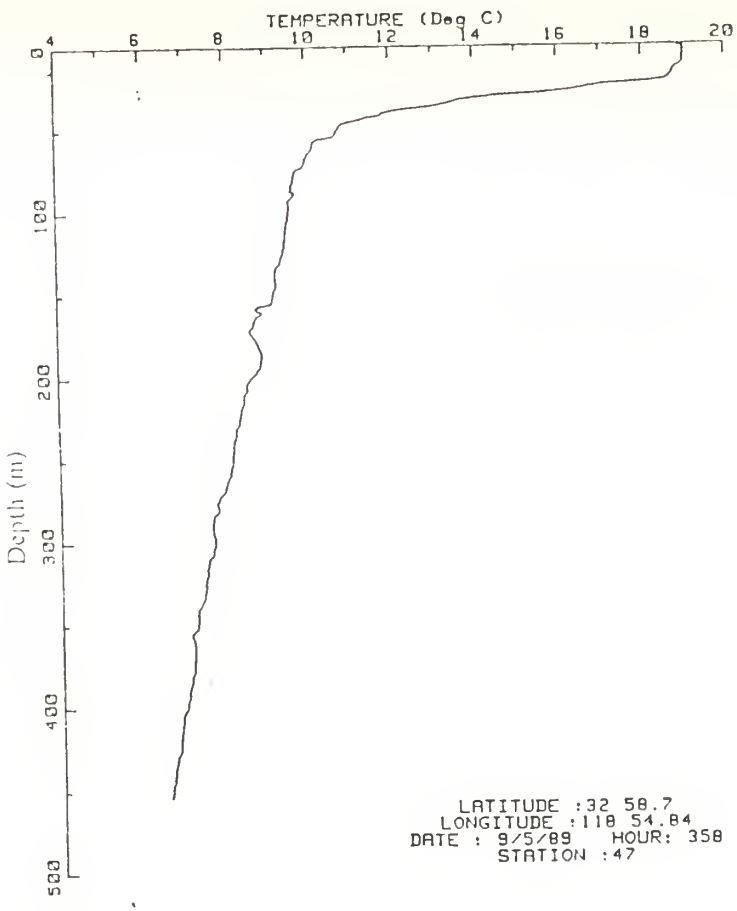

Figure 15.5 Vertical profile of temperature measured by XBT at station No. 47 in figure 5.

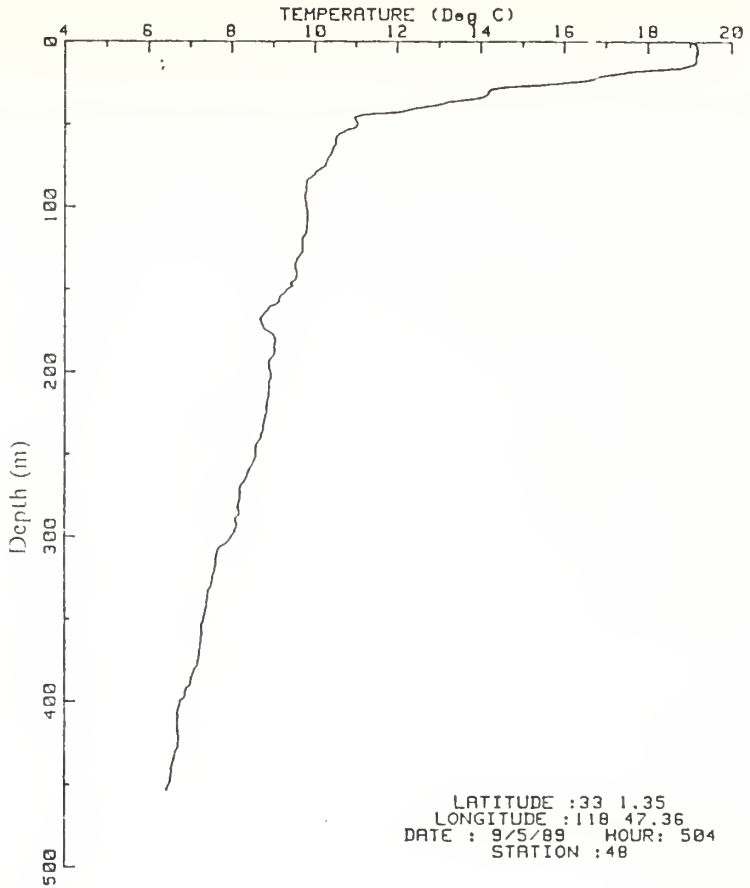

Figure 15.6 Vertical profile of temperature measured by XBT at station No. 48 in figure 5.

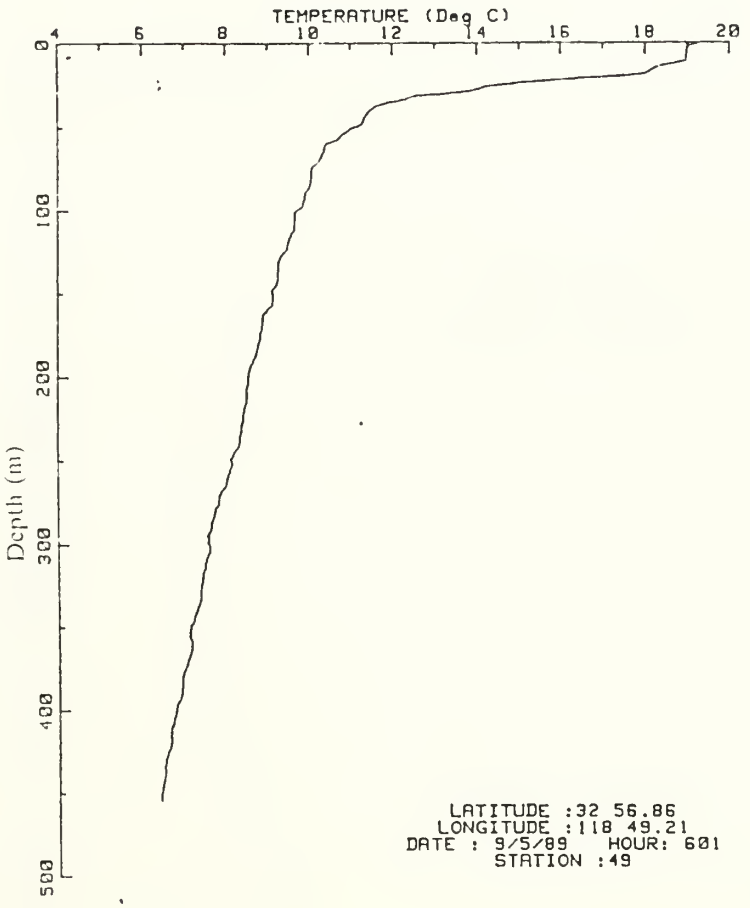

Figure 15.7 Vertical profile of temperature measured by XBT at station No. 49 in figure 5.

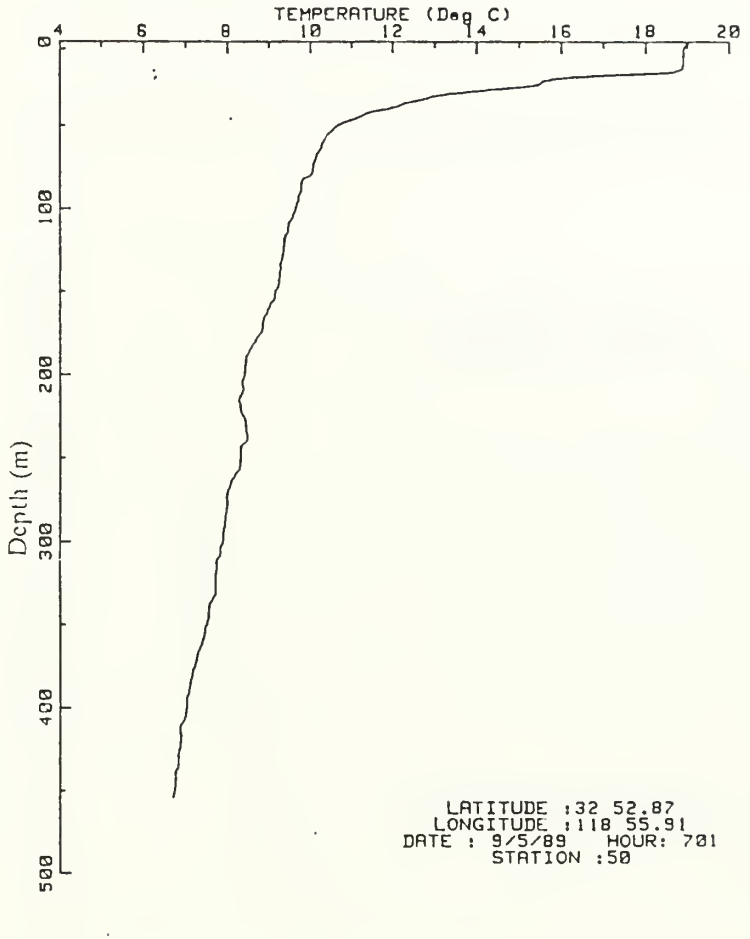

Figure 15.8 Vertical profile of temperature measured by XBT at station No. 50 in figure 5.

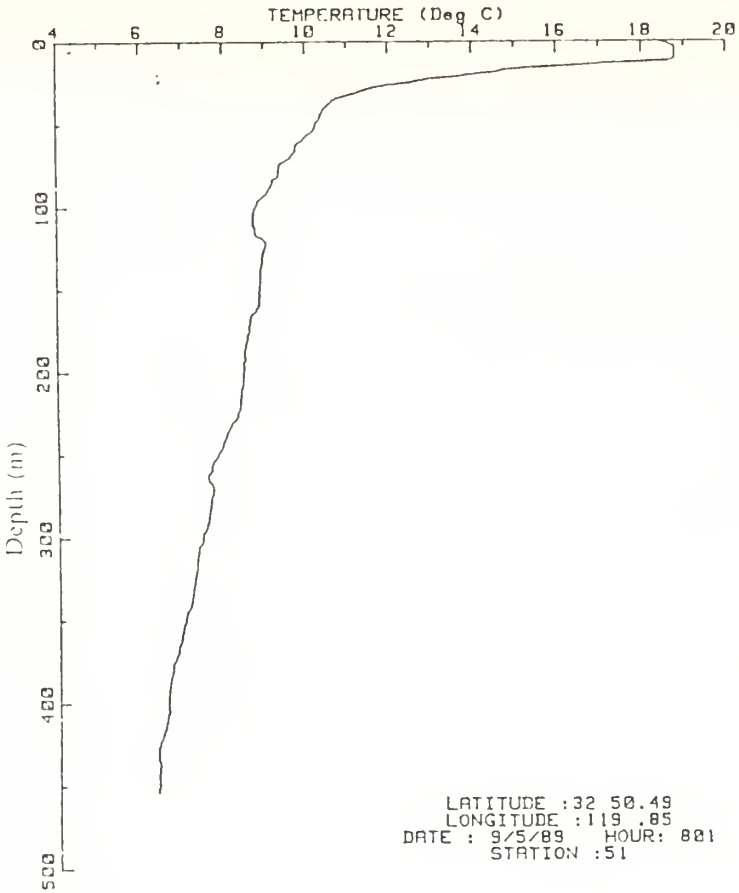

Figure 15.9 Vertical profile of temperature measured by XBT at station No. 51 in figure 5.

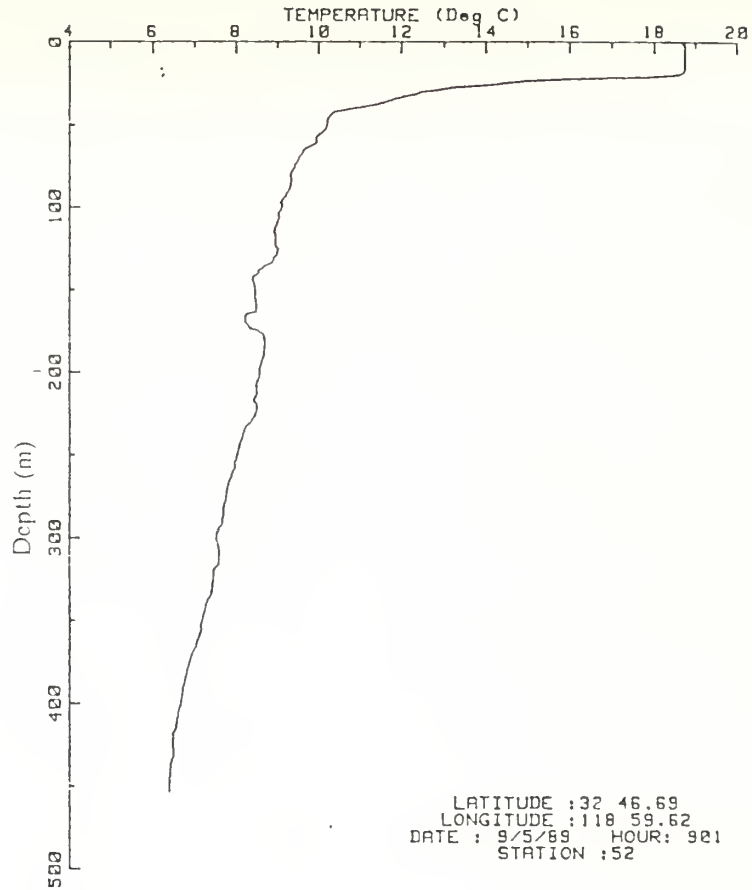

Figure 15.10 Vertical profile of temperature measured by XBT at station No. 52 in figure 5.

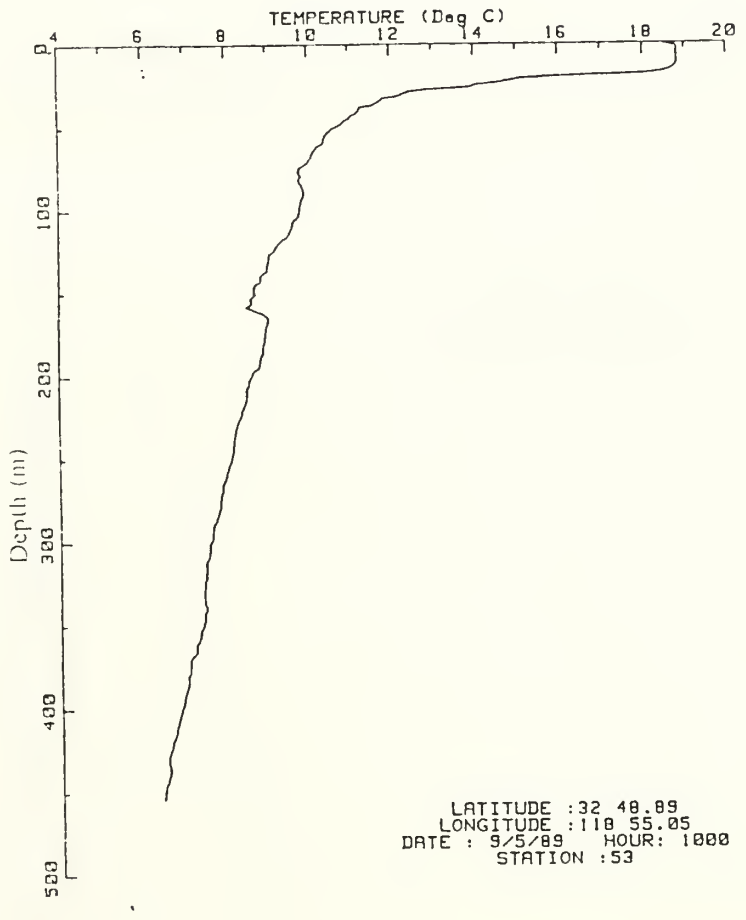

Figure 15.11 Vertical profile of temperature measured by XBT at station No. 53 in figure 5.

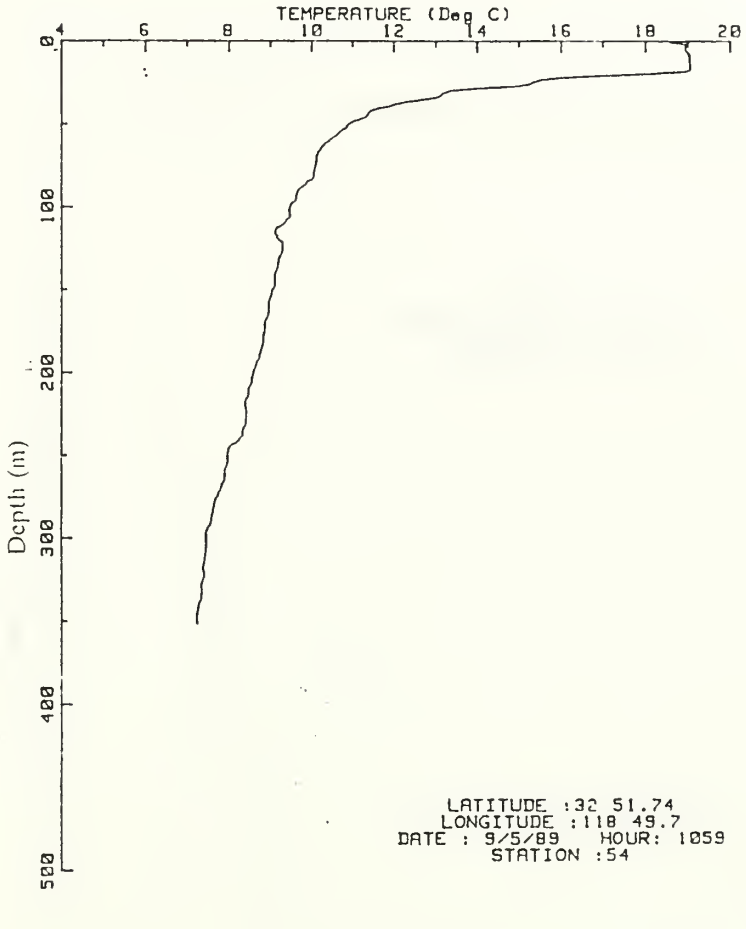

Figure 15.12 Vertical profile of temperature measured by XBT at station No. 54 in figure 5.

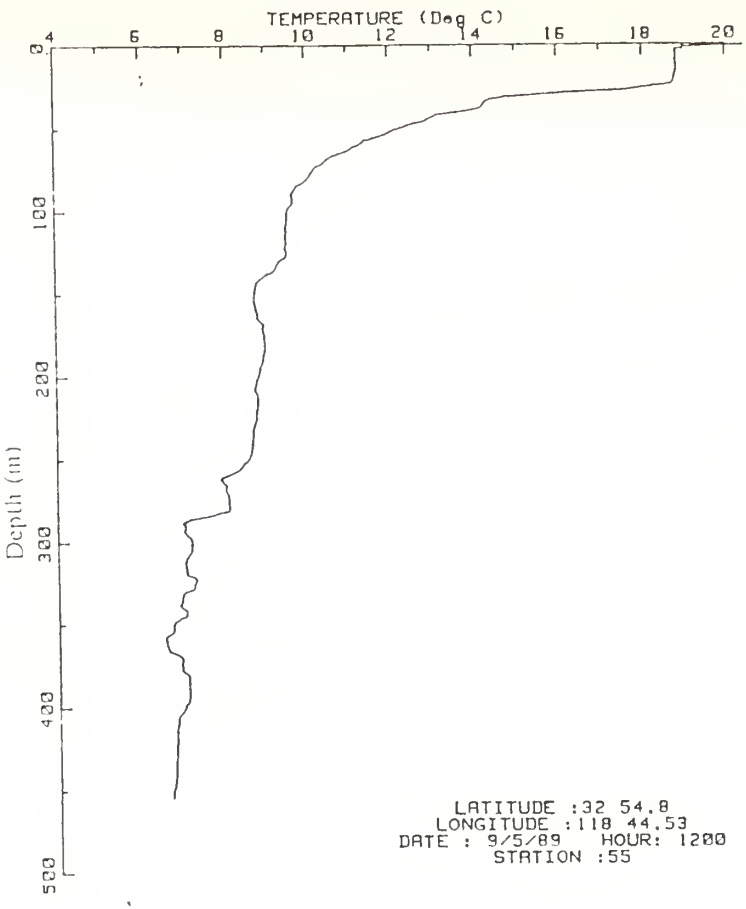

Figure 15.13 Vertical profile of temperature measured by XBT at station No. 55 in figure 5.

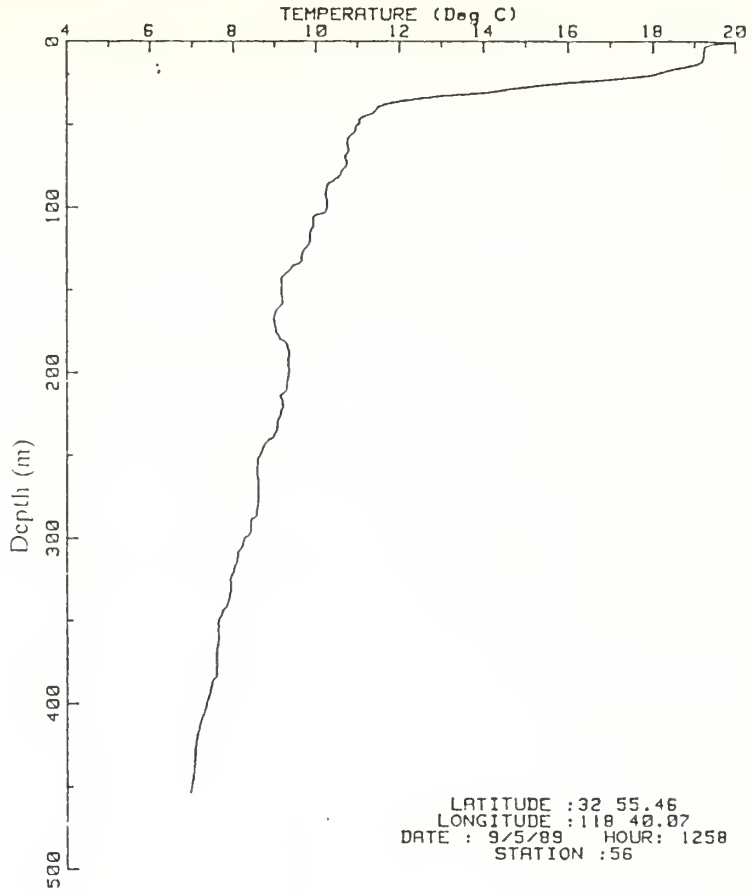

Figure 15.14 Vertical profile of temperature measured by XBT at station No. 56 in figure 5.

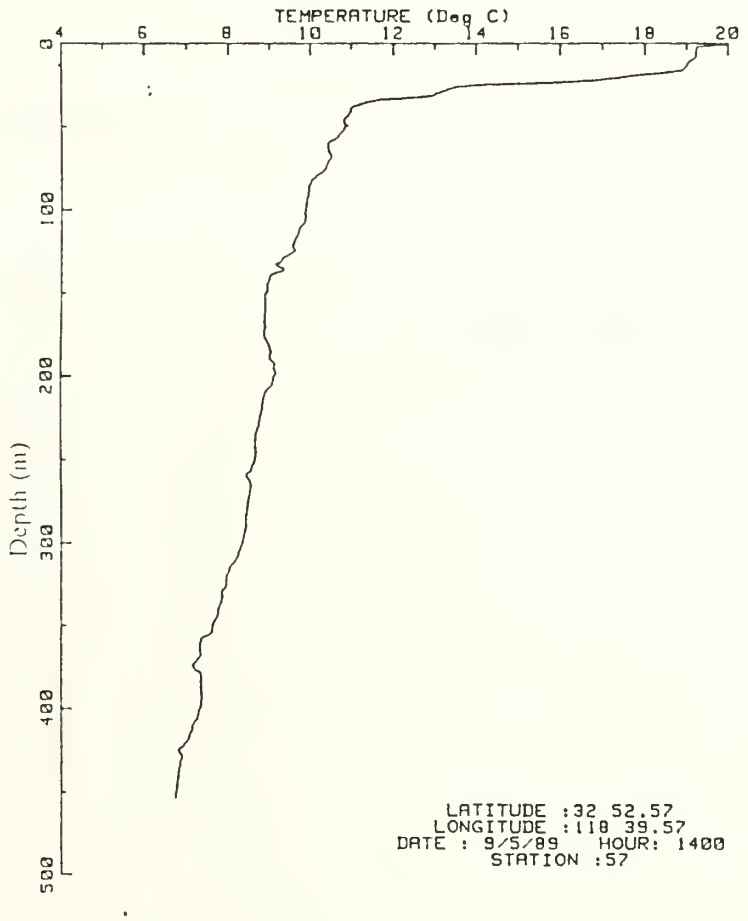

Figure 15.15 Vertical profile of temperature measured by XBT at station No. 57 in figure 5.

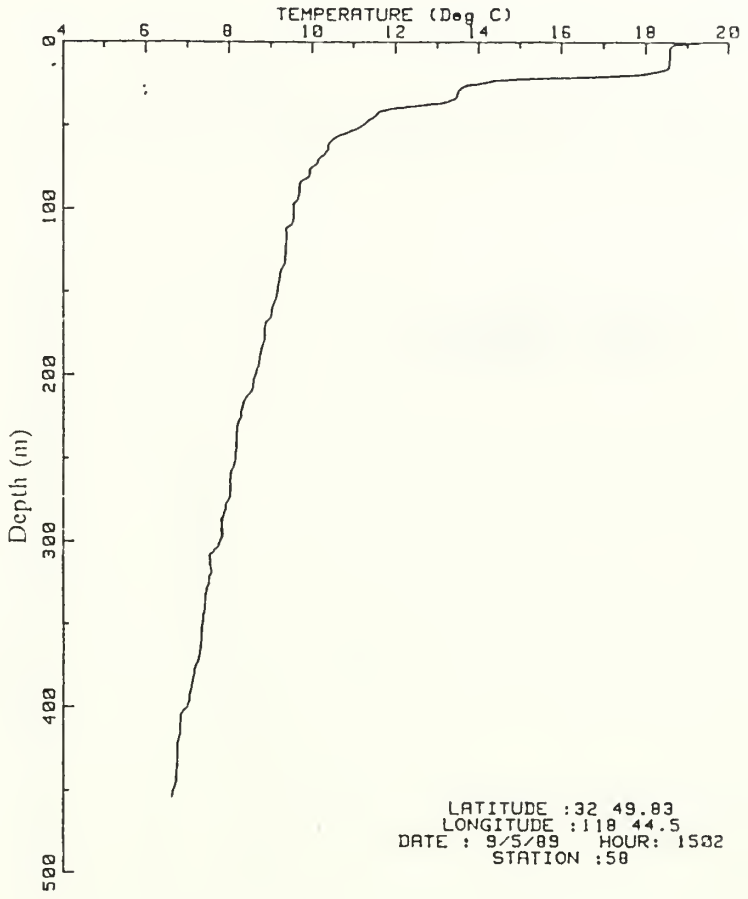

Figure 15.16 Vertical profile of temperature measured by XBT at station No. 58 in figure 5.

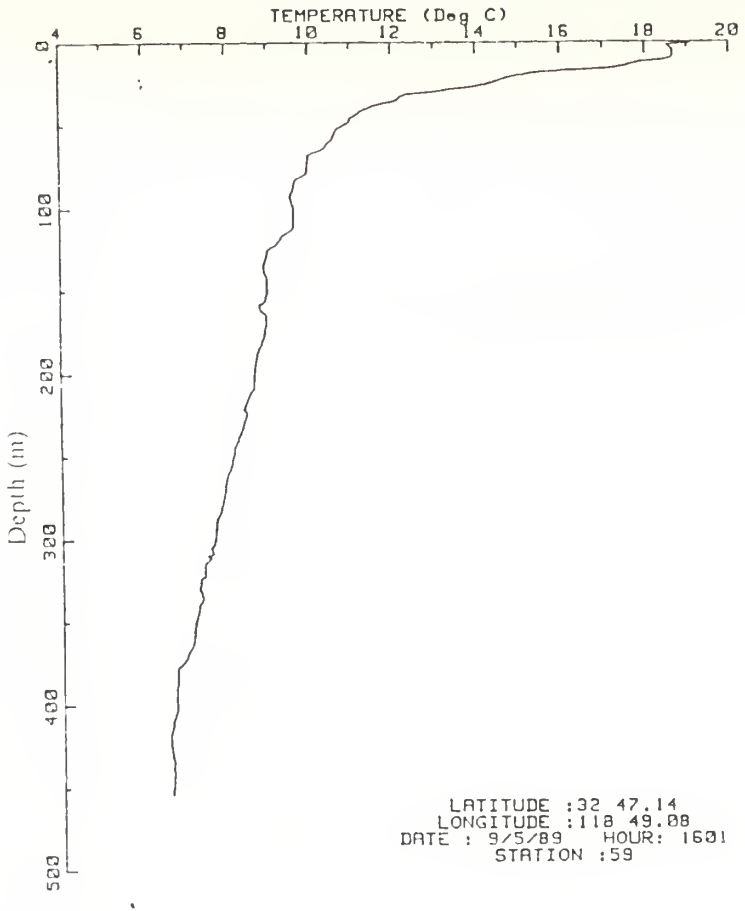

Figure 15.17 Vertical profile of temperature measured by XBT at station No. 59 in figure 5.

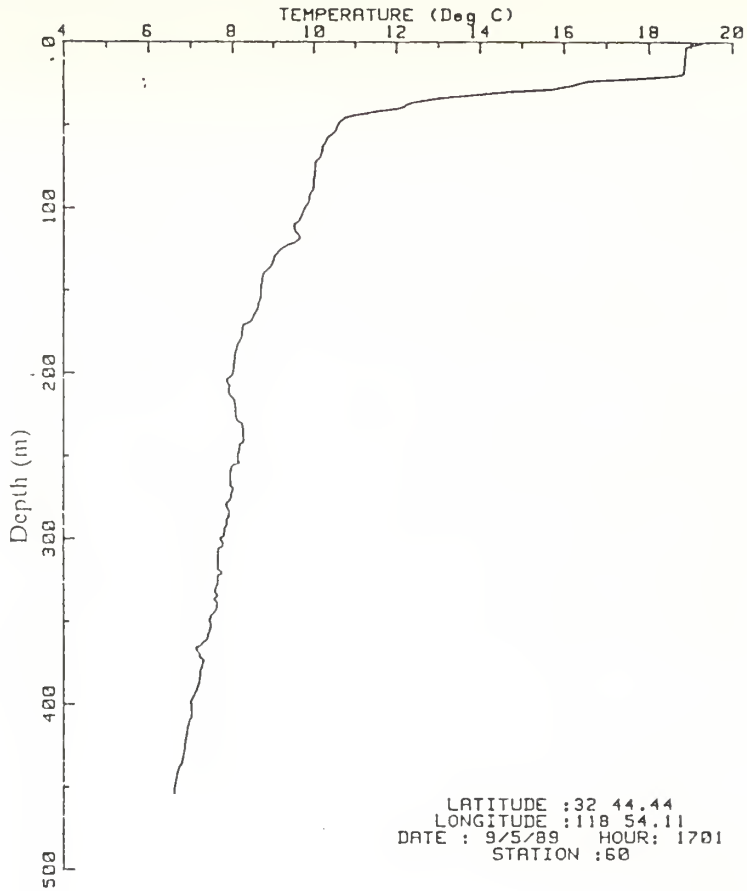

Figure 15.18 Vertical profile of temperature measured by XBT at station No. 60 in figure 5.

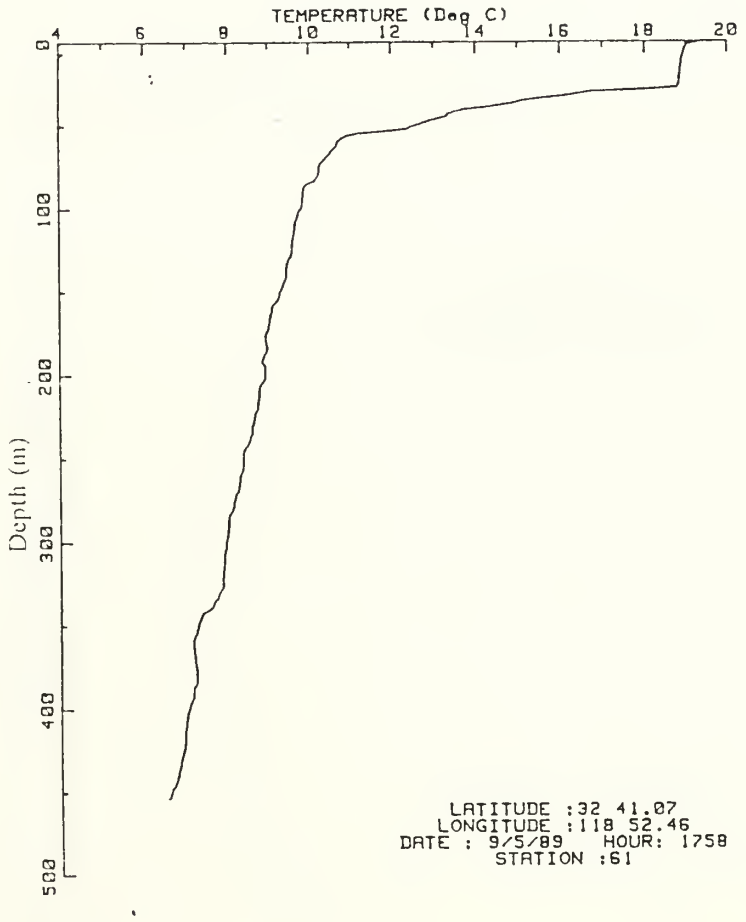

Figure 15.19 Vertical profile of temperature measured by XBT at station No. 61 in figure 5.

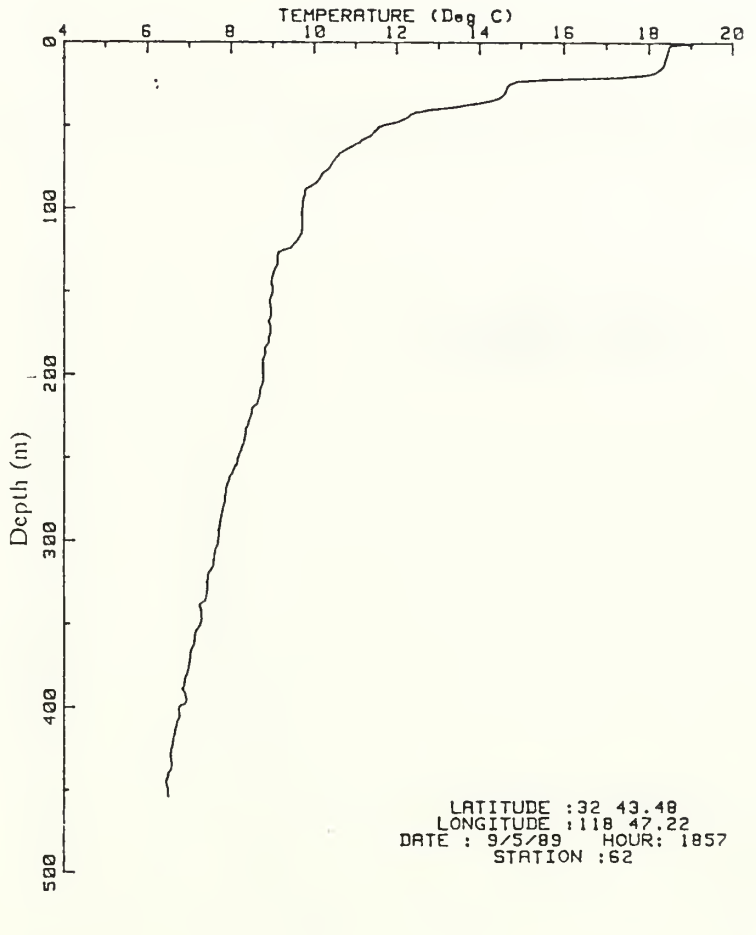

Figure 15.20 Vertical profile of temperature measured by XBT at station No. 62 in figure 5.

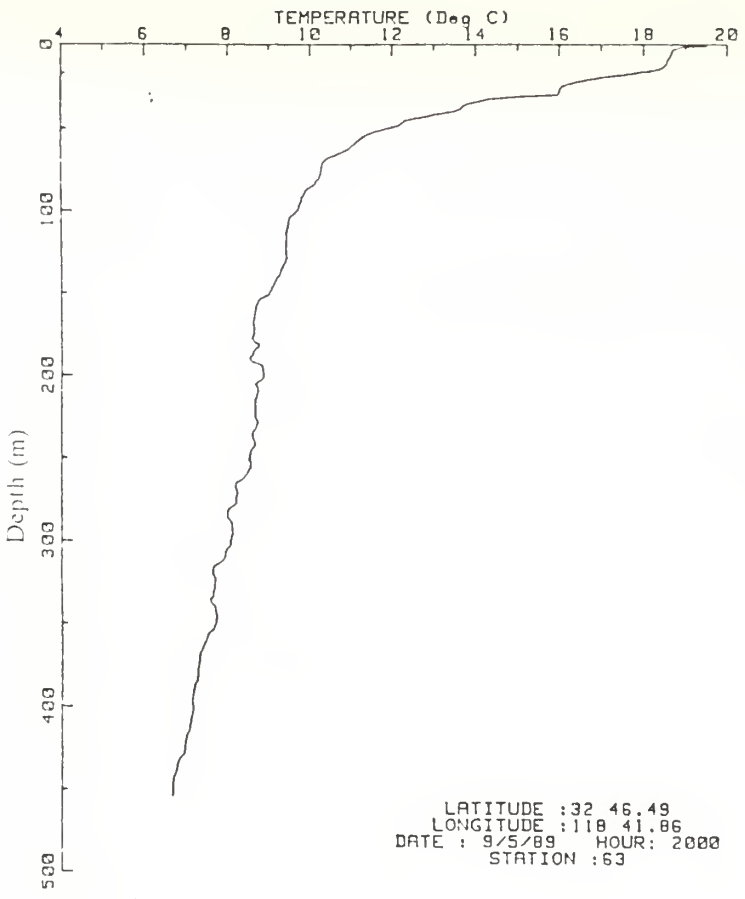

Figure 15.21 Vertical profile of temperature measured by XBT at station No. 63 in figure 5.

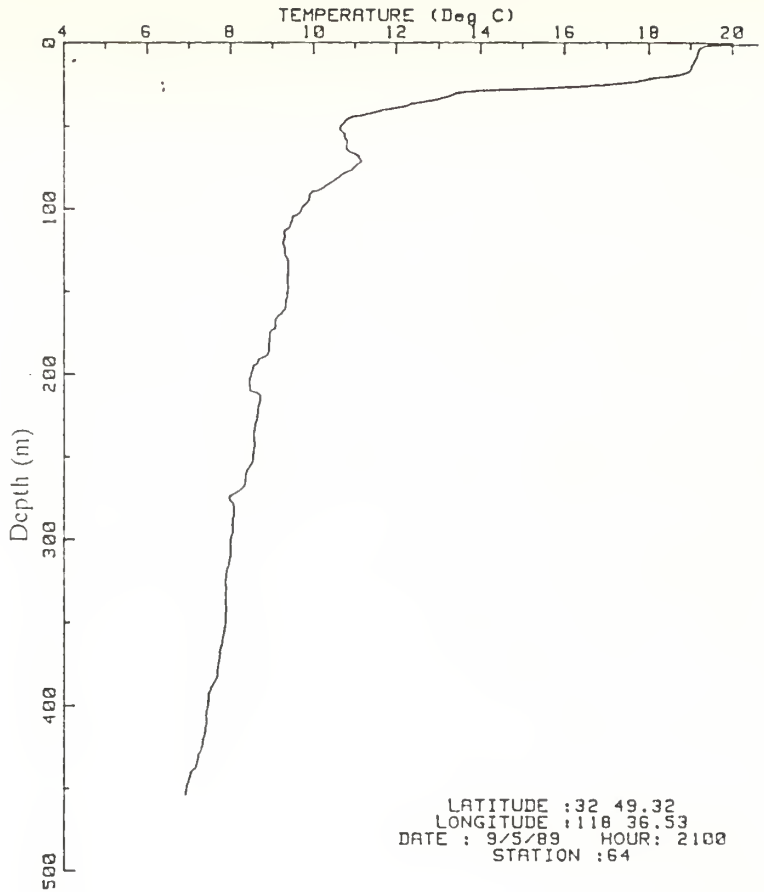

Figure 15.22 Vertical profile of temperature measured by XBT at station No. 64 in figure 5.

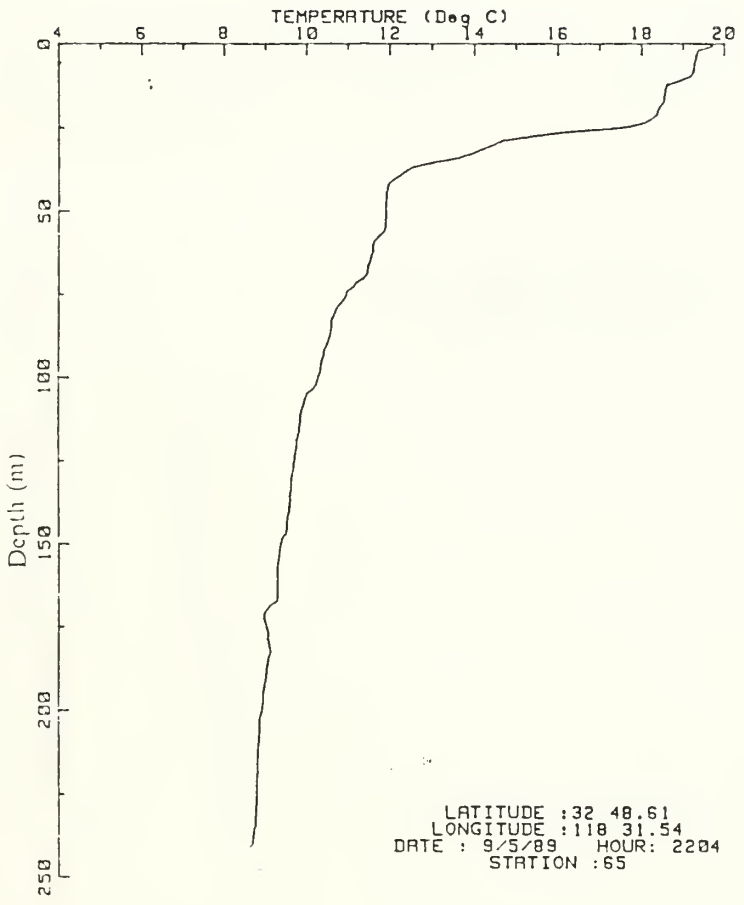

Figure 15.23 Vertical profile of temperature measured by XBT at station No. 65 in figure 5.

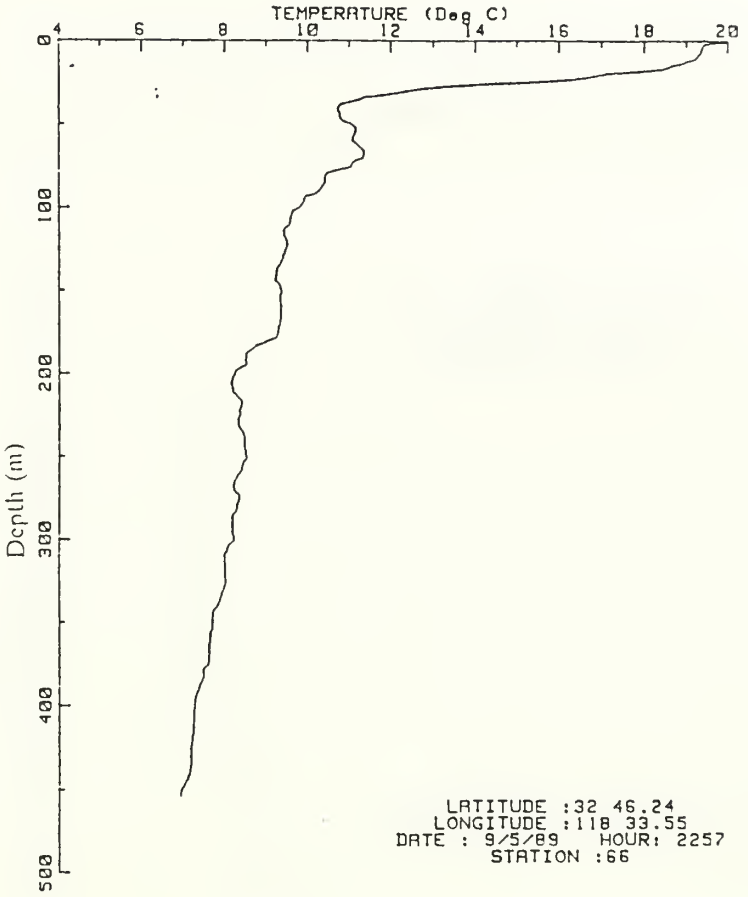

Figure 15.24 Vertical profile of temperature measured by XBT at station No. 66 in figure 5.

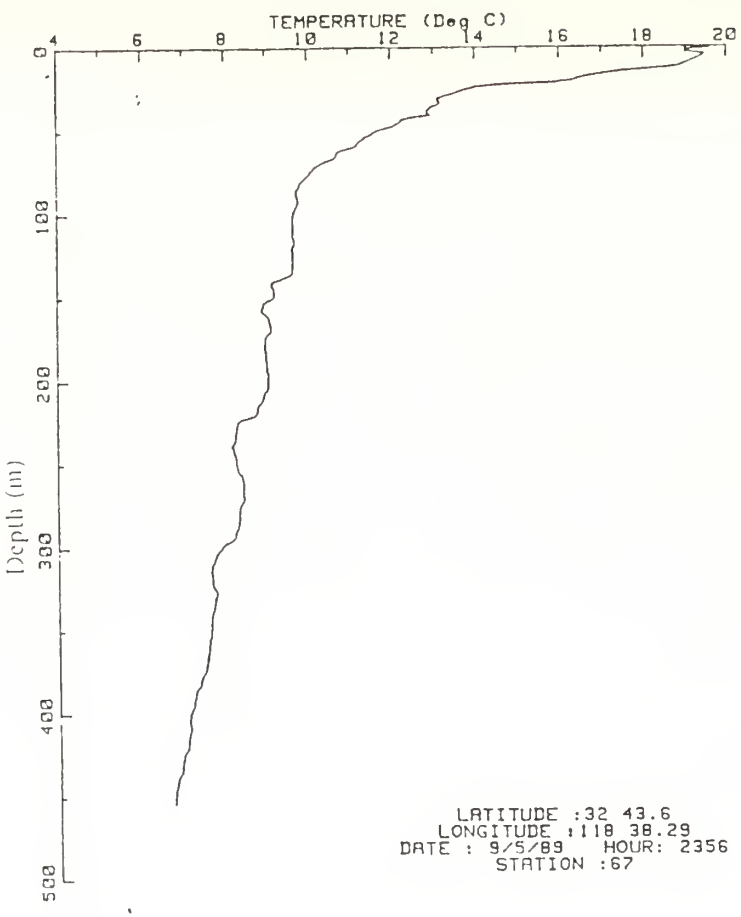

Figure 15.25 Vertical profile of temperature measured by XBT at station No. 67 in figure 5.

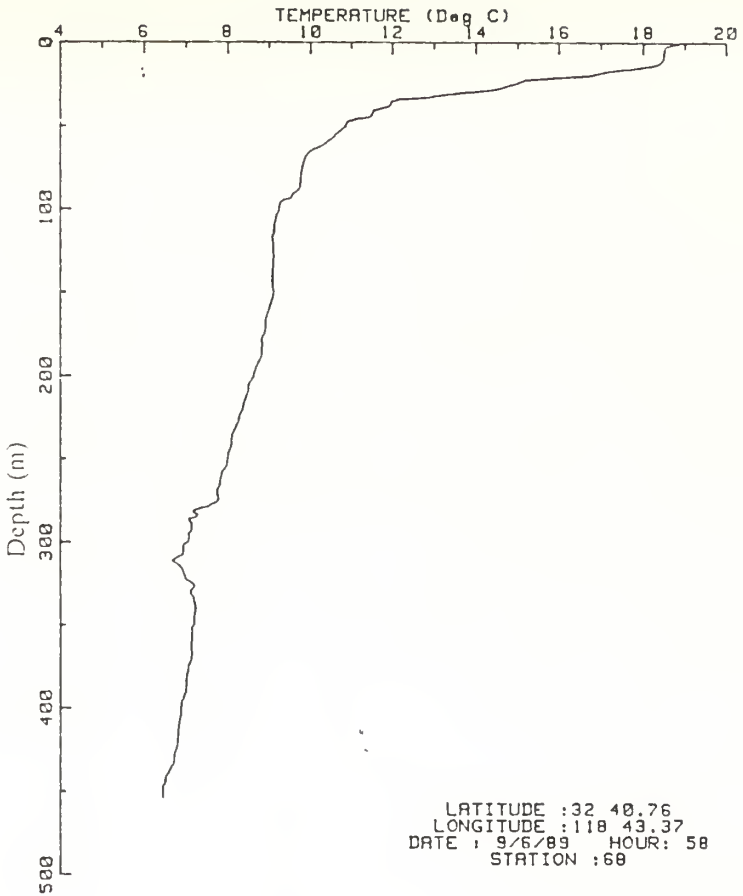

Figure 15.26 Vertical profile of temperature measured by XBT at station No. 68 in figure 5.

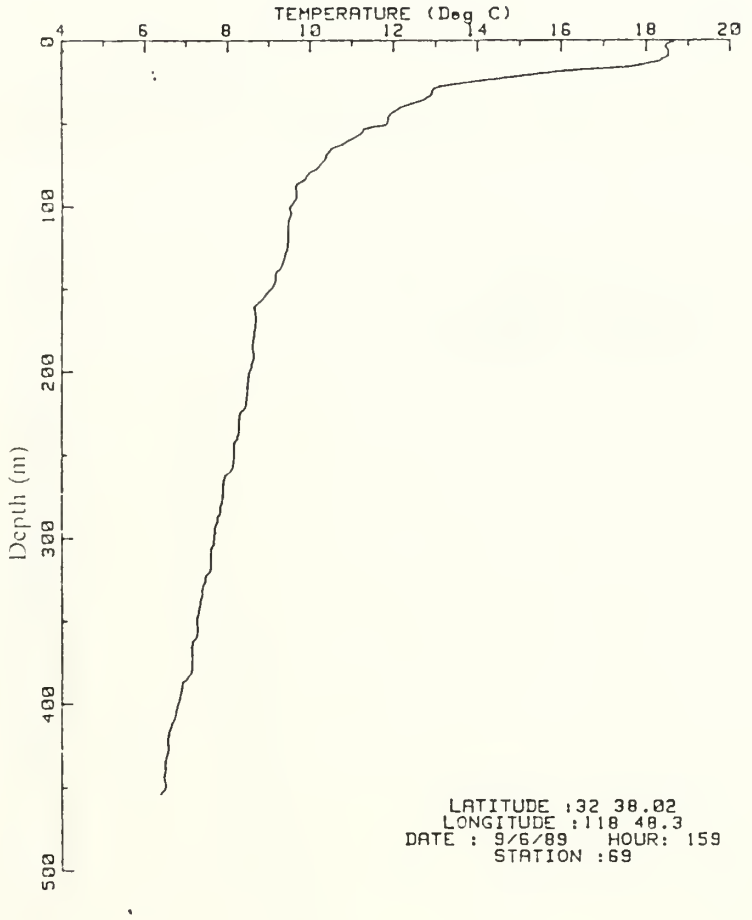

Figure 15.27 Vertical profile of temperature measured by XBT at station No. 69 in figure 5.

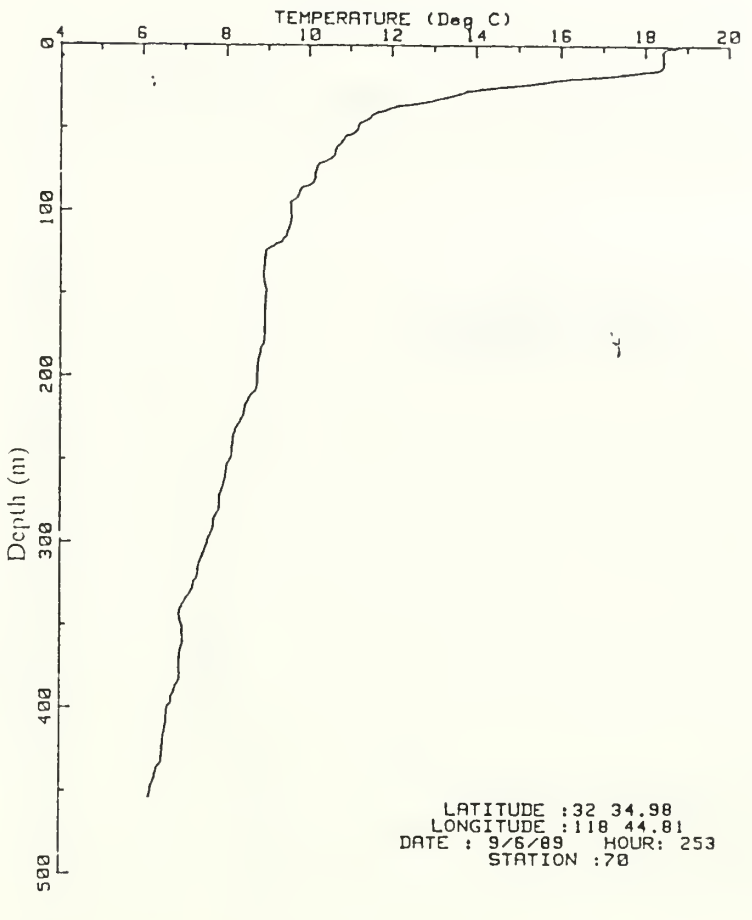

Figure 15.28 Vertical profile of temperature measured by XBT at station No. 70 in figure 5.

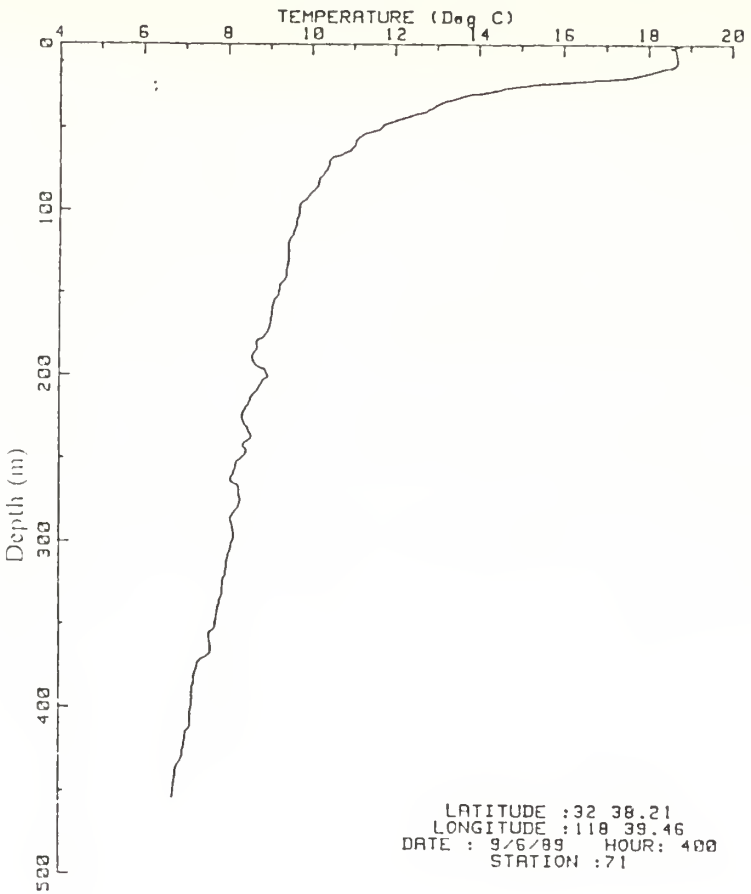

Figure 15.29 Vertical profile of temperature measured by XBT at station No. 71 in figure 5.

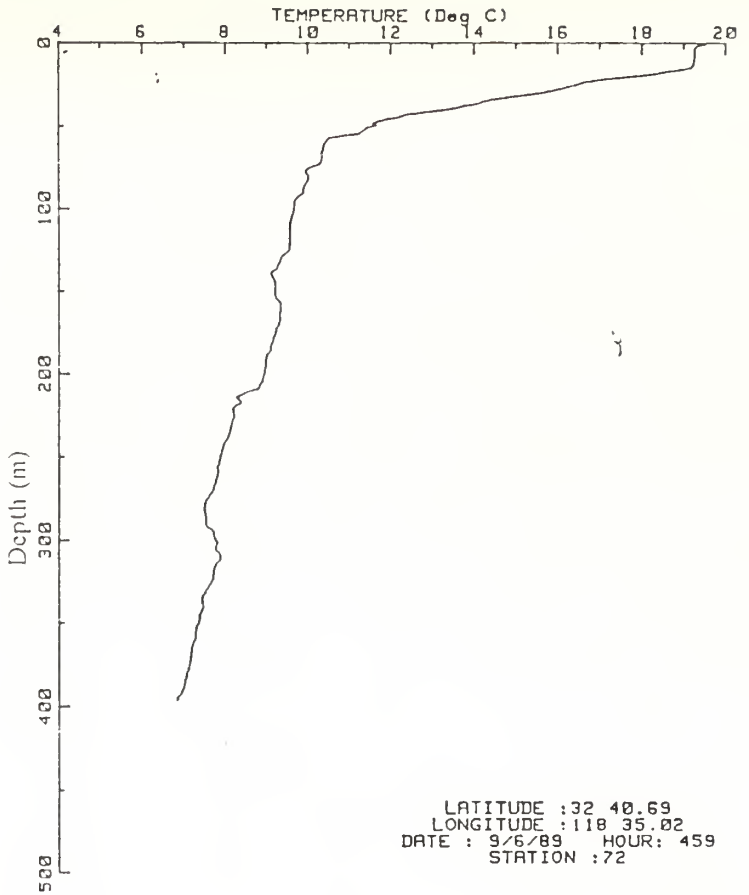

Figure 15.30 Vertical profile of temperature measured by XBT at station No. 72 in figure 5.

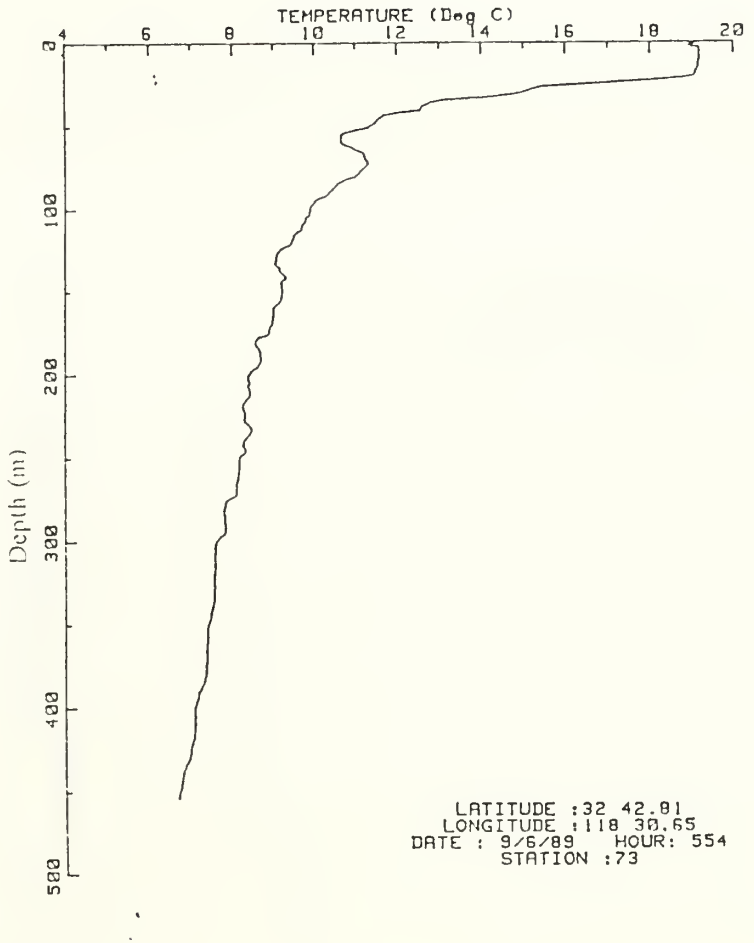

Figure 15.31 Vertical profile of temperature measured by XBT at station No. 73 in figure 5.

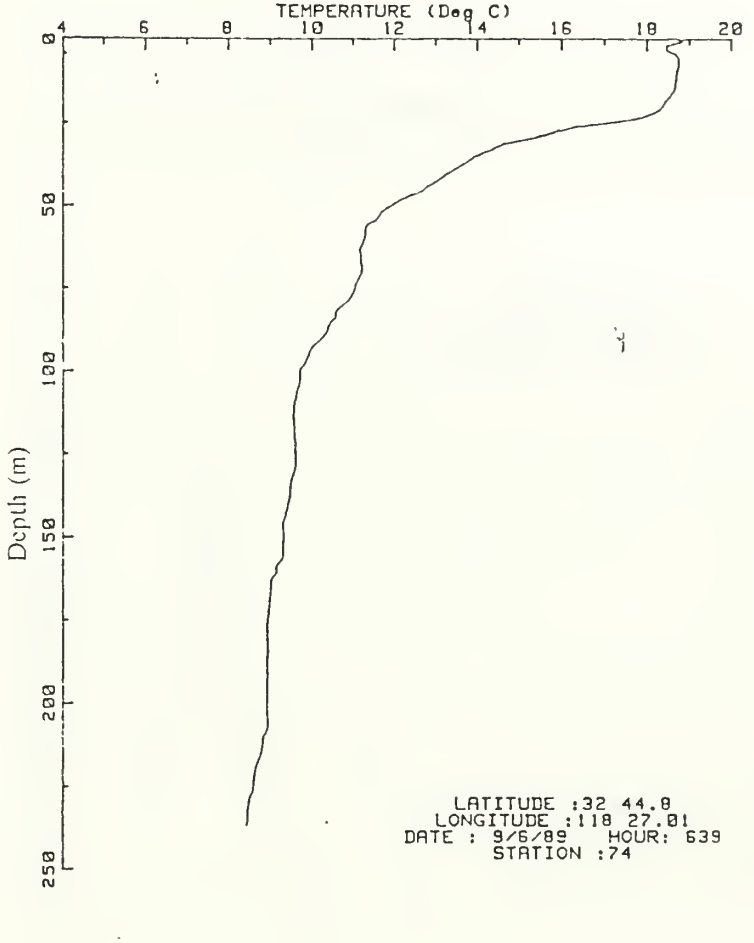

Figure 15.32 Vertical profile of temperature measured by XBT at station No. 74 in figure 5.

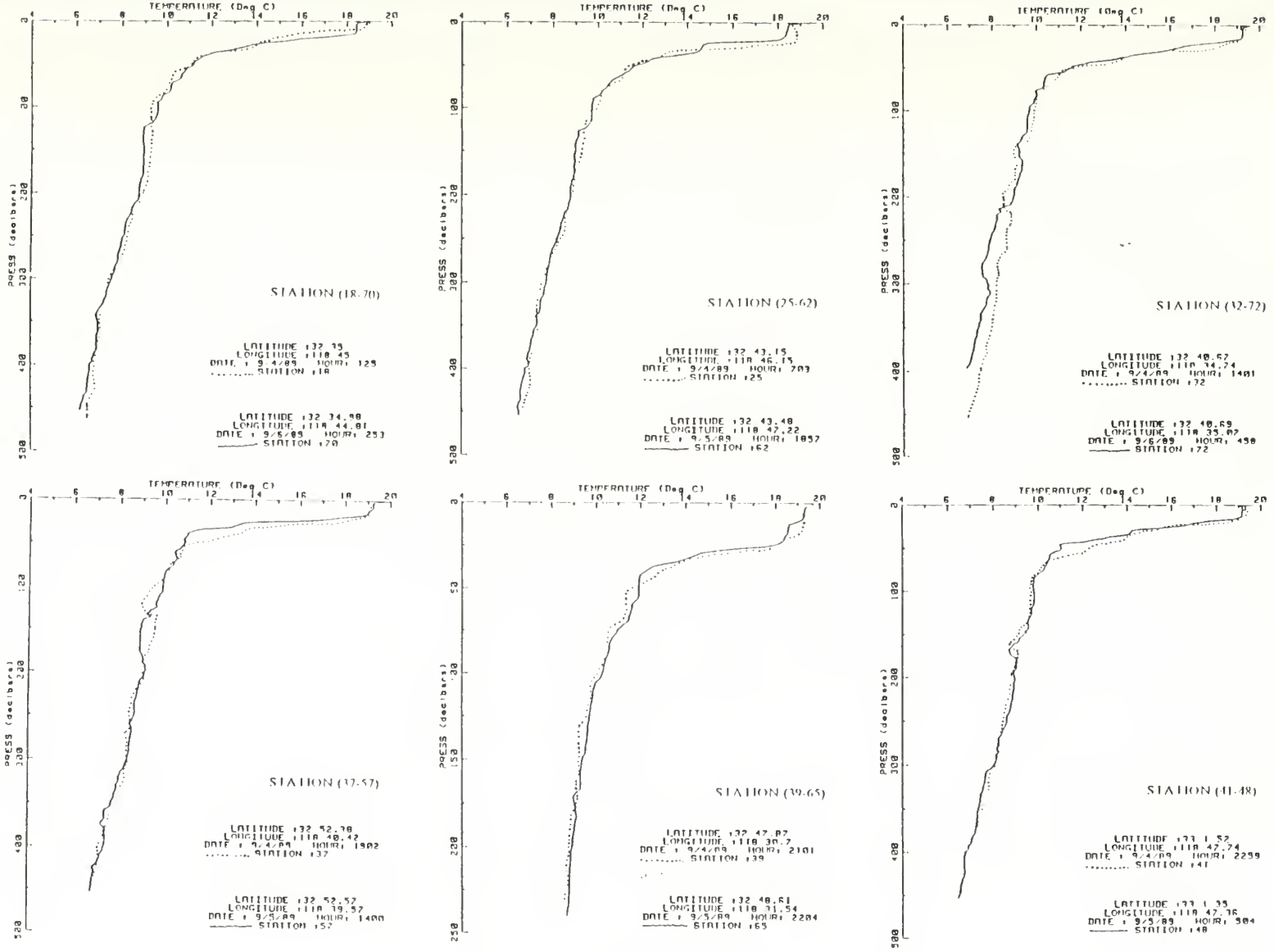

Figure 16. Six comparisons of temperature profiles between first and second pass over the study area for station (18-70)

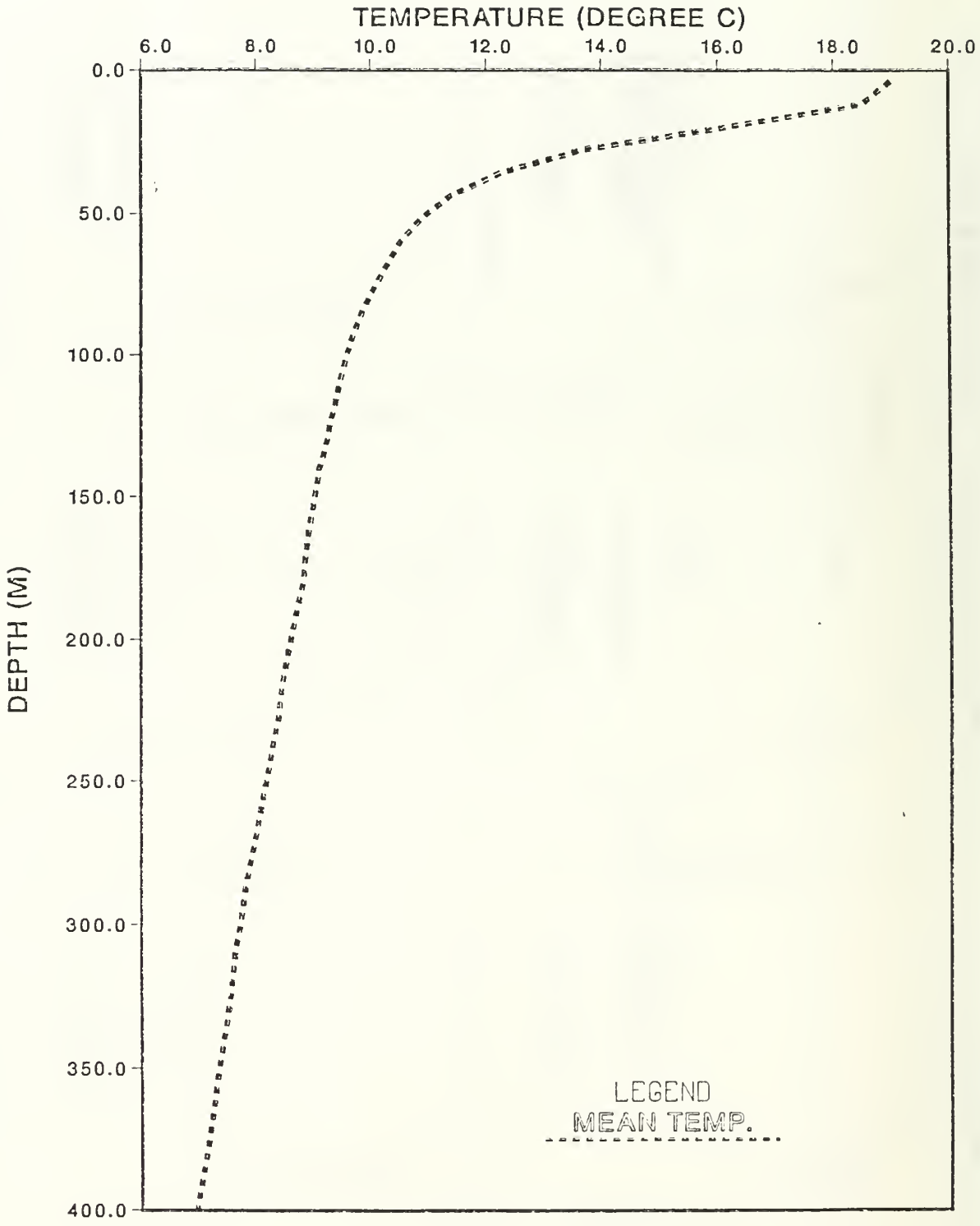

Figure 17. Mean temperature profile at study area given in figure 3 and figure 5.

INITIAL DISTRIBUTION LIST

		No.Copies
1.	Superintendent Naval Postgraduate School Attn:LCRD C.M. Tsai	15
	Paul F. Jessen	1
	Dr. P.C. Chu, Code 68Cu	1
	Chairman Department of Oceanography Code OC/CO	2
	Dr. Steve Ramp	1
	Toby Garfield	1
	Leslie Rosenfeld	1
	Chairman Department of Meteorology Code MR/RD	1
	Library, Code 0142	2
	Research Administration, Code 012	1
	Monterey, CA 93943-5000	
2.	Naval Facilities Engineering Command Chesapeake Division (FPO-1) Washington Naval Yard Washington D.C. 20374	5
3.	Ms. Maureen T. Smith Project Engineer Ocean Engineering and Construction Project Office Chesapeake Division (FPO-1) Naval Facilities Engineering Command Washington Naval Yard Washington D.C. 20374	2
4.	Defense Technical Information Center Cameron Station Alexandria, VA 22304-6145	1
5.	Director, Naval Oceanography Division Naval Observatory 34th and Massachusetts Avenue NW Washington D.C. 20390	1
6.	Commander Naval Oceanography Command Naval Oceanography Command Stennis Space Center, MS 39529-5000	1
7.	Commanding Officer Fleet Numerical Oceanography Center Monterey, CA 93943	1
8.	Commanding Officer Naval Oceanographic Office Stennis Space Center, MS 39522-5001	1

9. Commanding Officer 1
Naval Ocean & Atmosphere Research Laboratory
Stennis Space Center, MS 39522-5001

10. Commanding Officer 1
Naval Ocean & Atmosphere Research Laboratory (West)
Monterey, CA 93943-5006

11. Chairman, Oceanography Department 1
U.S. Naval Academy
Annapolis, MD 21402

12. Chief of Naval Research 1
800 North Quincy Street
Arlington, VA 22217

13. Dr. David L. Evans 1
Office of Naval Research
Physical Oceanography Program
Code 1122 PO
800 North Quincy Street
Arlington, VA 22217

14. Dr. Thomas H. Kinder 1
Office of Naval Research
Physical Oceanography Program
Code 1122 PO
800 North Quincy Street
Arlington, VA 22217

15. Dr. Jeff Smart 1
Applied Physics Laboratory
The Johns Hopkins University
Johns Hopkins Road
Laurel, MD 20707

16. Scripps Institution of Oceanography
Attn:Library 1
Dr. Jim Simpson 1
Prof. Joe Reid 1
P.O. Box 2367
La Jolla, CA 92037

17. School of Oceanography
University of Washington
Attn:Library 1
Dr.M. Gregg 1
Dr.Barbara Hickey 1
Dr.C. Eriksen 1
Seattle, WA 98195

18. School of Oceanography
Oregon State University
Attn:Library 1
Dr. Mike Kosro 1
Corvallis, OR 97331

19. Dr. Eric Firing 1
Department of Oceanography
University of Hawaii
Honolulu, HI 96822

20. Jeff H. Smart 1
The Johns Hopkins University
Applied Physics Laboratory
Johns Hopkins Road, Laurel,
Maryland 20707-6099

DUDLEY KNOX LIBRARY
3 2768 00327830 0